FUNDAMENTAL STUDIES OF CHEMICAL IONIZATION AND CHARGE EXCHANGE IONIZATION FOR QUADRUPOLE ION TRAP MASS SPECTROMETRY

By

DAVID WAYNE BERBERICH

A DISSERTATION PRESENTED TO THE GRADUATE SCHOOL
OF THE UNIVERSITY OF FLORIDA
IN PARTIAL FULFILLMENT OF THE REQUIREMENTS FOR THE
DEGREE OF DOCTOR OF PHILOSOPHY

UNIVERSITY OF FLORIDA

1989

To Kathleen with all of my love.

ACKNOWLEDGEMENTS

I wish to express my sincere gratitude to Dr. Richard A. Yost for his guidance and direction during the completion of this work. I would also like to acknowledge and thank the members of my graduate committee, Dr. John Dorsey, Dr. Gerhard Schmid, Dr. Kenneth Wagener, and Dr. Charles Thomas. A special thanks goes to Dr. John Dorsey for being a friend at the difficult moments that arise during graduate school.

I acknowledge the U. S. Army Chemical Research, Development, and Engineering Center for their support of this work.

I thank my fellow group members, especially Mark Hail for his assistance with the TQMS, Mike Lee, Ken Matuszak, Todd Gillespie, and Kevin Volk. I thank my special friends Stephen Brooks, Maria Torrez, Linda Volk, Mike Rutledge, and Moi Leong who provided my wife and I friendship and many special memories.

Sincere thanks go to my family, Mom and Dad Berberich, Debbie, Bill and Barb, Bob and Dana, and Mom and Dad Kennedy, for their support. A special thanks to Sister Marie Joan Harris and Patrick Roach, whose support and encouragement convinced me to attend and complete graduate school.

I have difficulty finding the words to express the debt of gratitude that I feel for my wife Kathleen. Kathleen was always there by my side providing me with support, encouragement, love, and laughter. Whenever I was down or discouraged she would know exactly what to do or say to cheer me up or encourage me. We have experienced many special moments

over the past four and a half years, but the happiest moments for me are those that I have shared with my wife.

TABLE OF CONTENTS

page

ACKNOWLEDGEMENTS iii

ABSTRACT vii

CHAPTERS

1 INTRODUCTION 1

- Historical Perspective 2
- Ionization Techniques 5
- Overview of Thesis Organization 15

2 EXPERIMENTAL 19

- Samples and Reagents 19
- Mass Spectrometers 19
  - Quadrupole Ion Trap 19
  - Triple Quadrupole 32

3 POSITIVE AND NEGATIVE IONIZATION IN QUADRUPOLE ION TRAP MASS SPECTROMETRY: EFFECTS OF APPLIED VOLTAGES AND REACTION TIMES 36

- Positive Electron, Chemical, and Charge Exchange Ionization . 41
  - Non-mass-selected Reactions 41
  - Mass-selected Ejection 58
  - Mass-selected Ion-molecule Reactions 67
- Negative Electron Capture and Chemical Ionization 81
  - Non-mass-selected Reactions 82
  - Mass-selected Ejection 87
  - Mass-selected Ion-molecule Reactions 97
- Conclusions 117

4 ION-MOLECULE REACTIONS FOR POSITIVE CHEMICAL IONIZATION AND CHARGE EXCHANGE IONIZATION IN QUADRUPOLE ION TRAP AND TRIPLE QUADRUPOLE MASS SPECTROMETERS 121

- Non-mass-selected Reactions 127
  - Electron Ionization 127
  - Charge Exchange Ionization 134
  - Chemical Ionization 139

Mass-selected Ion-Molecule Reactions 141
Charge Exchange Ionization 141
Chemical Ionization 156
Conclusions 163

5 CONCLUSIONS AND FUTURE WORK 165

LITERATURE CITED 171

BIOGRAPHICAL SKETCH 176

Abstract of Dissertation Presented to the Graduate School of the
University of Florida in Partial Fulfillment of the Requirements for
the Degree of Doctor of Philosophy

FUNDAMENTAL STUDIES OF CHEMICAL IONIZATION AND CHARGE EXCHANGE IONIZATION FOR QUADRUPOLE ION TRAP MASS SPECTROMETRY

by

David Wayne Berberich

May 1989

Chairman: Richard A. Yost
Major Department: Chemistry

Interest in quadrupole ion trap mass spectrometry (QITMS), in which positive and/or negative ions are trapped in a three-dimensional quadrupole RF field, has recently undergone a resurgence. Within this ion trap the functions of mass spectrometry (ionization, mass analysis, and ion activation) may be performed in a single region. These capabilities offer the opportunity to perform tandem mass spectrometry (MS/MS) sequentially in a single region (tandem-in-time), as opposed to the more familiar MS/MS approach of linking two discrete mass analyzers (tandem-in-space). Unique features of QITMS include the potential for extremely efficient MS/MS, to perform MS^n (MS/MS/MS...etc.), and for small, low-cost MS/MS systems.

This thesis emphasizes fundamental studies of the ionization processes in the QITMS. Selection of an ionization technique is of utmost importance, since it ultimately determines the characteristics of the resultant mass spectra. In this thesis, four forms of ionization are discussed: electron ionization (EI), positive chemical ionization (PCI) via proton transfer or hydride abstraction, negative chemical ionization (NCI) via proton abstraction or electron capture (EC), and charge exchange ionization (CE).

The QITMS is normally operated in the RF-only mode (non-mass-selected). The spectra obtained with this mode of operation may be the result of CE or CI with the desired reactant ion, as well as with undesired reactant ions, and EI. Operation of the QITMS with both DC and RF voltages allows for the storage of a narrow mass range of ions with a single polarity. Thus, unambiguous CE and CI reactions can be obtained by mass selecting reactant ions of a single m/z, and allowing specific ion-molecule reactions to occur. Mass-selected CE and CI spectra are compared with those obtained with a triple quadruple (TQMS) instrument by allowing ion-molecule reactions to occur in the center quadrupole collision cell. The characterization and optimization of operating parameters for the QITMS are described. A variety of reactant gases were examined, since it was anticipated that various gases would produce markedly different CE and CI spectra.

CHAPTER 1
INTRODUCTION

The objectives of this research were threefold: firstly, to characterize and optimize the parameters affecting the operation of the Finnigan MAT quadrupole ion trap mass spectrometer (ITMS), including for both positive and negative ionization; secondly, to develop and evaluate various operational modes for ionization of sample molecules, including non-mass-selected, mass-selected ejection, and mass-selected ionization; thirdly, to evaluate and compare various ionization modes with and without mass-selected ion-molecule reactions in a quadrupole ion trap mass spectrometer (QITMS) and a triple quadrupole mass spectrometer (TQMS). Five forms of ionization were evaluated which produce positive and negative ions by gas-phase ion-molecule reactions, namely electron ionization (EI), positive chemical ionization (PCI) via proton transfer and hydride abstraction, negative chemical ionization (NCI) by means of proton abstraction and electron capture (EC), and charge exchange (CE).

This introductory chapter provides a historical perspective on the QITMS, other instrumentation that is employed to examine ion-molecule reactions, and the ionization techniques that are used in this work, as well as an overview of the thesis organization.

Historical Perspective

In the late 1950s, the first discussion of ion storage and mass analysis with a quadrupole ion trap were reported [1-3]. J.F.J. Todd and coworkers coined the term "QUISTOR" referring to the quadrupole ion store (trap) [4]. The most common methods of scanning the quadrupole ion trap have been the resonance absorption and mass-selective stability modes. Resonance absorption detection involves the application of an AC voltage between the end cap electrodes to induce any ions that have an m/z such that their fundamental frequency of motion in the axial direction is the same as the perturbing field frequency to resonate; ions are ejected onto the end cap electrodes and the resulting current is detected [1]. The ions are detected within the ion trap in the resonance absorption technique, while with mass-selective stability ions are ejected out of the ion trap to a detector. The detection of ions by ejecting them from the ion trap was demonstrated in the late 1960s [5]. The mass-selective stability mode involves trapping ions (with RF and DC voltages) of only one value of m/z at a time and pulse-ejecting the ions from the ion trap (with DC voltages) to a detector [2,3].

Many groups have evaluated the quadrupole ion trap. Some of the studies that have been performed include evaluation of ion injection [6,7], ion-molecule reactions [8,9], mass-selected ejection [10], simultaneous positive and negative ion detection [11], various materials for construction of the ion trap (e.g., stainless steel mesh and solid stainless steel), and various applications of DC and RF voltages for the development of new operation modes [5,12,13].

The recent resurgence of interest in quadrupole ion trap mass spectrometry (QITMS) can be partially attributed to the introduction of the commercially available ion trap mass spectrometer (Finnigan MAT) ITMS and ion trap detector (ITD). Finnigan MAT has been actively involved in numerous areas of research with the QITMS including the following: operation modes (mass-selective instability) [14], mass-selective storage [15,16], and axial modulation [15]), MS^n (i.e., MS/MS/MS... etc.) [17], automatic gain control EI [18], and EI and CI MS/MS [16,17]. In this thesis, the mass-selective instability (only RF voltages) and the mass-selective storage (RF and DC voltages) modes will be referred to as non-mass-selected and mass-selected modes, respectively.

The QITMS consists of a hyperbolic ring electrode (solid stainless steel) and two hyperbolic end cap electrodes (solid stainless steel) shown in Figure 1.1 [19]. Application of an RF voltage to the ring electrode relative to the end cap electrodes creates a symmetrical three-dimensional quadrupole electric field within the electrode surfaces. When ions are created within or injected into this quadrupole field, they are either trapped or ejected depending upon the specific m/z of the ion and the applied field parameters (the magnitude and frequency of the RF voltage). The QITMS is normally operated in the non-mass-selected mode; the applied ring-RF voltage determines the low m/z cut-off, below which ions no longer have stable trajectories and are ejected from the trap [14]. A mass spectrum of the trapped ions is obtained by ramping the RF voltage so that ions of increasing m/z are sequentially ejected from the ion trap to a detector. Tandem mass spectrometry (MS/MS) is achieved on the QITMS by applying a supplemental RF voltage across the end caps with a frequency

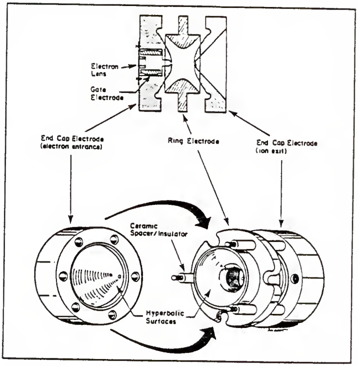

Figure 1.1. Schematic drawing of a quadrupole ion trap illustrating the quadrupole shape of the electrode surfaces [19].

which matches the secular frequency of the parent ion of interest [14]. This supplemental RF voltage is used in this work to develop a new scan mode referred to as mass-selected ejection. This scan mode will be discussed in greater detail in Chapter 3.

Ionization Techniques

The QITMS has the capability of performing electron ionization (EI), chemical ionization (CI), and charge exchange (CE) ionization through control of the magnitude of the ring-RF voltage and supplemental RF voltage and the length of time for which each parameter is applied. Indeed, it is possible to mass-select reactant ions for CI or CE in order to control the energetics of the sample ionization process. As the processes of ionization, mass-selection of reactant ion, ion-molecule reactions, and mass analysis are all performed in the same physical space but sequentially in time, the QITMS is a "tandem-in-time" mass spectrometer. This is in contrast to conventional "tandem-in-space" mass spectrometers where these processes occur sequentially in separate regions of the instrument.

In order to appreciate the significance of the various operation modes, it is necessary to briefly discuss the theory governing ion motion in quadrupole ion traps. The motion of ions in a quadrupole ion trap mass spectrometer can be described by the Mathieu equation [20]:

$$\frac{d^2u}{d\xi^2} + (a_u - 2aq_u \cos 2\xi)u = 0 \qquad (1.1)$$

with 'a' and 'q' defined as follows:

$$a_z = -2a_r = \frac{-8eU}{mr_o^2\omega^2} = \frac{-4eU}{mz_o^2\omega^2} \tag{1.2}$$

$$q_z = -2q_r = \frac{-4eV}{mr_o^2\omega^2} = \frac{-2eV}{mz_o^2\omega^2} \tag{1.3}$$

where u represents either x or y, ξ is the phase of RF voltage, e is the charge on an electron, U is the applied DC voltage, V is the zero-to-peak RF voltage, m is the m/z of a given ion, ω is the angular frequency of the applied field, and r_o and z_o are the radii in the r and z direction, respectively. Since e,ω, r_o and z_o are constant for a particular analysis, it is helpful to consider the Mathieu parameter 'a' simply as the DC voltage applied to ion trap ring electrode, divided by the m/z of a given ion, multiplied by a constant. Similarly, the Mathieu parameter 'q' can be considered simply as the RF voltage applied to the ring electrode divided by the m/z of a given ion, multiplied by a constant. Using this simplification, it becomes evident that for a given DC potential, each m/z has a unique value of 'a'. Similarly for a given RF potential, each m/z has a unique value of 'q'.

The theoretical stability of a given ion is dependent upon whether the substitution of its 'a' and 'q' values into the Mathieu equation of motion yields a stable periodic trajectory. A plot of the regions of stability in 'a' and 'q' space providing theoretical stable trajectories, called a stability envelope [13] of the Mathieu type, is shown in Figure 1.2. The ions with values of 'a' and 'q' which lie within the stability

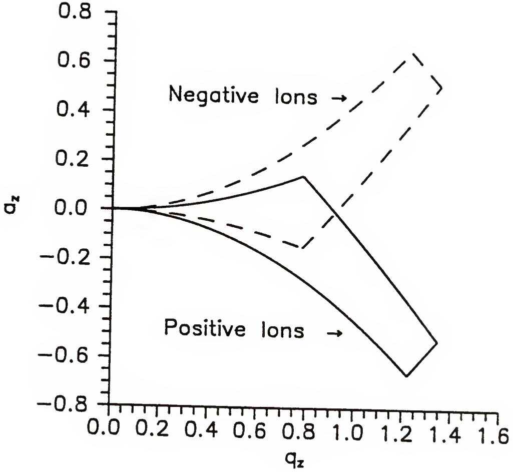

Figure 1.2. Mathieu stability envelope for both positive and negative ions in a quadrupole ion trap.

envelope will have stable trajectories. Conversely, all ions with values of 'a' and 'q' which lie outside the stability envelope will have unstable trajectories and will not be stored in the ion trap. The solid and dashed lines in Figure 1.2 represent the stability envelopes for positive and negative ions, respectively. It is readily apparent from examination of the stability envelopes that by operation of the ion trap with appropriate values of 'a' and 'q', ions of a single polarity (negative or positive) can be stored in the ion trap. This concept is further discussed in Chapter 3.

Ion-molecule reactions may be examined with a variety of mass spectrometers, including quadrupole ion trap (QITMS), Fourier transform (FTMS), sector, and triple quadrupole (TQMS) mass spectrometers. These mass spectrometers may be divided into two classes: trapping devices (QITMS and FTMS), and conventional devices (sector and TQMS). This thesis will not cover the basic operation and experimental parameters in detail for each type of instrument, but rather will briefly compare trapping and conventional instruments. Excellent articles including applications and operation parameters can be found in the literature for each instrument: QITMS [5,19,21,22], FTMS [23-26], sector [27-28], and triple quadrupole [28-31].

The mass spectrometers that trap ions have similar operating conditions including the following: reactant gas pressure, sample pressure, ionization time, and reaction time (Table 1.1) [23-26]. The major differences in the QITMS and FTMS are their respective methods of detection. In the quadrupole ion trap, ions are normally ejected prior to detection (5), although ions have been detected within the ion trap

Table 1.1. Operating Parameters of FTMS, QITMS, TQMS, and Sector Mass Spectrometers

Instrument	Ionization	Pressure	Ion Residence Time	Ionization/ Mass Analysis Configuration	Detection
FTMS	Pulsed	0.1 - 10 μtorr (Reactant gas)	milliseconds-seconds	Separated in time	Separated in time
QITMS	Pulsed	1 mtorr He (Buffer gas) 10 μtorr (Reactant gas)	milliseconds	Separated in time	Separated in space
TQMS & Sector	Continuous	1 torr (source) (Reactant gas)	microseconds	Separated in space	Separated in space

with FT methods (32). In FTMS, ion detection involves the measuring of the image current created within the ion cyclotron cell. Once again, conventional mass spectrometers have very similar operating conditions including the following: reactant gas pressure, sample pressure, ionization time, reaction time, and detection (Table 1.1). The conventional instruments operate with much higher reactant gas pressures (~ 1 torr) for CE and CI as compared to the trapping devices (~ 10^{-5} - 10^{-7} torr) and much shorter ion residence times (μs) as compared to the trapping devices (ms to s) (Table 1.1) [27-31]. These respective conditions on both instruments allow for efficient CI or CE ionization to occur.

The selection of an ionization technique in mass spectrometry is of utmost importance, since the ionization process ultimately determines the characteristics of the resultant mass spectra. Currently several ionization modes exist that are amenable to ionization of gas-phase samples in mass spectrometry, including electron ionization (EI), positive ion chemical ionization (PCI) via proton transfer or hydride abstraction, negative ion CI (NCI) via proton abstraction or electron capture (EC), and charge exchange (CE). Each ionization technique has its inherent advantages and disadvantages. By the selection of gaseous reactant ions, the energetics of the gas-phase ion-molecule reactions and the resultant degree of fragmentation that appears in a given spectrum can be controlled.

Electron ionization is the most commonly used ionization technique for the production of positive ions in mass spectrometry [33,34]. Traditionally, EI spectra are used for the positive identification of a compound due to the extensive fragmentation of the odd-electron molecular ion $[M]^{+\cdot}$. As a result, EI spectra provide primarily structural information, as well as molecular weight information provided some $[M]^{+\cdot}$ remains. Some work has been done with negative electron ionization, but due to production of structurally insignificant ions ($[CN]^-$, $[Cl]^-$, and $[F]^-$) and its very low sensitivity, negative electron ionization is not commonly used [35].

Besides EI, PCI is one of the most widespread ionization techniques used in modern mass spectrometry. The mass spectra produced by PCI are generally characterized by abundant pseudo-molecular, even-electron ions (either $[M+H]^+$ or $[M-H]^+$) with less fragmentation occurring than with EI. Some other common ions seen in PCI include adduct ions with the reactant gas ions and pseudo-molecular ions. Due to the small degree of fragmentation that occurs in PCI, it is traditionally the ionization method of choice when performing trace analysis or for the determination of molecular weights [35]. An ionization mode that is seldom used analytically is positive CE. This may be due to the fact that CE ionization is an odd-electron process; hence, the ionization and fragmentation that results are similar to those more easily provided by EI [36,37].

Negative chemical ionization (NCI) has not been studied as extensively as PCI [38]. There are two primary processes that may form negative ions, either ion-molecule or electron molecule interactions [39]. In this thesis, the term NCI will refer to ion-molecule reactions, while the term electron capture will refer to electron-molecule interactions. Electron capture ionization is an ionization process which normally requires electrons of near-thermal energy. The three basic reactions that occur upon interaction of an electron with a neutral molecule are [40]:

Electron capture: $AB + e^- \rightarrow AB^-$ (1.4)

Dissociative electron capture: $AB + e^- \rightarrow A^- + B^\cdot$ (1.5)

Ion pair production: $AB + e^- \rightarrow A^- + B^+ + e^-$ (1.6)

These processes will be discussed in greater detail in Chapter 3. Negative-ion-molecule reactions may occur by a number of different processes including: proton transfer, charge exchange, nucleophilic addition, and nucleophilic displacement, producing primarily $[M-H]^-$, $[M]^-$, $[M+X]^-$, and $[M-X]^-$ ions, respectively [41]. NCI via proton transfer reactions will also be further discussed in Chapter 3. The resonance electron capture rate constants are considerably higher than rate constants for ion-molecule reactions (either positive or negative), due to the high mobility of the electron [42]. As a result of these higher rate constants, resonance capture (electron-molecule interaction) can have a much higher sensitivity than normal CI and CE (ion-molecule interactions); this is the primary motivation for derivatization with electron-capturing groups for EC studies [43].

One advantage of CI or CE (in which ion-molecule reactions lead to sample ion formation) is the ability to control the amount of energy deposited into the ion (and thereby the degree of fragmentation) by selection of the reactant gas. The selection of reactant gas and its pressure in the ion source determines the ions which will serve as reactant ions in the ion-molecule reactions to form sample ions. The degree of fragmentation of the sample ions observed with CI or CE will be determined by the various reactant gas ions that interact with the sample molecules. Another advantage of CI and CE is the ability to perform selective ionization. This selectivity can be used to ionize certain components of a mixture, while not ionizing other mixture components. For example, it has been shown that the $[C_6H_6]^{+\cdot}$ ion generated from benzene ionize only the unsaturated fatty acids in a mixture of saturated and unsaturated fatty acids [44].

Traditionally, CI or CE is carried out in a high-pressure ionization source with approximately 1 torr of reactant gas. The reactant gas is normally introduced into the ion source in 1000-fold or greater excess of the sample [45]. The gaseous mixture is ionized by EI with high-energy (70 - 100 eV) electrons. This results in both the reactant gas and the sample being ionized. Since the reactant gas is in great excess of the sample, it will have a greater probability of ionization. The reactant gas ions are able to interact with neutral reactant gas molecules to form other reactant gas ions, as well as with sample molecules which may result in CI or CE ionization. The mass spectra obtained with such an ion source configuration will include sample ions produced by EI, as well as by CI and/or CE with the variety of reactant ions present. Thus, one problem associated with CI or CE with traditional high-pressure ion sources is that selection of a single reactant ion is not possible. For example, with methane as a reactant gas, a number of reactant ions are produced which can react with the sample [46]. Some of the reactions to form various reactant ions observed with methane are shown in the following equations:

$$CH_4 + e^- \rightarrow CH_4^{+\cdot} + 2e^- \quad (1.7)$$
$$CH_4^{+\cdot} \rightarrow CH_2^{+\cdot} + H_2 \quad (1.8)$$
$$CH_4^{+\cdot} \rightarrow CH_3^{+} + H^{\cdot} \quad (1.9)$$
$$CH_4^{+\cdot} + CH_4 \rightarrow CH_5^{+} + CH_3^{\cdot} \quad (1.10)$$
$$CH_3^{+} + CH_4 \rightarrow C_2H_5^{+} + H_2 \quad (1.11)$$
$$CH_2^{+\cdot} + CH_4 \rightarrow C_2H_3^{+} + H_2 + H^{\cdot} \quad (1.12)$$
$$C_2H_3^{+} + CH_4 \rightarrow C_3H_5^{+} + H_2 \quad (1.13).$$

Under typical CI conditions, the major ions that result are $[CH_5]^+$, $[C_2H_5]^+$, and $[C_3H_5]^+$. The resultant mass spectra can contain sample ions produced by a combination of initial EI, proton transfer from $[CH_5]^+$, $[C_2H_5]^+$, and $[C_3H_5]^+$ (with a range of internal energies and degrees of fragmentation), hydride abstraction with $[C_3H_5]^+$, and CE with $[CH_4]^{+\cdot}$. Each of these competing reactions can cause different degrees of fragmentation which may lead to ambiguity and confusion in spectral interpretation.

The above-mentioned difficulties associated with CI and CE ionization can be eliminated by taking advantage of the inherent capabilities of tandem mass spectrometry (MS/MS). The ability to mass-select a single reactant ion produced from a reactant gas (or even a mixture of reactant gases) and to allow only this ion to interact with a sample molecule in a subsequent step provides a high level of control over sample ionization by CI and CE. Most MS/MS studies involve mass-selection of a sample ion which is reacted then with a collision gas atom or molecule, either by collisionally-activated dissociation [47], or less frequently by reactive collisions [48]. In this paper, we report the advantages of first mass-selecting a reactant ion, which then is used to ionize sample molecules. Although similar mass-selective CI or CE processes have been previously reported [49,50], these studies generally have been designed to investigate the underlying CI or CE reactions rather than to provide a new analytical capability on widely available mass spectrometers. A number of papers have been published on charge stripping via mass-selected ions [51,52]. Mass-selective CE reactions have been demonstrated with a double quadrupole instrument [53]. Proton-transfer CI reactions have been studied by trapping ions in the center quadrupole of a TQMS and pulsing the ions out with an ion lens [54]. Non-mass-selected CE and CI reactions in a quadrupole ion trap mass spectrometer (QITMS) have been demonstrated [10,21,22]. Recently, a number of papers in which mass-selected CE and CI reactions were demonstrated in a QITMS were presented at the 36th Annual Conference on Mass Spectrometry and Allied Topics of the American Society for Mass Spectrometry [55-57].

The QITMS and the TQMS are uniquely suited to perform mass-selected CI or CE reactions. In the TQMS, ionization, mass-selection of the reactant ion, CI or CE, and mass analysis occur in discrete regions of the instrument, and thus MS/MS is tandem-in-space [Figure 1.3 (a)]. This is in contrast to tandem mass spectrometry with the QITMS, where these processes occur sequentially in the same region in space, and thus, MS/MS is tandem-in-time [Figure 1.3 (b)].

Overview of Thesis Organization

This thesis addresses the development, characterization, and optimization of instrumental parameters for various ionization modes with the quadrupole ion trap mass spectrometer. The following chapters provide a detailed description of the scan functions used with each ionization mode and discussion of the results of our fundamental studies of chemical ionization and charge exchange ionization. Chapter 2 will describe the instrumentation that was used in these studies, which includes Finnigan MAT triple quadrupole and quadrupole ion trap mass spectrometers. In Chapter 3, the results of the evaluation of the operational modes, and the parameters affecting the operation modes (e.g., applied voltages and reaction times), for the QITMS and negative ionization studies are discussed. Non-mass-selected and mass-selected ion-molecule reactions

Figure 1.3. Schematic representation of mass-selected and non-mass-selected scan modes for (a) triple quadrupole mass spectrometer (TQMS) and (b) quadrupole ion trap mass spectrometer (QITMS).

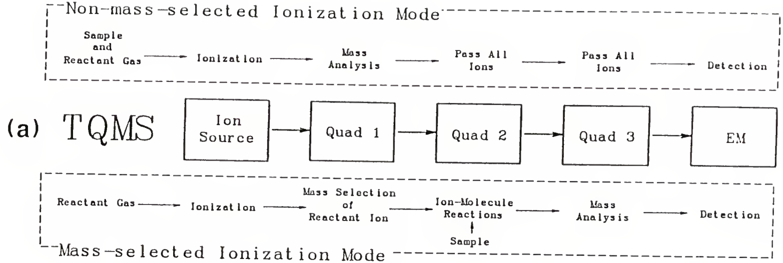
Non-mass-selected Ionization Mode
Sample and Reactant Gas
Ionization
Mass Analysis
Pass All Ions
Pass All Ions
Detection
(a) TQMS
Ion Source
Quad 1
Quad 2
Quad 3
EM
Reactant Gas
Ionization
Mass Selection of Reactant Ion
Ion-Molecule Reactions
Sample
Mass Analysis
Detection
Mass-selected Ionization Mode

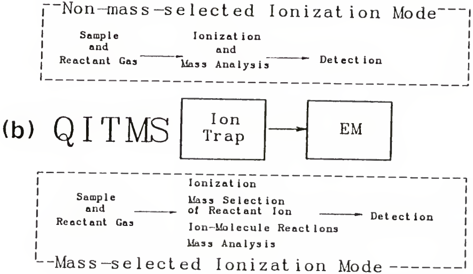
Non-mass-selected Ionization Mode
Sample and Reactant Gas
Ionization and Mass Analysis
Detection
(b) QITMS
Ion Trap
EM
Sample and Reactant Gas
Ionization
Mass Selection of Reactant Ion
Ion-Molecule Reactions
Mass Analysis
Detection
Mass-selected Ionization Mode

with the QITMS and TQMS are discussed and compared in Chapter 4. The last chapter of this thesis (Chapter 5) contains conclusions and suggestions for future ionization studies and applications for the QITMS.

CHAPTER 2
EXPERIMENTAL

Samples and Reagents

Nitrogen (zero grade), helium (zero grade), and argon (zero grade) reactant gases were obtained from Liquid Air Corporation. Ethylene (C.P.), methane (ultra-high purity), and sulfur hexafluoride (high purity) were obtained from Matheson. Carbon dioxide (zero grade) and nitrous oxide (U.S.P) were obtained from Jacksonville Welding Supply Incorporated and Ohio Medical Products, respectively. Phenylacetonitrile (high purity), o-cresol (practical grade), methyl benzoate (high purity), ethyl benzoate (high purity), aniline (high purity), and nitrobenzene (high purity) benzamide (high purity) were obtained from Chem Service. Glycine (ammonia-free crystalline), benzoic acid (Certified ACS grade), and n-butylbenzene (98% pure) were obtained from Sigma Chemical, Fisher Scientific, and Eastman Kodak, respectively. The structures of the sample molecules are shown in Figure 2.1.

Mass Spectrometers

Quadrupole Ion Trap

The quadrupole ion trap mass spectrometer (QITMS) used in these studies was a Finnigan MAT Ion Trap Mass Spectrometer (ITMS), which was operated at 100 C. The buffer gas, He, was introduced directly into the ion trap

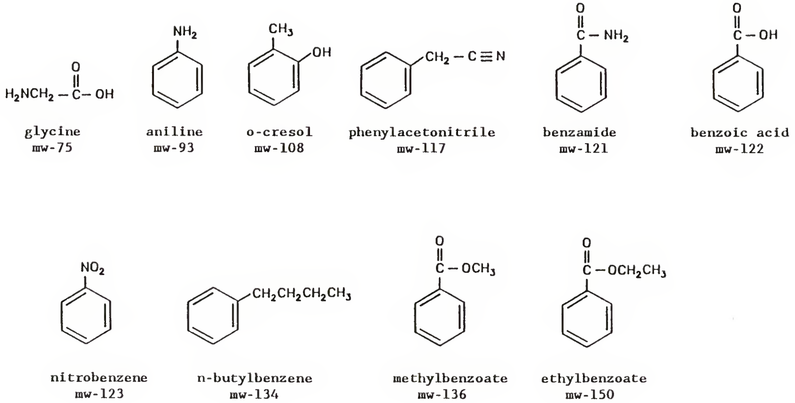

Figure 2.1. Structures and molecular weights of sample molecules.

via a variable leak valve (Granville-Phillips). The reactant gases (N_2, Ar, CO_2, N_2O, CH_4, C_2H_4, and SF_6) were introduced into the vacuum chamber of the QITMS through the normal reactant gas lines via a needle valve (Negretti Valve Division), while H_2O reactant gas was introduced via a variable leak valve (Granville-Phillips) at indicated pressures between 1.0×10^{-5} and 2.0×10^{-5} torr. All liquid samples were introduced into the vacuum chamber, near the ion trap, through a variable leak valve (Granville-Phillips) (mounted on a 1/2 inch o.d. probe inserted through the solids probe inlet assembly) to yield indicated pressures of 2.0×10^{-6} torr. All solid samples were introduced into the vacuum chamber, near the ion trap by means of a standard solids probe inserted through a solids probe inlet assembly. These pressures were measured with a Bayard-Alpert ionization gauge (Granville-Phillips) mounted on the vacuum chamber. Since sample and reactant gases were introduced into the vacuum chamber, these readings should be reasonable estimates of the pressure inside the ion trap itself. The standard dynode and channeltron electron multiplier assembly was modified in order to permit detection of negative ions. This modification involved the removal of the resistor between the dynode and the multiplier; the dynode was then connected to a separate external high-voltage power supply (Bertan), while the electron multiplier voltage was still under computer control of the QITMS. Typical dynode voltages were + 3 kV for negative ion detection and - 3 kV for positive ion detection. Electron multiplier voltages were typically - 2.2 kV for negative ion detection and -1.6 kV for positive ion detection.

The scan modes used for ionization in the QITMS are shown in Figures 2.2-2.5. The QITMS non-mass-selected EI scan function consists of three

Figure 2.2. QITMS scan function for non-mass-selected EI.

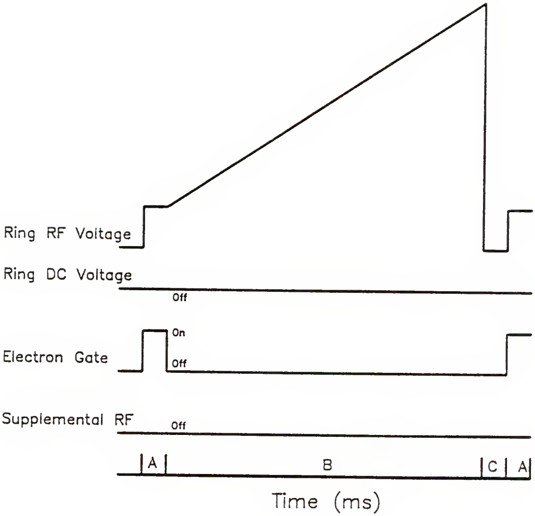

A — Ionization

B — Analytical scan

C — Drop RF to sweep ions out of ion trap

Figure 2.3. QITMS scan function for non-mass-selected CE or CI.

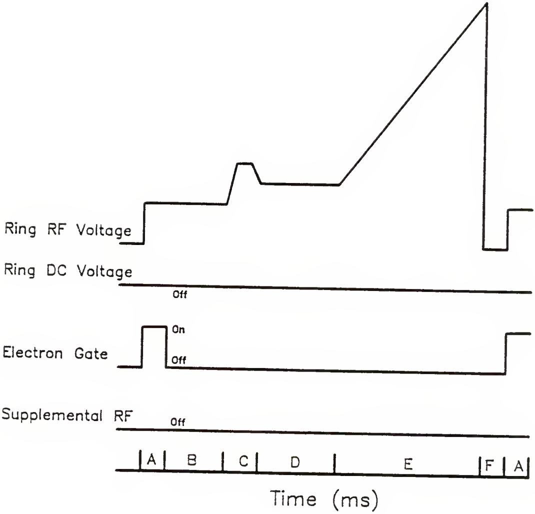

A – Ionization

B – Formation of reactant ions (CI)

C – Isolation of reactant ions with low mass cut–off

D – Formation of sample ions

E – Analytical scan

F – Drop RF to sweep ions out of ion trap

Figure 2.4. QITMS scan function for mass-selected ejection CE or CI.

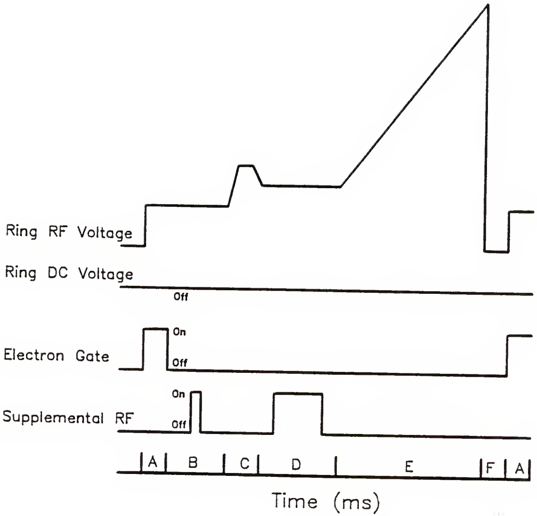

A — Ionization

B — Formation of reactant ions (CI) and ejection of unwanted reactant ions with supplemental RF

C — Isolation of reactant ions with low mass cut-off

D — Formation of sample ions and ejection of unwanted reactant ions with supplemental RF

E — Analytical scan

F — Drop RF to sweep ions out of ion trap

Figure 2.5. QITMS scan function for mass-selected CE or CI.

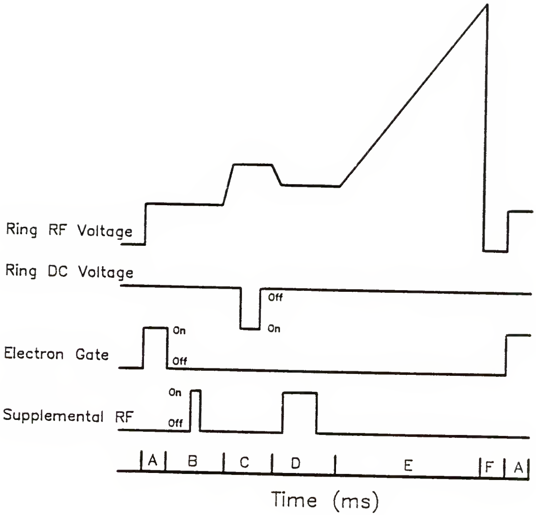

A — Ionization

B — Formation of reactant ions (CI) and ejection of unwanted reactant ions with supplemental RF

C — Isolation of reactant ions with DC

D — Formation of sample ions and ejection of unwanted reactant ions with supplemental RF

E — Analytical scan

F — Drop RF to sweep ions out of ion trap basic time periods (Figure 2.2). In period A, electrons are introduced into the ion trap, resulting in electron ionization of both the sample and reactant gas. The RF level during this period is set so that ions above m/z 10 have stable trajectories and are stored. The average energy of electrons at this RF level is approximately 30 eV [58]. Ionization times were varied between 0.1 and 2.0 ms depending upon the sensitivity required. During period B, ions are sequentially ejected from the ion trap (and detected) by ramping the ring electrode RF voltage from the low to high mass of interest at a rate of 5.5 amu/ms. Finally, the RF voltage is lowered to a very low level during period C, which effectively ejects all remaining ions from the QITMS. The entire scan function is repeated several times during typical acquisition of data. The results of several of these scans are averaged and stored by the data system as one analytical scan.

The non-mass-selected CE or CI scan function (Figure 2.3) is very similar to the non-mass-selected EI scan function, and consists of six basic time periods. In period A, electrons are introduced into the ion trap, resulting in electron ionization of both the sample and reactant gas. The RF level during this period is set so that ions above m/z 10 have stable trajectories and are stored, providing efficient storage of reactant ions. Ionization times were varied between 0.1 and 4.0 ms depending upon the sensitivity required. The reactant ions initially formed during ionization are allowed to interact with the reactant gas for a period of 10 - 50 ms (period B). Note that period B is omitted for the CE scan, since the reactant ions for CE ionization are formed directly by EI during period A. Then the RF voltage is increased linearly to a value corresponding to a m/z that is slightly lower than the reactant ion of interest (period C). For example, when $[N_2]^{+\cdot}$ is used as a reactant ion, the RF voltage is increased to a value corresponding to m/z 25. Prior to period D, the RF voltage is lowered to a value corresponding to m/z 10. During period D, the reactant ions are allowed to interact with the sample molecules for 10 - 100 ms. It should be noted that ion-molecule reactions involving sample molecules and sample ions are also occurring during the previous three periods. During period E, ions are sequentially ejected from the ion trap (and detected) by ramping the ring electrode RF voltage from the low to high mass of interest at a rate of 5.5 amu/ms. Finally, the RF voltage is lowered to a very low level during period F, which effectively ejects all remaining ions from the QITMS. Similar to non-mass-selected EI, the entire scan function is repeated several times during typical acquisition of data.

In addition to the low m/z cut-off imposed by the amplitude of the RF ring voltage, there are two other approaches to controlling which masses are stored in the ion trap. One approach involves the application of a supplemental RF voltage applied across the end cap electrodes with the resonant frequency of a particular m/z ion. This approach is referred to as mass-selected ejection CE or CI and the scan function is shown in Figure 2.4. Provided the magnitude of this supplemental RF voltage is large enough, an ion of interest can be ejected from the ion trap. This technique can be used to eject an undesired ion (reactant or product) from the ion trap and thereby prevent it from increasing in intensity during a reaction time (Period B or D). Similarly, it has been shown that the application of a supplemental RF voltage "tickle voltage" applied across the end cap electrodes with the resonant frequency of a single m/z ion can be used to promote collisionally-activated dissociation (CAD) [16].

Another approach (referred to as mass-selected CE or CI) employs a DC voltage applied to the ring electrode in conjunction with the RF voltage. This allows a narrow mass range of m/z's (typically one amu wide) to have stable trajectories within the ion trap [16]. This mode of operation is analogous to a quadrupole mass filter [20]. The mass-selected CE or CI scan function (Figure 2.5) which employs this RF/DC mode is similar to the non-mass-selected CE or CI scan function. The primary difference is that after reaction period B for CI, or after the ionization period A for CE, a DC voltage pulse (negative to mass-select positive ions) is applied to the ring electrode. Thus, the products of any ion-molecule reactions which occurred during the previous periods, but are not in the m/z range of interest, can be ejected from the ion trap. The remaining periods of the two scan functions are identical. The ability to mass-select ions of a single m/z enables specific ion-molecule reactions to be monitored.

Triple Quadrupole

The triple quadrupole mass spectrometer (TQMS) used in these studies was a Finnigan MAT TSQ70 (Figure 2.6) equipped with a dual EI/CI source. All reactant gases were introduced into the TQMS through the CI gas line to yield indicated ion source pressures of 0.2 to 0.8 torr. For reactions performed in the ion source [Figure 1.3 (a)], a sample was leaked into the ion source to yield an indicated analyzer pressure of 1.0×10^{-6} torr, using a variable leak valve (Granville-Phillips) mounted on a 1/2 inch o.d. stainless steel probe that could be inserted into the ion source

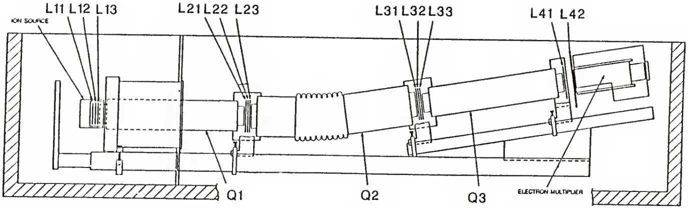

Figure 2.6. Schematic diagram of the Finnigan MAT TSQ70, showing the ion source, electrostatic lenses (L11-L42), quadrupoles (Q1-Q3), and electron multiplier.

through the direct probe inlet assembly. The ion source temperature was 150 C and the electron energy was 70 eV. For reactions in the second quadrupole collision cell (Q2) [Figure 1.3 (a)], the reactant gases were introduced into the ion source as before (same pressures) and the samples were leaked into Q2 (indicated sample pressures ~ 2.0 x 10^{-6} torr). The collision cell was maintained at 100 C to minimize sample memory effects. For mass-selected ion-molecule reactions, the reactant ion was mass-selected with the first quadrupole (Q1) and allowed to react with the neutral sample gas in Q2. The third quadrupole (Q3) was scanned to mass-analyze the products of the Q2 ion-molecule reactions.

Samples were introduced into the ion source or into Q2 via variable leak valves (Granville-Phillips). Samples were admitted into Q2 through the line normally used for collision gas introduction. Reactant gas pressures were monitored in the ion source with a capacitance manometer (MKS Instruments) with a resolution of 0.1 mtorr. Sample pressures in Q2 were too low to be measured by the Convectron thermocouple gauge (Granville-Phillips) normally used for collision gas pressure measurement; therefore reproducible sample pressures were obtained by adjusting the sample pressure to give the same analyzer pressure reading on the Bayard-Alpert ionization gauge mounted on the vacuum manifold outside Q2.

The TQMS was tuned with perfluorotributylamine (PFTBA or FC43) and no additional tuning was needed for the acquisition of spectra that were the result of CE or CI in the ion source. However, the use of mass-selective reactions in Q2 did require some additional optimization of the ion optical parameters. The instrument was optimized by introducing argon in the ion source and n-butylbenzene into Q2. The first quadrupole (Q1) was set to pass $[\mathrm{Ar}]^{+\cdot}$ (m/z 40) and the resulting charge exchange products of $[\mathrm{Ar}]^{+\cdot}$ with n-butylbenzene were mass-analyzed with Q3. The ion optics were then optimized for maximum transmission of the CE product ions.

CHAPTER 3
POSITIVE AND NEGATIVE IONIZATION IN QUADRUPOLE ION TRAP MASS SPECTROMETRY: EFFECTS OF APPLIED VOLTAGES AND REACTION TIMES

This chapter deals with the characterization and optimization of reaction times and applied voltages with the QITMS. Some of the time intervals that will be addressed are ionization time, reactant ion formation time, and sample ion formation time. This chapter also addresses the application of various voltages to the ion trap in order to implement the various modes of operation for the QITMS. Three modes of operation will be discussed: RF-only mode (non-mass-selected reactions), RF voltage and supplemental RF voltage (mass-selected ejection of unwanted reactant ions), and RF and DC voltage plus supplemental RF voltage (mass-selected reactions). The basic forms of the scan functions for the various modes of operation are shown in Figures 2.3, 2.4, and 2.5, respectively. The experimental results with positive and negative ionization methods will be discussed. Additionally, the preliminary results from negative ionization are discussed in the last portion of Chapter 3, while the results for positive ionization techniques are discussed in more detail in Chapter 4. The ionization techniques that will be addressed are electron ionization (EI), positive ion chemical ionization (PCI) (via proton transfer, hydride abstraction, and adduct formation), negative ion chemical ionization (NCI) [via proton abstraction and electron capture (EC)], and charge exchange (CE) ionization.

In order to appreciate the significance of the various operational modes, it is necessary to briefly discuss the stability diagram for quadrupole ion traps (Figure 3.1). Motion of ions in a quadrupole ion trap can be described by the Mathieu equation. A more detailed discussion of the Mathieu equations may be found in Chapter 1. One may consider the Mathieu parameter 'a_z' as the DC voltage (U) applied to the quadrupole ion trap ring electrode, divided by m/z (m) of a given ion, multiplied by some constant (C). Similarly, the Mathieu parameter 'q_z' can be considered simply as the RF voltage (V) applied to quadrupole ion trap ring electrode divided by the m/z (m) of a given ion, multiplied by some constant (K):

$$a_z = C(U/m) \quad \text{and} \quad q_z = K(V/m) \qquad (3.1,3.2).$$

Using this simplification, it becomes evident that for a given DC potential, each m/z has a unique value of 'a_z' assigned to it. Similarly for a given RF potential, each m/z has a unique value of 'q_z' assigned to it.

In the normal mode of operation (mass-selected instability or non-mass-selected storage), the quadrupole ion trap mass spectrometer (QITMS) is operated with only a radio frequency (RF) voltage applied to the ring electrode [14]. The magnitude and frequency of the applied RF voltage determines the mass range of ions that will have stable ion trajectories. Since this is an RF-only mode ($U = 0$ and hence 'a_z' = 0) only those ions which have a value of 'q_z' between 0 and 0.908 have stable trajectories and are trapped. The stability envelopes in Figure 3.1 show the envelopes for the ions which have stable trajectories defined by 'a_z' and 'q_z'. All ions whose 'a_z' and 'q_z' values fall within the solid line (positive ions)

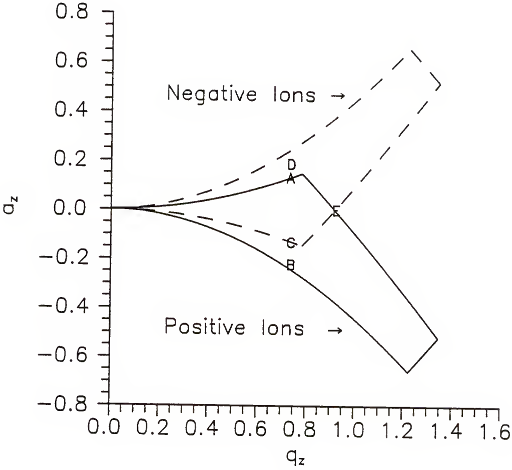

Figure 3.1. Mathieu stability envelopes for positive (solid line) and negative (dashed line) ions. Points 'A', 'B', 'C', 'D', and 'E' have corresponding 'a_z' values of 0.134, - 0.223, - 0.133, 0.176, and 0.00, and 'q_z' values of 0.738, 0.738, 0.738, 0.738, and 0.908. Ions with 'a_z' and 'q_z' values that fall inside the stability envelopes will have stable trajectories and be stored within the ion trap; those with 'a_z' and 'q_z' values that lie outside of the stability envelopes will have unstable trajectories and will be ejected from the ion trap.

or dashed line (negative ions) have stable ion trajectories and will be stored in the ion trap. All ions whose 'a_z' and 'q_z' values lie outside the stability envelopes (solid and dashed lines) will have unstable ion trajectories and will not be stored in the ion trap. Since 'q_z' is inversely proportional to m/z, the m/z corresponding to a 'q_z' of 0.908 (point 'E') is the lowest m/z stable at that RF voltage; theoretically all ions with a m/z larger than that corresponding to 'q_z' = 0.908 will be trapped.

The mass-selected ejection mode is analogous to the non-mass-selected mode in respect to only an RF voltage being applied to the ring electrode. In addition to the RF voltage applied to the ring electrode; however, a supplemental RF voltage is applied across the end cap electrodes at the resonant frequency of a particular m/z ratio. This supplemental RF voltage will prevent an ion of that m/z from being stored in the ion trap provided the magnitude and application time of the voltage are sufficient to increase the ion trajectory until it exceeds the ion trap dimensions. The supplemental RF-voltage (tickle voltage) is the same voltage that is applied for CAD/MS/MS experiments [16].

The application of a direct current (DC) voltage in addition to the RF voltage to the ring electrode results in a mode of operation referred to as the mass-selective storage mode [8]. This mode of operation has recently been introduced on the commercial QITMS [55-57]. The mass-selected mode ionization employs a DC voltage applied to the ring electrode in conjunction with the RF voltage. This allows a narrow mass range of m/z 's (typically one amu wide) to have stable trajectories within the ion trap [15]. The application of a negative DC voltage results in moving up the y-axis (a_z) (point A); while the application of a positive DC voltage results in moving down the y-axis (a_z) (point B) (Figure 3.1). Hence, if the appropriate DC voltages are applied to the ring electrode, a particular mass range (as small as one amu wide) can be stored. This is the familiar operational mode of the quadrupole mass filter [20]. The theoretical apex of the stability diagram corresponds to point E with values of 'a_z' and 'q_z' corresponding to 0.15 and 0.79, respectively [15]. Experimentally, the apex was found to correspond to a 'q_z' value of 0.813 and an 'a_z' value of ~ 0.134. In addition, the polarity of ions can be selected by operation of the ion trap beyond the apex (points B and D) of the stability diagram (i.e., for isolation of ions with a negative charge, operation of the ion trap with values of 'a_z' larger than +0.15 will insure that all positive ions are ejected from the ion trap).

The various ionization modes that were addressed above are significant in the operation of the QITMS and the commercially available ITD. The RF-only mode of operation is of importance since it is currently the only operational mode that is available on the ITD. The mass-selected-ejection and mass-selected ion-molecule reaction modes are significant since they both increase the selectivity of the ionization techniques. This chapter deals with the characterization and optimization of reaction times and applied voltages with the QITMS. The characterization and optimization of these parameters for positive and negative ions, respectively will be discussed. The main sections of positive and negative ions are each divided into the three subsections: non-mass-selected reactions, mass-selected-ejection, and mass-selected ion-molecule reactions. Under each subsection the various ionization techniques that are applicable will be discussed. Finally, the conclusions that can be drawn from this work are summarized.

Positive Electron, Chemical, and Charge Exchange Ionization

Non-mass-selected Reactions

Electron ionization. Electron ionization (EI) is the most commonly used ionization technique in mass spectrometry. For this work, EI was the first mode of operation characterized and optimized. The scan function for EI is shown in Figure 2.2. The parameters that affect the EI spectra are ionization time (period A) and the RF voltage during the ionization time. The ionization time is limited by the onset of space charge in the ion trap. Space charge effects are noted in the profile data in Figure 3.2 showing the fragment ions m/z 91^+ and 92^+ of n-butylbenzene. Space charge is a phenomenon that is characterized by shifting of mass assignments as well as severe loss of resolution. Space charge is an effect that is initiated by a large number of ions being confined in a specific region [59]. The ions will begin to interact with one another in terms of coulombic repulsion, and hence the trajectories of the ions will be altered. The onset of space charge is compound- and pressure-dependent; hence, an exhaustive study of space charge was not performed, but rather the characteristics of mass spectra that exhibit space charge were noted. If space charge is significant in the mass spectra [as in Figure 3.2 (c)], there are several options to reduce the degree of space

Figure 3.2. The EI non-mass-selected profile data of n-butylbenzene with ionization times of (a) 0.1 ms, (b) 0.5 ms, and (c) 1.0 ms. The m/z 91^+ and 92^+ ions are fragment ions of n-butylbenzene.

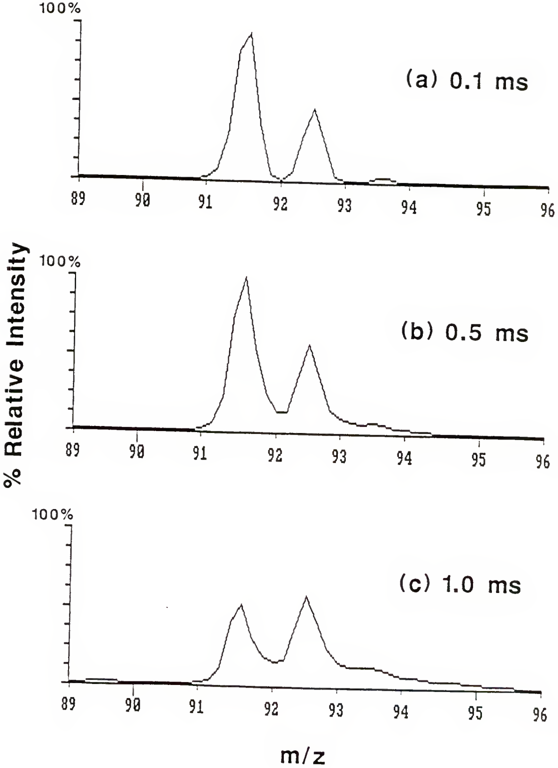
100%
(a) 0.1 ms
89
90
91
92
93
94
95
96
100%
(b) 0.5 ms
89
90
91
92
93
94
95
96
100%
(c) 1.0 ms
89
90
91
92
93
94
95
96
% Relative Intensity
m/z

charge, including: reduce sample size or pressure, reduce ionization time, increase RF level after ionization to eliminate low mass ions.

Chemical ionization. Chemical ionization (CI) is a product of ion-molecule reactions of reactant ions with sample molecules. The reactant ion population (percent relative abundance %RA of different reactant ions) varies as a function of reaction time and pressure of reactant gas. The nature of CI reactant ion production makes it the most complex ionization technique examined in this study. The scan function for non-mass-selected (NMS) CI is shown in Figure 2.3. The pressures of the reactant gases were held constant for the results reported in this work. The most important time parameter for the production of reactant ions is the post-ionization time (reaction time to form reactant ions [period B]).

Three different reactant gases (methane, water, and ammonia) were examined for the characterization and optimization of the reactant ion formation time (period B) for CI. The graphs in Figures 3.3-3.5 show the characterization of the reactant ion abundances with various formation times for the respective reactant gases. The graphs for water and ammonia as reactant gases follow the same general trend, characterized by intense EI-produced molecular ions at short reactant ion formation times, which rapidly undergo ion-molecule reactions with the reactant gas and are thus replaced by protonated molecular ions at long reaction times. The optimum reactant ion formation times correspond to the shortest time periods at which the maximum ion intensity is observed for the chosen reactant ions. Hence, the optimum reactant ion formation times with water and ammonia as reactant gases are 20 ms and 5 ms, respectively. It is interesting to note that ammonia did not ionize (by proton transfer) any of the compounds

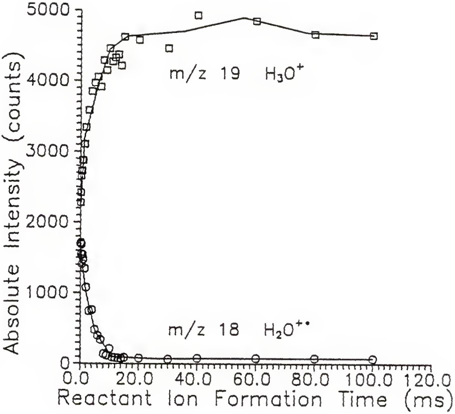

Figure 3.3. Characterization of reactant ion formation time (period B) with water as the reactant gas.

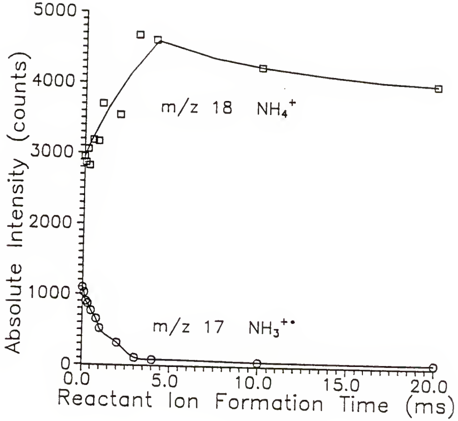

Figure 3.4. Characterization of reactant ion formation time (period B) with ammonia as the reactant gas.

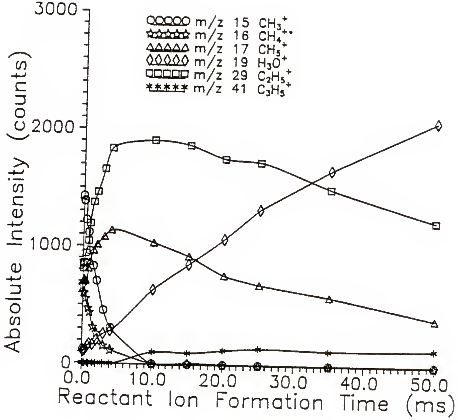

Figure 3.5. Characterization of reactant ion formation time (period B) with methane as the reactant gas.

examined (o-cresol, phenylacetonitrile, and n-butylbenzene). This was predicted based upon the PA's of the compounds and ammonia.

The graph for methane is more complex than those for water and ammonia due to competing reactions. Some of the reactions that occur for methane are the following [34,45]:

$$CH_4 + e^- \rightarrow CH_4^{+\cdot} + 2e^- \tag{3.3}$$

$$CH_4^{+\cdot} \rightarrow CH_2^{+\cdot} + H_2 \tag{3.4}$$

$$CH_4^{+\cdot} \rightarrow CH_3^+ + H^\cdot \tag{3.5}$$

$$CH_4^{+\cdot} + CH_4 \rightarrow CH_5^+ + CH_3^\cdot \tag{3.6}$$

$$CH_3^+ + CH_4 \rightarrow C_2H_5^+ + H_2 \tag{3.7}$$

$$CH_2^{+\cdot} + CH_4 \rightarrow C_2H_3^+ + H_2 + H^\cdot \tag{3.8}$$

$$C_2H_3^+ + CH_4 \rightarrow C_3H_5^+ + H_2 \tag{3.9}$$

The major reactant ions observed in the QITMS in this study were $[CH_4]^{+\cdot}$, $[CH_5]^+$, $[C_2H_5]^+$, and $[C_3H_5]^+$; additionally large quantities of $[H_3O]^+$ (due to protonation of residual H_2O) were also observed at long reaction times (Figure 3.5). Hence, the optimum reactant ion formation times for the formation of reactant ions from methane reactant gas were different for each reactant ion; e.g., for m/z 29 ($[C_2H_5]^+$) the optimum reactant ion formation time was 5 ms, while for m/z 19 ($[H_3O]^+$) the optimum reactant ion formation time was greater than 50 ms. The eventual dominance of the $[H_3O]^+$ is expected based upon the greater proton affinity of H_2O compared to CH_4 and C_2H_4.

The time period that was optimized next was the sample ion formation time (period C). The CH_4 NMS (without RF cut-off) spectrum of n-butylbenzene [Figure 3.6 (a)] can be compared to the CH_4 NMS (with RF

Figure 3.6. Methane CI mass spectra of n-butylbenzene (mw - 134) (a) CH_4 non-mass-selected without RF cut-off, (b) CH_4 non-mass-selected with RF cut-off (RF level ~ 28 amu), (c) ($[C_2H_5]^+$) mass-selected ejection (ejection of m/z 41), (d) $[C_2H_5]^+$ mass-selected. Mass scan range was from m/z 15 to 300.

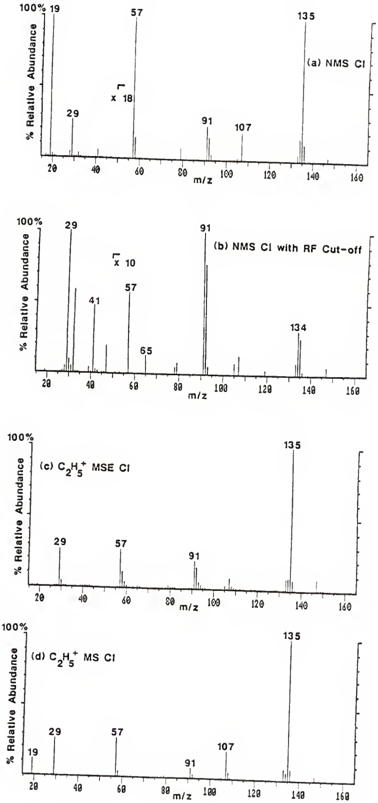
100%
19
57
135
% Relative Abundance
(a) NMS CI
x 18
29
91
107
20
40
60
80
m/z
100
120
140
160
100%
29
91
(b) NMS CI with RF Cut-off
x 10
57
41
134
65
% Relative Abundance
20
40
60
80
100
m/z
120
140
160
100%
135
(c) $C_2H_5^+$ MSE CI
% Relative Abundance
29
57
91
20
40
60
80
m/z
100
120
140
160
100%
135
(d) $C_2H_5^+$ MS CI
% Relative Abundance
29
57
19
107
91
20
40
60
80
m/z
100
120
140
160

cut-off ~ 28 amu) spectrum [Figure 3.6 (b)]. The ionization process illustrated in Figure 3.6 (b) should be better defined due to the ejection of all but the $[C_2H_5]^+$ and $[C_3H_5]^+$ reactant ions, but the spectra illustrate that both ionization processes suffer from interfering reactant ions (i.e., CH_4 NMS CI (without RF cut-off) has as reactant ions $[H_3O]^+$, $[C_2H_5]^+$, and $[C_3H_5]^+$, while with an RF cut-off of ~ 28 amu, the $[H_3O]^+$ reactant ion is ejected leaving $[C_2H_5]^+$, $[O_2]^{+\cdot}$, and $[C_3H_5]^+$). Clearly even with ejection of reactant ions below m/z 29, a variety of reactant ions are observed in the spectra which can cause mixed-mode ionization to occur. Particularly notable in Figure 3.6 (b) is the relatively large abundance of $[O_2]^{+\cdot}$ (m/z 32), which is responsible for the unexpectedly high abundance of $M^{+\cdot}$ (m/z 134) of n-butylbenzene (in addition to residual EI). It should be noted that sample ions formed by EI and CI in the previously mentioned time periods (periods A and B) may be present in these mass spectra.

The optimization of the sample ion formation time [excluding the time in previous periods (A and B)] was performed for each reactant gas with n-butylbenzene as the sample. The graph with methane as the reactant gas and n-butylbenzene as the sample without the use of the RF cut-off at m/z 28 is shown in Figure 3.7. The reactant and sample ions are shown in Figures 3.7 (a) and (b), respectively. These figures illustrate that with reaction times greater than 100 ms, the dominant ionization process will be protonation with the $[H_3O]^+$ ion formed from residual water. Residual EI ions present in the ion trap can not be eliminated by using this mode of ionization. The initial amount of the n-butylbenzene molecular ion (m/z 134) compared to the pseudo-molecular ion (m/z 135) is indicative of

Figure 3.7. Characterization of reaction period C (sample ion formation time) with methane as the reactant gas and n-butylbenzene (mw - 134) as the sample: (a) reactant ions, and (b) sample ions.

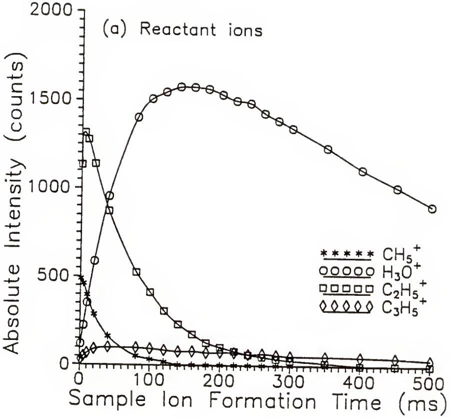
(a) Reactant ions
Absolute Intensity (counts)
2000
1500
1000
500
0
0
100
200
300
400
500
Sample Ion Formation Time (ms)
CH_5^+
H_3O^+
$C_2H_5^+$
$C_3H_5^+$

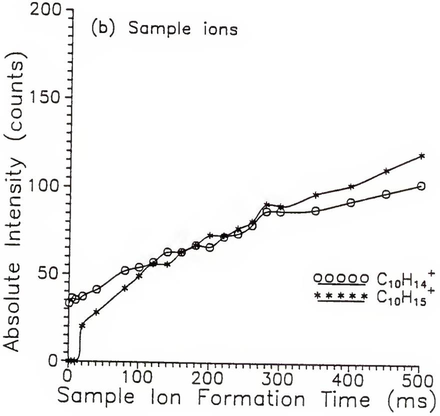
(b) Sample ions
Absolute Intensity (counts)
200
150
100
50
0
0
100
200
300
400
500
Sample Ion Formation Time (ms)
$C_{10}H_{14}^+$
$C_{10}H_{15}^+$

residual sample ions formed from EI. The increase in the molecular ion intensity with increasing reaction time must be due to ion-molecule reactions, presumably CE with $[O_2]^{+\cdot}$.

Charge exchange ionization. Charge exchange (CE) ionization is a product of ion-molecule reactions of reactant ions with sample molecules. The reactant ion population (relative abundance of different reactant ions) varies as a function of ionization time and pressure of reactant gas. The nature of CE process is similar to the CI process. The scan function for non-mass-selected (NMS) CE is shown in Figure 3.8. The most important time parameter for the production of reactant ions is ionization time (period A), since the CE reactant ions are formed directly by EI, not by ion-molecule reactions. Once again, the pressures of the reactant gases were held constant for the results reported in this work.

Argon was examined for the characterization and optimization of the ionization time for reactant ion formation (period A) for CE. As in EI, the ionization time is limited by the onset of space charge in the ion trap. EI of argon gas produces one reactant ion (m/z 40 $[Ar]^{+\cdot}$). The optimum reactant ion formation time (ionization time) for argon was 1.0 ms.

The time period that was optimized next was sample ion formation time (period C). The N_2O NMS (without RF cut-off) CE spectrum [Figure 3.9 (a)] of n-butylbenzene can be compared to the N_2O NMS (with RF cut-off ~ 40 amu) CE spectrum [Figure 3.9 (b)]. The ionization process illustrated in Figure 3.9 (b) is better defined than in the previous example; for example ejection of the $[H_3O]^+$ reactant ions has reduced the amount of CI which occurs to produce m/z 135. Similar to NMS CI, sample ions formed by EI,

Figure 3.8. QITMS non-mass-selected scan function for CE.

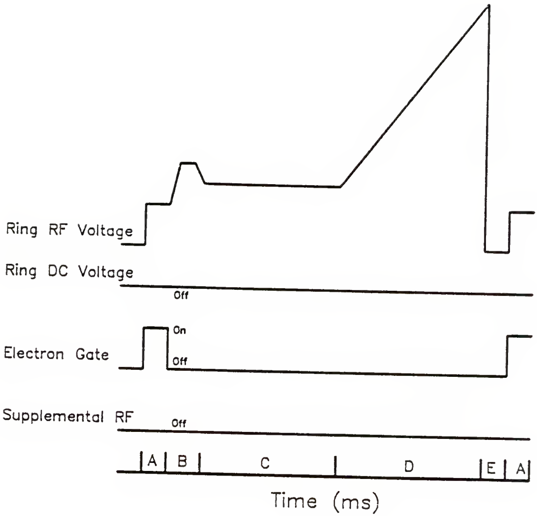

A — Ionization

B — Isolation of reactant ions with low mass cut—off

C — Formation of sample ions

D — Analytical scan

E — Drop RF to sweep ions out of ion trap

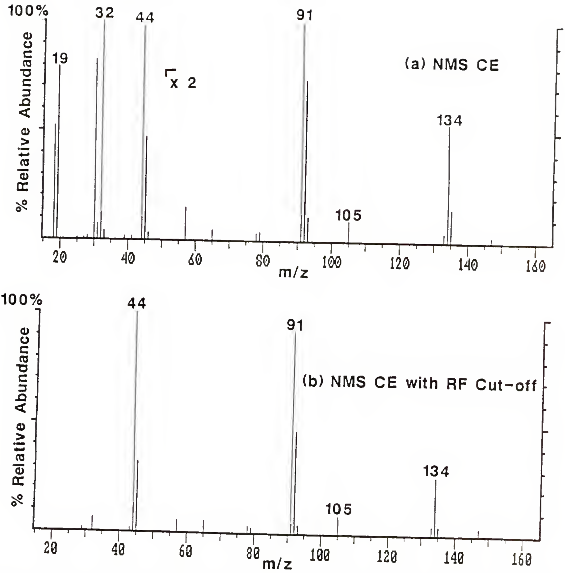

Figure 3.9. Non-mass-selected CI mass spectra with nitrous oxide as the reactant gas and n-butylbenzene (mw - 134) as the sample (a) without RF cut-off and (b) with RF cut-off (RF level ~ 40 amu). Mass scan range was from m/z 15 to m/z 300.

CI, and CE ions in the previously mentioned time periods (A and B) can still be present in the mass spectra. The graph of nitrous oxide as the reactant gas and n-butylbenzene as the sample showing the variation of reactant and sample ion abundances with sample ion formation time (period C) is shown in Figure 3.10. These figures clearly illustrate that with various reaction times, the dominant ionization process (most abundant reactant ion) varies. Hence, some control of the icnization process can be achieved with various sample ion formation times.

Mass-selected Ejection

Chemical ionization. The scan function for mass-selected ejection (MSE) CI with supplemental RF is shown in Figure 2.4. The MSE technique allows additional selectivity as compared to the NMS ionization mode. Since the formation of the reactant ions is the same as with NMS ionization, the only parameters that were varied are the magnitude of the supplemental RF voltage and the reaction time to form sample ions. The frequency of the RF voltage was that calculated by the QITMS software to be the resonant frequency of the ion of interest. Methane and water were examined as reactant gases for these studies.

The effect of the magnitude of the supplemental RF voltage on the ejection of undesired reactant ions was characterized and optimized visually on the computer screen. If a large supplemental RF voltage is used, not only the selected m/z but also reactant ions of interest are ejected from the ion trap. The best conditions appear to be small supplemental RF voltage, since, as the reaction time increases, the

Figure 3.10. Characterization of reaction period C (sample ion formation time) with nitrous oxide as the reactant gas and n-butylbenzene (mw - 134) as the sample: (a) reactant ions, and (b) sample ions.

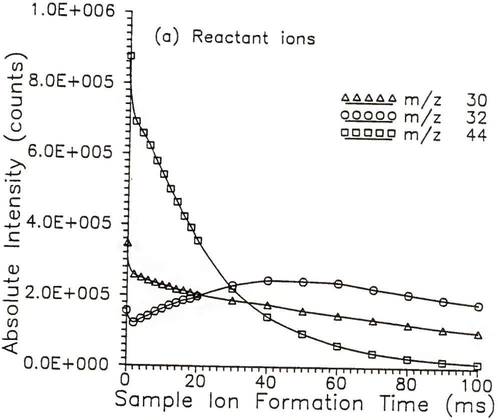
1.0E+006
8.0E+005
6.0E+005
4.0E+005
2.0E+005
0.0E+000
Absolute Intensity (counts)
(a) Reactant ions
m/z 30
m/z 32
m/z 44
0
20
40
60
80
100
Sample Ion Formation Time (ms)

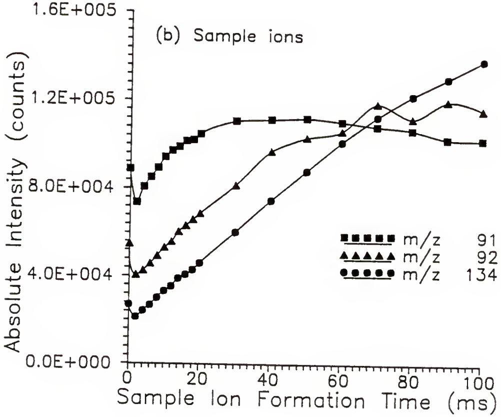
1.6E+005
1.2E+005
8.0E+004
4.0E+004
0.0E+000
Absolute Intensity (counts)
(b) Sample ions
m/z 91
m/z 92
m/z 134
0
20
40
60
80
100
Sample Ion Formation Time (ms)

ejection of the unwanted reactant ion becomes more efficient. For sample ion formation times less than 100 ms, the supplemental RF voltage is applied for the duration of this reaction time; however, for sample ion formation times greater than 100 ms, the supplemental RF voltage is only applied for the first 100 ms. The graph in Figure 3.11 (a) shows the ejection of m/z 41 ($[C_3H_5]^+$) ions from the ion trap during period D when methane is used as a reactant gas. The efficiency of ejection of m/z 41 is best seen as the decrease compared to when no supplemental RF is used. In Figure 3.7 (a), the $41^+/29^+$ is ~ 8% versus ~ 2% here at 10 ms, while in Figure 3.7 (a), the $41^+/29^+$ is ~ 15% versus ~ 0.01% here at 60 ms. Hence the mass-selected ejection of m/z 41 is more efficient with longer reaction times. This graph can be compared to that in Figure 3.7 (a), in which m/z 41 ions were not ejected. For these studies the supplemental RF voltage was held constant (3 V) and the reaction time for period D was varied. By comparison of Figures 3.11 (b) and 3.7 (b), the onset of CI is readily seen in the $[C_2H_5]^+$ MSE CI graph [Figure 3.11 (b)] by comparing it with the NMS CI graph [Figure 3.7 (b)]. The onset of CI is noted by monitoring the m/z 134 and 135 ions; if the m/z 135 ion is greater than that expected from ^{13}C contributions (10% of the m/z 134 ion) then CI via proton transfer is occurring. In the $[C_2H_5]^+$ MSE CI spectra, this ion (m/z 29) has not been completely isolated; however, it is initially the most abundant reactant ion present in the ion trap. Residual oxygen was not present in the $[C_2H_5]^+$ MSE CI spectra, which explains the differences in the m/z 134 ion intensity.

The large difference in the absolute intensities (number of counts) for these two cases (Figures 7 and 11) can be readily explained. The data

Figure 3.11. Characterization of period D (sample ion formation time) with $[C_2H_5]^+$ mass-selected ejection CI of n-butylbenzene (mw- 134): (a) reactant ions, and (b) sample ions. The m/z 41 ion ($[C_3H_5]^+$) was mass-selectively ejected from the ion trap.

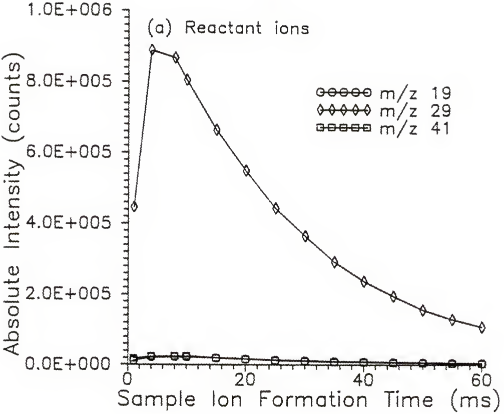
(a) Reactant ions
m/z 19
m/z 29
m/z 41
Absolute Intensity (counts)
1.0E+006
8.0E+005
6.0E+005
4.0E+005
2.0E+005
0.0E+000
0
20
40
60
Sample Ion Formation Time (ms)

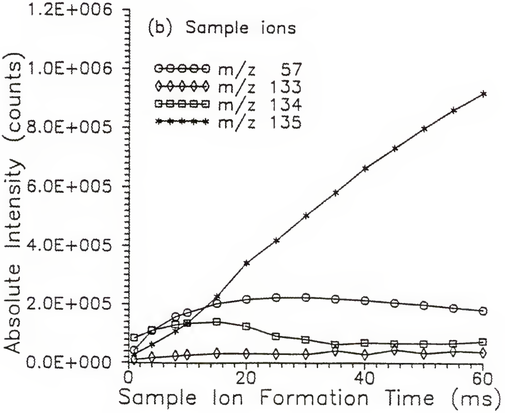
(b) Sample ions
m/z 57
m/z 133
m/z 134
m/z 135
Absolute Intensity (counts)
1.2E+006
1.0E+006
8.0E+005
6.0E+005
4.0E+005
2.0E+005
0.0E+000
0
20
40
60
Sample Ion Formation Time (ms)

were collected using two versions of software; therefore, the absolute intensities (counts) from the two versions cannot be directly compared. All other conditions for the two experiments, multiplier voltage, ionization time, sample pressure, and reactant gas pressure were held constant.

The CH_4 NMS (with RF cut-off ~ 28 amu) CI spectrum [Figure 3.6 (b)] of n-butylbenzene is compared to the $[C_2H_5]^+$ MSE spectrum [Figure 3.6 (c)] where all ions below m/z 28 are ejected from the ion trap by using the RF low mass cut-off and the supplemental RF voltage is used to eject m/z 41. The added selectivity of mass-selected ejection is easily seen in this example, by noting the absence of the interfering reactant ions at m/z 32 and 41 in the CH_4 MSE spectrum. Ejection of m/z 41 from the ion trap should prevent proton abstraction from occurring. It is difficult to make a definite conclusion based upon these spectra. However, the absence of m/z 32 in the $[C_2H_5]^+$ MSE CI spectrum causes significant differences to appear in the mass spectra, as discussed above. One limitation of this technique is that only one unwanted reactant ion can be eliminated during a reaction time. Hence, if two or more reactant ions are present, the reactant ion that would cause the largest interference must be selected to be ejected from the ion trap. Similar to non-mass selected ionization, sample ions present in the previously mentioned time periods (A, B, and C), formed by EI, CI, and CE of the sample molecule can be present in the mass spectra. The resulting sample ions are not ejected from the ion trap with this technique.

Charge exchange ionization. The scan function for MSE CE with supplemental RF is shown in Figure 3.12. As in the MSE CI study, the

Figure 3.12. QITMS mass-selected ejection scan function for CE.

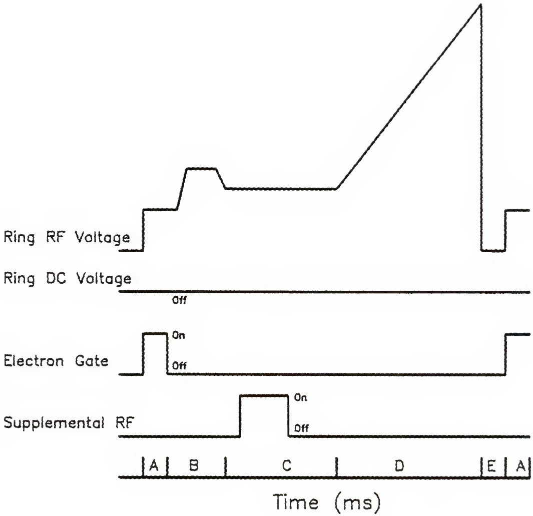

A — Ionization

B — Isolation of reactant ions
with low mass cut-off

C — Formation of sample ions and ejection of
unwanted reactant ions with supplemental RF

D — Analytical Scan

E — Drop RF to sweep ions out of ion trap

supplemental RF voltage was characterized and optimized visually. The best conditions appeared to be small supplemental RF voltage (~3 V), since, as one increases the reaction time, the ejection of the unwanted reactant ion becomes more efficient. The reaction time for formation of reactant ions (20 ms) was held constant in this study. The time period that was optimized for this ionization mode was the reaction time for the formation of sample ions (period C). Graphs similar to Figure 3.11 were generated for nitrous oxide which show the ejection of various reactant ions from the ion trap during period C. These graphs indicate that the reactant ions for nitrous oxide behave in a similar manner as the reactant ions of methane.

The N_2O NMS (without RF cut-off) CE spectrum [Figure 3.13 (a)] of n-butylbenzene is compared to the $[NO]^+$ MSE CE spectrum [Figure 3.13 (b)] where all ions below m/z 29 are ejected from the ion trap by using the RF low mass cut-off and the supplemental RF voltage is used to eject m/z 44. In the $[NO]^+$ MSE CE spectrum, this ion (m/z 30) has not been completely isolated; however, it is initially the most abundant reactant ion present in the ion trap. Again, the added selectivity of mass-selected ejection is easily seen in this example. MSE CE has the same limitations as MSE CI.

Mass-selected Ion-molecule Reactions

Chemical ionization. The scan function for mass-selected (MS) CI is shown in Figure 2.5. The most significant time parameter for the production of reactant ions is the post-ionization time (period B). The optimization of this parameter was discussed previously in the NMS CI

Figure 3.13. Nitrous oxide CE mass spectra of n-butylbenzene (mw - 134) (a) non-mass-selected, (b) $[NO]^+$ mass-selected ejection (ejection of m/z 44) with RF level cut-off of m/z 29, and (c) $[NO]^+$ mass-selected. Mass scan range was from m/z 15 to m/z 300.

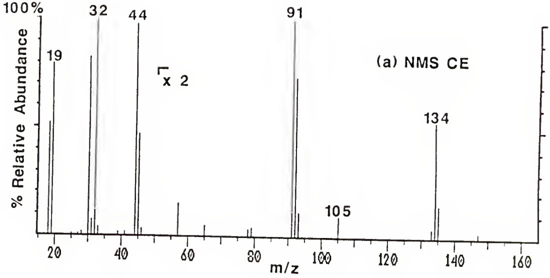
100%
% Relative Abundance
19
32
44
x 2
91
(a) NMS CE
134
105
20
40
60
80
100
120
140
160
m/z

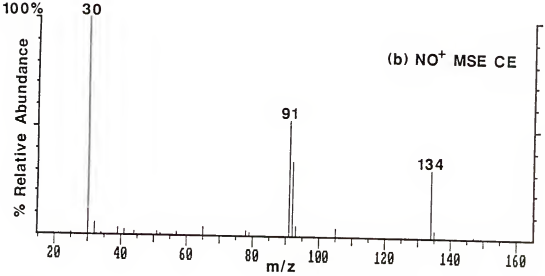
100%
% Relative Abundance
30
(b) NO$^+$ MSE CE
91
134
20
40
60
80
100
120
140
160
m/z

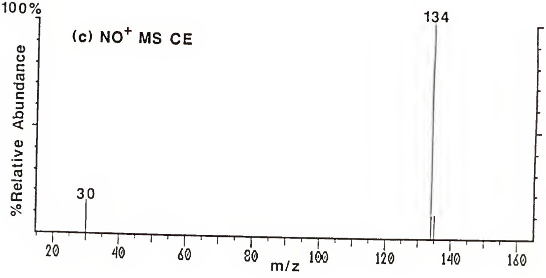
100%
%Relative Abundance
(c) NO$^+$ MS CE
134
30
20
40
60
80
100
120
140
160
m/z

section. The most important time intervals for MS CI are the isolation of the reactant ion and the formation of the sample ions. The isolation of the reactant ion was the first parameter that was characterized and optimized for this ionization mode.

The interpretation of the isolation of the reactant ion with DC voltage requires the use of the Mathieu stability envelope discussed previously (Figure 3.1). The theoretical apex of the stability diagram corresponds to values of 0.78 and 0.15 for 'q_z' and 'a_z', respectively [15]. This stability envelope illustrates two different points. Firstly, the application of -25 V DC (with a RF voltage ~ 132 V zero-to-peak, corresponding to a 'q_z' of 0.738) to the ring electrode m/z 29 for methane $[C_2H_5]^+$ will correspond to an 'a_z' value of 0.139 (point 'A') on the stability diagram. The 'q_z' value of 0.738 was determined visually to be the optimum for the isolation of a particular m/z with DC voltage. This is in contrast to the theoretical value for 'q_z' which should be equal to 0.78 for operation underneath the apex of the stability diagram. It is apparent that at this value of 'a_z' a very narrow mass range is stored in the ion trap. The experimental values of 'a_z' and 'q_z' lie within the region of stability for both positive and negative ions; therefore, both positive ions (narrow mass range) and negative ions (wider mass range) are stored at this point. Secondly, the positive DC voltage required to reach the lower boundary of the positive ion stability envelope is greater than the negative DC voltage required to reach the upper boundary. The DC voltage applied to the ring electrode was characterized by selecting a 'q_z' value of 0.738 for the m/z ion that was to be isolated (e.g., to isolate m/z 29, the low mass cut-off was set to a value of 23.56 amu corresponding to a 'q_z' of 0.908, yielding a 'q_z' value for m/z 29 of 0.738). The 'q_z' value was kept constant for these experiments and the DC voltage ('a_z' value) was varied, allowing the width of ions trapped to be controlled. The spectra in Figure 3.14 were obtained with the following DC voltages: (a) -28 V ('a_z' = 0.156), (b) -25 V ('a_z'= 0.139), (c) -5 V ('a_z' = 0.028), and (d) +40 V ('a_z' = - 0.223). Figure 3.15 is a graph showing the absolute intensities of m/z 19, 28, 29 and 41 as the DC voltage is varied. The drop off in the plateau region of Figure 3.15 (a) is unexpected and unexplained at this time. Figure 3.15 (b) is an enlargement of Figure 3.15 (a) showing the cut-off region for various ions with negative DC voltage. These figures help illustrate that high mass ions (m/z 41) are ejected with smaller applied DC voltages than are low mass ions (m/z 28). The ion at m/z 19 ($[H_3O]^+$) should not be stable in the ion trap since the RF cut-off value is corresponds to m/z 23.58. Therefore this ion must be formed during the subsequent sample ion formation time.

The $[C_2H_5]^+$ MS CI spectrum is shown in Figure 3.6 (d). The selectivity of this ionization technique can be seen by comparing the spectra in Figure 3.6. The only mass spectrum with low intensity m/z 91 and 92 ions is the $[C_2H_5]^+$ MS CI spectrum. This was predicted since the m/z 91 and 92 ions are produced primarily by EI and the only operation mode that completely eliminates EI-produced ions is MS CI. This mass spectrum is also characterized by a very low intensity molecular ion (m/z 134) and no interferent reactant ions at m/z 32 and 41. The ion at m/z 19 ($[H_3O]^+$) is present in the $[C_2H_5]^+$ MS CI spectrum; once again this is predicted since H_2O has a higher proton affinity than C_2H_4.

Figure 3.14. Characterization of the applied DC voltage for mass-selected CI spectra with methane as the reactant gas ('q_z' is held constant at a value of 0.738 for m/z 29): (a) -15 V ('a_z' = 0.0836), (b) -20 V ('a_z'= 0.111), (c) -25 V ('a_z' = 0.139), and (d) 40 V ('a_z' = - 0.223). QITMS mass-selected ejection scan function for CE.

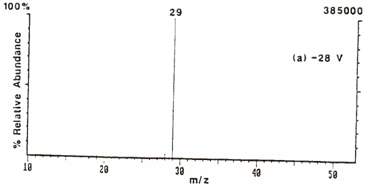
100%
29
385000
(a) −28 V
% Relative Abundance
10
20
30
40
50
m/z

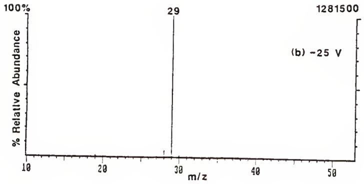
100%
29
1281500
(b) −25 V
% Relative Abundance
10
20
30
40
50
m/z

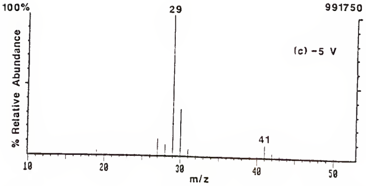
100%
29
991750
(c) −5 V
% Relative Abundance
41
10
20
30
40
50
m/z

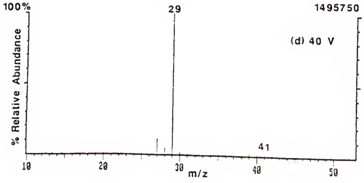
100%
29
1495750
(d) 40 V
% Relative Abundance
41
10
20
30
40
50
m/z

Figure 3.15. Characterization of the applied DC voltage for mass-selected CI with methane as the reactant gas (a) complete range of DC voltages and (b) DC voltages from - 30 V to -26 V.

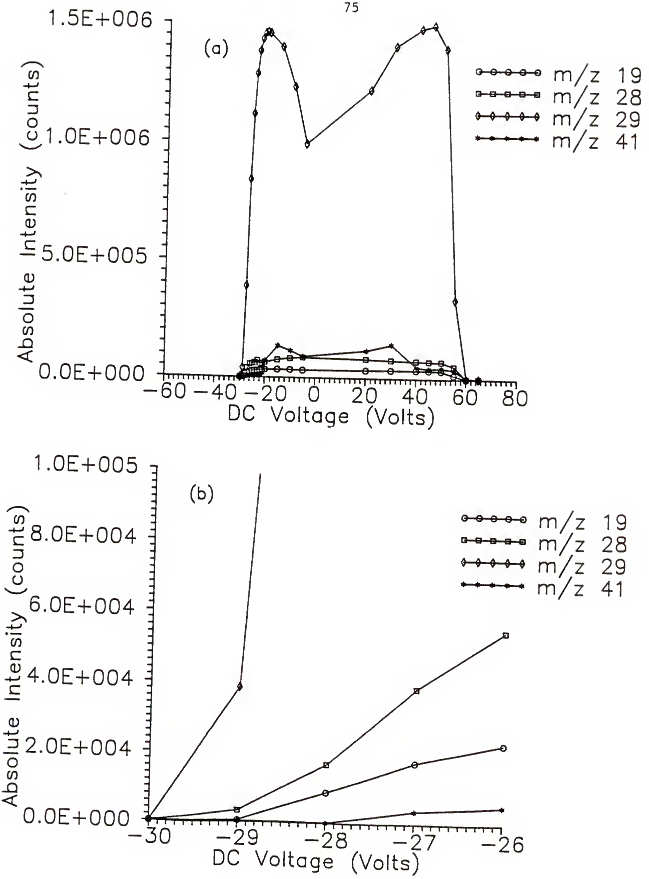
(a)
Absolute Intensity (counts)
1.5E+006
1.0E+006
5.0E+005
0.0E+000
DC Voltage (Volts)
−60
−40
−20
0
20
40
60
80
m/z 19
m/z 28
m/z 29
m/z 41
(b)
Absolute Intensity (counts)
1.0E+005
8.0E+004
6.0E+004
4.0E+004
2.0E+004
0.0E+000
DC Voltage (Volts)
−30
−29
−28
−27
−26
m/z 19
m/z 28
m/z 29
m/z 41

The conclusions that were drawn from this experiment were twofold. Firstly, as the amplitude of the applied DC voltage was increased, the mass range of the ions stored within the ion trap was decreased, and the corresponding intensities of the ions stored within the ion trap were decreased. Secondly, the amplitude of the negative DC voltage to reach upper boundary of the stability envelope (- 30 V) was less than the corresponding positive voltage (+ 60 V) to reach the lower edge of the stability envelope. Furthermore, with negative DC voltages, a narrow range of masses around the m/z of interest is stored, whereas with positive DC voltages only ions of m/z higher than the ion of interest can be eliminated. Therefore, for the isolation of positive reactant ions negative DC voltages were used. A DC voltage at which the selected m/z was reduced to half its maximum intensity was used in the next optimization study (i.e., m/z 29 in Figure 3.15 drops from its maximum intensity to zero between -20 and -30 V; therefore, a DC voltage of -25 V was selected).

The next parameter that was characterized was reaction time for the formation of sample ions (period D). This study was performed using the optimum values obtained for reactant ion formation (20 ms) and isolation (DC voltage of -25 V applied for 1 ms). The CH_4 NMS (with RF cut-off ~28 amu) spectrum [Figure 3.6 (b)] of n-butylbenzene is compared to the $[C_2H_5]^+$ MS CI spectrum [Figure 3.6 (d)]. It should be noted that sample ions produced by EI, CI, and CE in the previously mentioned time periods (periods A, B, and C) are ejected from the ion trap with the DC pulse. This is noted by the decrease in the intensities of the m/z 134, 91, and 92 ions. The times that are reported for the optimization of sample ion formation (~ 60 ms) do not include the times in period A through C. The optimum times were usually characterized by the absence or near-absence of selected reactant ions (i.e., all of the reactant ions have reacted to form sample ions).

Charge exchange ionization. The scan function for mass-selected (MS) CE is shown in Figure 3.16. As in the MS CI characterization, for MS CE ionization the isolation of the reactant ion was the first parameter that was characterized and optimized. As in the isolation of m/z 29 for mass-selected CI, the reactant ion m/z 30 from nitrous oxide was isolated in the ion trap for CE via the application of a negative DC voltage.

The N_2O NMS spectrum of the reactant ions [Figure 3.17 (a)] is compared to the $[NO]^+$ MS CE spectrum [Figure 3.17 (b)]. The mass-selected isolation of the m/z 30 ion is very efficient with 'a_z' and 'q_z' values of 0.156 and 0.738, respectively. The results obtained for the isolation of m/z 30 from nitrous oxide are much better in comparison to the isolation of m/z 29 from methane. The m/z 19 ion in the NMS spectrum does not appear in the $NO^{+\cdot}$ MS CE spectrum, as predicted since there is not a source of protons for the formation of the $[H_3O]^+$ ion. Also the m/z 32 ion ($[O_2]^{+\cdot}$) does not increase in intensity, this is also readily explained, based on the recombination energies of $[N_2O]^{+\cdot}$, $[NO]^+$, and $[O_2]^{+\cdot}$. The $[O_2]^{+\cdot}$ ion is formed in the N_2O NMS CE spectra from CE of $[N_2O]^{+\cdot}$ with residual O_2. The $[N_2O]^{+\cdot}$ ion is ejected from the ion trap with the DC pulse with $[NO]^{+\cdot}$ MS CE, hence the $[O_2]^{+\cdot}$ ion cannot be formed.

The next parameter that was characterized and optimized was the sample ion formation time (period C). This study was performed using the optimum values obtained for reactant ion formation (20 ms) and isolation (DC

Figure 3.16. QITMS mass-selected scan function for CE.

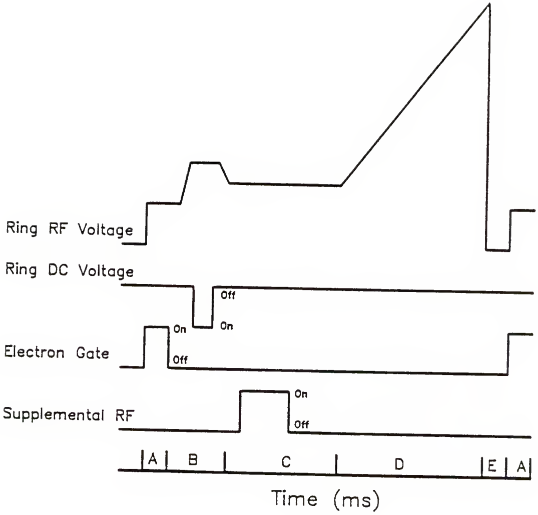

A — Ionization

B — Isolation of reactant ions with DC

C — Formation of sample ions and ejection of unwanted reactant ions with supplemental RF

D — Analytical scan

E — Drop RF to sweep ions out of ion trap

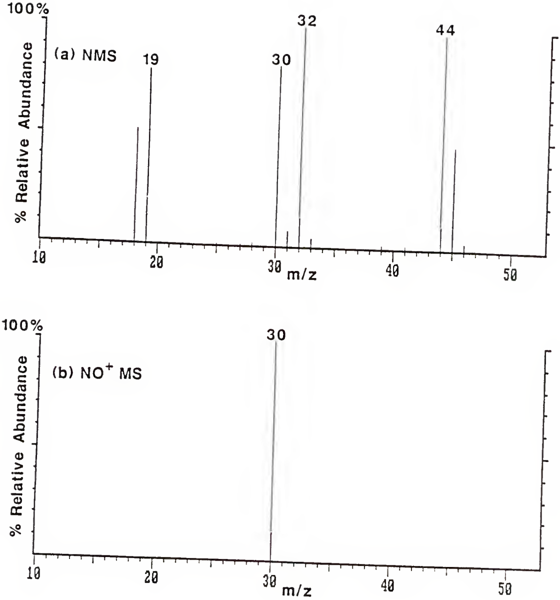

Figure 3.17. Mass spectra of nitrous oxide (a) non-mass-selected without RF cut-off and (b) mass-selection of m/z 30.

voltage of -29 V applied for 1 ms). The N_2O MSE (of m/z 44) CE spectrum [Figure 3.13 (b)] of n-butylbenzene and the $[NO]^+$ MS CE spectrum [Figure 3.13 (c)] are compared. The differences in the spectra are easily seen. The $[NO]^+$ MS CE mass spectrum exhibits no fragmentation and a very intense molecular ion, while the N_2O MSE (of m/z 44) CE mass spectrum is clearly the result of mixed-mode ionization, since the only significant reactant ion in (b) is m/z 30, the difference must be due to residual EI-produced ions (91^+ and 92^+). Positive ion MS CE and MS CI will be discussed in more detail in Chapter 4.

Negative Electron Capture and Chemical Ionization

As mentioned previously, negative ionization techniques in mass spectrometry have not been studied as thoroughly as positive ionization techniques. The primary processes that may form negative ions are ion-molecule and electron-molecule interactions [38]. In this thesis, the term negative chemical ionization (NCI) will refer to ion-molecule reactions; the term electron capture (EC) will refer to electron-molecule interactions. Electron affinity (EA) is defined as the lowest energy required to remove an electron from a negative ion [41]. For the reaction:

$$[A]^- \rightarrow A + e^- \qquad \Delta H^o = EA([A]^-) \tag{3.10}$$

ΔH^o = EA provided $[A]^-$ and A are in their ground rotational, vibrational, and electronic states, and provided the electron has zero kinetic and potential energy [41]. The processes that are addressed in this chapter are NCI via proton abstraction and EC. Negative ionization in QITMS has been reported in the literature [11,22,60], but the description of the experimental parameters necessary for the successful production of negative ions has not been well defined. This portion of the thesis will address the characterization and optimization of reaction times and applied voltages for the formation and detection of negative ions with the QITMS. Three modes of operation will be discussed in conjunction with negative ions: non-mass-selected reactions, mass-selected ejection, and mass-selected reactions.

Non-mass-selected Reactions

Electron capture. Electron capture (EC) is an ionization process which normally requires electrons of thermal or near-thermal energy. The three basic EC reactions that can occur upon ionization of an electron with a neutral molecule are [40]:

Electron capture: $AB + e^- \rightarrow [AB]^{-\cdot}$ (3.11)

Dissociative electron capture: $AB + e^- \rightarrow [A]^- + B\cdot$ (3.12)

Ion pair production: $AB + e^- \rightarrow [A]^- + B^+ + e^-$ (3.13)

All of the EC processes are resonance processes since no electron is produced to carry away the excess energy. These processes are observed for electrons with kinetic energies from thermal up to ~15 eV [61]. For EC, two cases arise depending on whether the EA of AB is less than or greater than zero [62]. When the EA is less than zero, a molecular anion $[AB]^{-\cdot *}$ may be formed which may disappear by autodetachment [43] or if above the dissociation limit, may dissociate to $[A]^-$ + $B^\cdot$. Dissociative EC occurs if capture of an electron leads to a repulsive state of $[AB]^{-\cdot}$, which dissociates to form $[A]^-$ + $B^\cdot$, with possible excess internal and translational energy. The species $[AB]^{-\cdot *}$ may also distribute its excess energy into the vibrational modes of the anion and undergo collisional stabilization (i.e., at pressures of ~ 1 torr the lifetime of the $[AB]^{-\cdot *}$ species must be greater than 1 μs). With ion pair formation (the least common ionization process), the electron provides the energy necessary to form an excited molecule which dissociates to give a positive ion and a negative ion. The EC rate constants are considerably higher than rate constants for ion-molecule reactions (either positive or negative), due to the high mobility of the electron [42]. As a result of these higher rate constants, EC (electron-molecule interaction) can have a much higher sensitivity than normal CI and CE (ion-molecule interactions); this is the primary motivation for derivatization with electron-capturing groups for negative electron-capture ionization studies [15].

For this work, EC was the first mode of operation that was characterized. The scan function for non-mass selected (NMS) EC is the same as the scan function for NMS EI shown in Figure 2.2. The parameters that effect the EC spectra are ionization time (period A) and the RF level during the ionization time. A number of reactant gases were examined for the production of thermal electrons including methane, water, ammonia, nitrous oxide, carbon tetrachloride, and sulfur hexafluoride. The sample compounds examined for EC were n-butylbenzene, nitrobenzene, and benzoic acid. Electron capture did not occur for any of the sample molecules examined and only occurred for the reactant gases. Since EC for most compounds is favored only for thermal electrons, electrons with higher energy generally lead to electron ionization (EI) to form positive ions. In high-pressure (~ 1 torr) CI sources employed in conventional mass spectrometry, electrons are thermalized by repeated collisions with a reactant or buffer gas. Even if electrons could undergo enough collisions at the 1000 times lower pressures in the ion trap, they would still not reach thermal energies; electrons have a m/z value thousands of times lower than the low m/z cut-off of the ion trap. As a result, electrons will have unstable trajectories, and have much too short a residence time in the ion trap to be thermalized. Indeed, electron capture is only observed in the ion trap for compounds with extremely high electron affinities (e.g., SF_6). Hence, the added sensitivity for EC as an ionization technique is not found in the QITMS.

It was discovered that, when the QITMS was operated to detect negative ions, positive ions were detected as well. This was determined by the observation of m/z 19, corresponding to $[H_3O]^+$, in the negative ion mass spectrum of water. When the QITMS is configured for negative ion detection, a conversion dynode placed before the electron multiplier is operated at + 3000 V. A conversion dynode functions by converting negative ions to positive particles by impact on its surface [63]; the positive particles produced are then accelerated to the negatively biased electron multiplier and are detected in the usual manner. The detection of positive ions during negative ion operation can be explained by two possible processes. The most likely process involves positive ions ejected through the grounded end cap closest to the detector being repelled by the + 3000 V dynode, and striking the end cap electrode, thus ejecting electrons or negative ions which are then detected. The other process involves the positive ions bypassing the + 3000 V conversion dynode and directly striking the multiplier (held at -2400 V). Due to the poor performance of non-mass-selected EC, the operating conditions for this ionization mode were not optimized.

Negative chemical ionization. Negative ion-molecule reactions may occur by a number of different processes, including proton abstraction, charge exchange, nucleophilic addition, and nucleophilic displacement producing primarily $[M\text{-}H]^-$, $[M]^-$, $[M+R]^-$, and $[M\text{-}H]^-$ ions, respectively [61]. This thesis will address only proton abstraction reactions in the ion trap. These reactions:

$$[R\text{-}H]^- + M \rightarrow R + [M\text{-}H]^- \qquad (3.14)$$

will be exothermic if the gas-phase acidity of M is greater than the gas phase acidity of $[R\text{-}H]^-$ [35]. The gas-phase acidity scale is defined in terms of the ΔH for the reaction [41]:

$$RH \rightarrow [R\text{-}H]^- + H^+ \quad \Delta H = \Delta H_{acid} \qquad (3.15)$$

Since ΔH is positive, the acidity is greater the smaller the ΔH_{acid}. Alternatively ΔH_{acid} represents the proton affinity of $[R\text{-}H]^-$; therefore, an equivalent statement is that reaction (3.16) will be exothermic if the PA of $[R\text{-}H]^-$ is greater than PA of $[M\text{-}H]^-$ [33]. $[OH]^-$ is one of the most commonly used reactant ions in NCI [64]. The $[OH]^-$ ion from water is produced by dissociative electron capture to form $[H]^-$, followed by proton abstraction from another H_2O molecule to form $[OH]^-$ [65]:

$$H_2O + e^- \rightarrow [H]^- + OH \qquad (3.16)$$

$$[H]^- + H_2O \rightarrow [OH]^- + H_2 \qquad (3.17).$$

In $[OH]^-$ NCI, the major reaction that transpires is [41]:

$$[OH]^- + M \rightarrow [M\text{-}H]^- + H_2O \qquad (3.18)$$

$$\Delta H = PA([M\text{-}H]^-) - PA([OH]^-) \qquad (3.19).$$

Little of the exothermicity of the reaction appears as vibrational energy in the $[M\text{-}H]^-$ ions, so little or no fragmentation occurs [41].

Negative chemical ionization (NCI) is a product of ion-molecule reactions of negative reactant ions with sample molecules. The reactant gases examined for NCI were water, carbon tetrachloride, and sulfur hexafluoride. The samples examined for NCI were glycine, aniline, o-cresol, phenylacetonitrile, benzoic acid, nitrobenzene, n-butylbenzene, methylbenzoate, benzamide, and ethylbenzoate. The scan function for non-mass-selected (NMS) NCI is the same as the scan function for NMS PCI shown in Figure 2.3. The ionization time and the initial RF levels were the most significant operating parameters for NCI. Once again, the NMS NCI experiments yielded poor results. The negative reactant ions as well as the more abundant positive ions are stored in the ion trap. Hence, positive-negative ion recombination leads to rapid loss of the negative ions, limiting the ability to perform NCI in the ion trap. The spectrum observed for water NMS NCI of n-butylbenzene is shown in Figure 3.18. The spectrum is clearly the result of NCI ($[OH]^-$reactant ion plus $[M-H]^-$), and PCI ($[H_3O]^+$ reactant ion plus $[M+H]^+$ and $[C_4H_9]^+$), as discussed previously. Due to the poor performance of non-mass-selected NCI (the 133^- ion is approximately eight times less intense than the 135^+ ion) as well as the confusion that arises from the presence of both positive and negative ions in the spectrum, the operating conditions for this ionization mode were not further pursued.

Mass-selected Ejection

Electron capture. The scan function for negative ion mass-selected ejection (MSE) EC (with supplemental RF) is shown in Figure 3.19. The MSE technique allows the major positive reactant ion (m/z 19, $[H_3O]^+$) to be ejected from the ion trap, minimizing the probability of ion-ion recombination for NCI, and allowing negative ions to be detected. Once again, the sample molecules of interest did not undergo electron capture, but the reactant gases examined did undergo dissociative electron capture. The resulting negative reactant ions can be used for NCI, as shown below. The ionization time and the ejection of m/z 19 from the ion trap were the most important parameters for MSE EC. The ionization times were varied between 60 and 100 ms depending upon the reactant gas of interest. The spectrum of H_2O with MSE EC is shown in Figure 3.20. This spectrum indicates that the ionization process that is occurring for water is dissociative electron capture, ultimately producing the reactant ion $[OH]^-$.

Figure 3.18. Water non-mass-selected NCI mass spectrum of n-butylbenzene (mw -134). Mass scan range was from m/z 15 to 300.

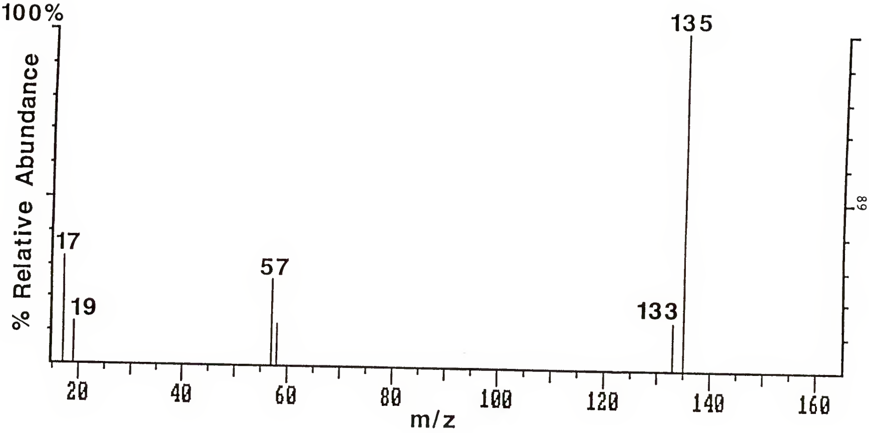
100%
% Relative Abundance
17
19
57
133
135
20
40
60
80
100
120
140
160
m/z

Figure 3.19. QITMS mass-selected ejection scan function for EC.

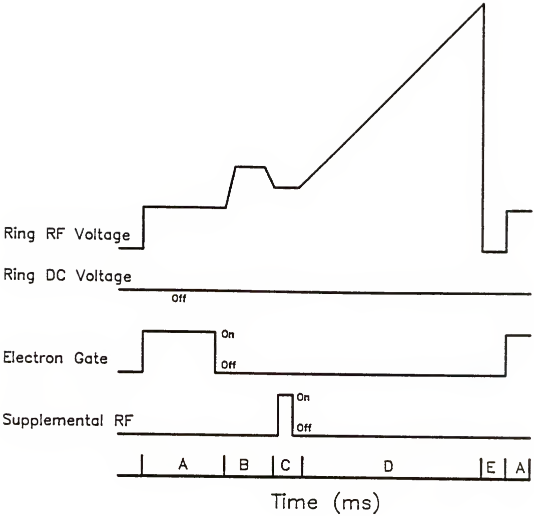

A — Ionization

B — Isolation of sample ions
with low mass cut—off

C — Ejection of unwanted
ions with supplemental RF

D — Analytical scan

E — Drop RF to sweep ions out of ion trap

Figure 3.20. Mass-selected ejection EC mass spectrum of water. Mass scan range was from m/z 15 to 300.

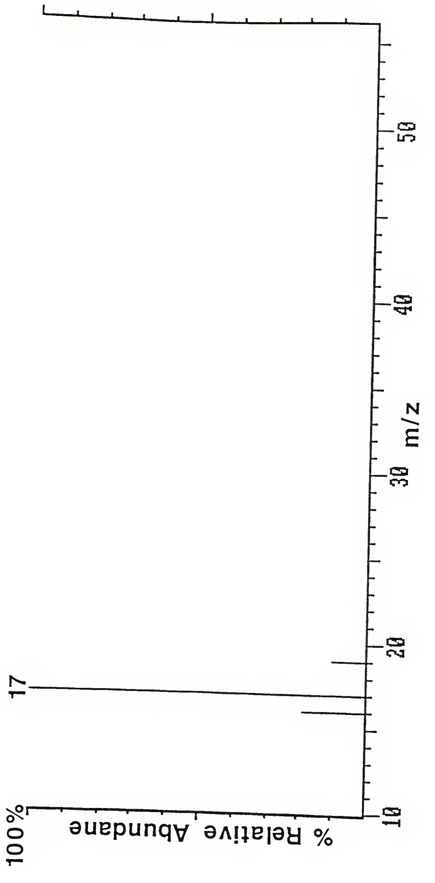
100%
% Relative Abundance
17
10
20
30
40
50
m/z

Similar to positive MSE, the voltage of the supplemental RF was characterized and optimized visually on the computer screen. The magnitude of the supplemental voltage is very important in the ejection of unwanted reactant ions. If too large a supplemental RF voltage is used, both the reactant ion of interest (e.g., m/z 17) and interfering reactant ions (e.g., m/z 19) are ejected from the ion trap. The best conditions appear to be small supplemental RF voltage; as the reaction time is increased the ejection of the unwanted reactant ion becomes more efficient.

Negative chemical ionization. The scan function for mass-selected ejection (MSE) NCI is shown in Figure 3.21. The major difference in the scan functions for PCI and NCI is that with NCI the formation of the negative reactant ions occurs during the ionization time (filament on time), while with PCI the formation of positive reactant ions occurs after the ionization time. The main factors contributing to this appear to be positive-negative ion recombination that quickly eliminates the less abundant negative ions. The other factor is that ionization times for NCI are 100 to 1000 times longer than ionization times in PCI. Hence, in NCI, ion-molecule reactions to form negative ions can occur during the relatively long ionization times (60 to 100 ms). The important operating parameters for MSE NCI were ionization time, the amplitude of the supplemental RF voltage used for mass-selected ejection of m/z 19, and the reaction time to form sample ions. As mentioned previously, optimum ionization times (to form reactant ions) were between 60 and 100 ms, which is much longer than with PCI (ionization times are typically between 0.1 and 1 ms) approximately . The necessity of long ionization times for MSE NCI can be readily explained. The EC process is much less efficient due

Figure 3.21. QITMS mass-selected ejection scan function for NCI.

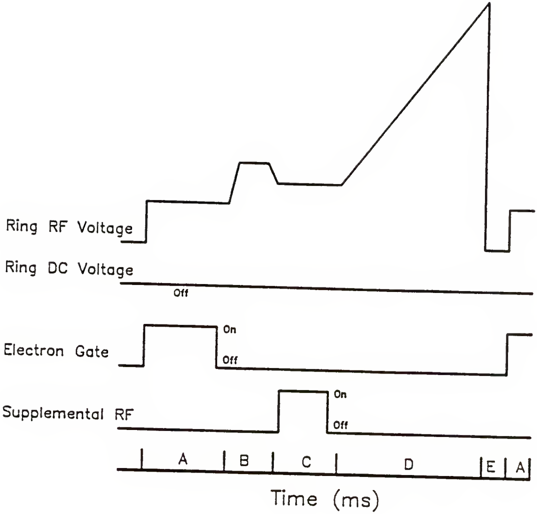

A — Ionization

B — Isolation of reactant ions with low mass cut—off

C — Formation of sample ions and ejection of unwanted reactant ions with supplemental RF

D — Analytical Scan

E — Drop RF to sweep ions out of ion trap

to the lack of thermal electrons; therefore, longer ionization times are required to produce an adequate number of reactant ions. The mass-selected ejection of m/z 19 ($[H_3O]^+$) immediately after ionization was characterized and optimized as with NMS EC. The characterization of sample ion formation time is shown in Figure 3.22. This figure illustrates that positive ion interferences are not significant in the mass spectrum of the sample molecules, due to the ejection of $[H_3O]^+$. The optimum sample formation reaction time is 70 ms for water MSE NCI of n-butylbenzene (Figure 3.23). This spectrum is characterized by pseudo-molecular ion at m/z 133 ($[M-H]^-$) and no fragmentation. Comparison with Figure 3.19 shows that ejection of m/z 19 has prevented formation of any positive ions (e.g., 135^+), eliminating the problem of positive ions in the NCI spectrum.

Mass-selected Ion-molecule Reactions

Electron capture. Once again, sample molecules were not observed to produce negative ions with electron capture mass-selected reactions; however negative ions from various reactant gases were detected. The scan function for mass-selected (MS) EC is the same as the scan function for MS CE shown in Figure 3.16. The most significant time parameters for the production of negative reactant ions are the ionization time, application of DC voltage and the mass-selected ejection of m/z 19. The first parameter that was characterized was the ionization time. Ionization times varied between 10 and 100 ms. The other operating parameters were held constant during this characterization. The graph in Figure 3.24 shows the characterization and optimization of the ionization time with

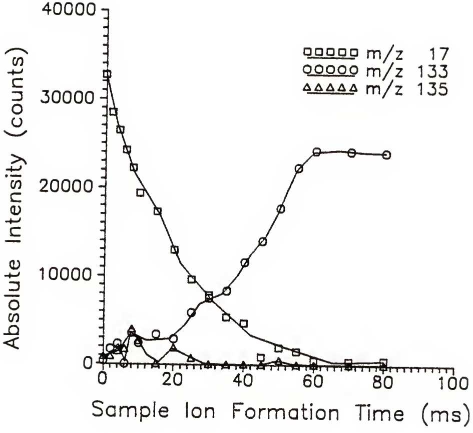

Figure 3.22. Characterization of water mass-selected ejection NCI with m/z 19·($[H_3O]^+$) ejected from the ion trap.

Figure 3.23. Water mass-selected ejection NCI mass spectrum of n-butylbenzene (mw - 134) with a sample ion formation time of 70 ms. Mass scan range was from m/z 15 to 300.

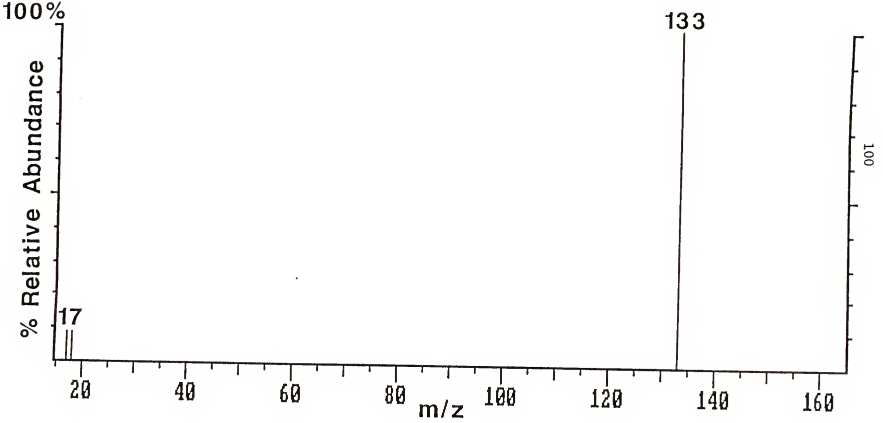
100%
% Relative Abundance
17
133
100
m/z
20
40
60
80
100
120
140
160

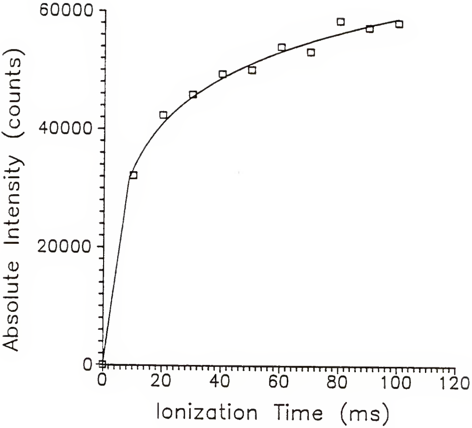

Figure 3.24. Characterization of ionization time for the mass-selected storage of m/z 17 ([OH]$^-$) from water.water as the reactant gas.

The only parameter that limited the useful ionization time was the onset of space charge, which is similar to the observations with positive electron ionization. Without space charge effects, one would expect the intensity of the $[OH]^-$ ion to increase linearly with increasing ionization times; in this case, curvature due to space charge is apparent above ~ 10 ms. The optimum ionization time for EC was determined to be 60 ms. The DC voltage was the next parameter that was characterized and optimized.

The discussion of the characterization and optimization of DC voltage (isolation of the reactant ion) requires the Mathieu stability envelopes for positive and negative ions [Figure 3.1]. The dashed line represents the stability envelope for negative ions, while the solid line represents the stability envelope for positive ions. In positive mass-selected CI, the ion trap was operated near the apex of the stability envelope (point 'A', negative DC voltage) for positive ions. When the ion trap was operated at the apex of the stability diagram for negative ions (point 'C', positive DC voltage), negative ions were detected, but at very low intensities. The ions observed when positive DC voltages are used are m/z 57 and 135, which actually correspond to $[C_4H_9]^+$ and $[M+H]^+$ [Figure 3.25 (a)], respectively, and not to negative ions. These ions are most likely formed with positive CI by $[H_3O]^+$. The lack of negative ions is due to positive-negative ion recombination, since both the abundant positive and less abundant negative ions have stable trajectories in the ion trap at this point. Alternatively, when the ion trap was operated with negative DC voltages (point 'D'above the apex of the stability diagram for positive ions), the efficient isolation of negative reactant ions was obtained [Figure 3.25 (b)]. With the application of - 18 V DC (with a constant 'q_z'

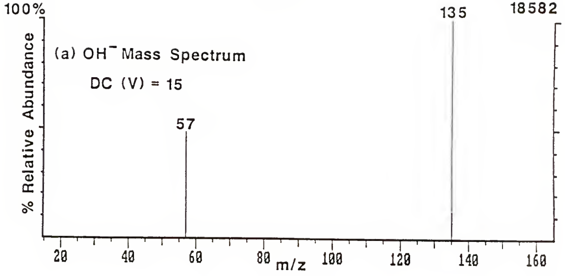

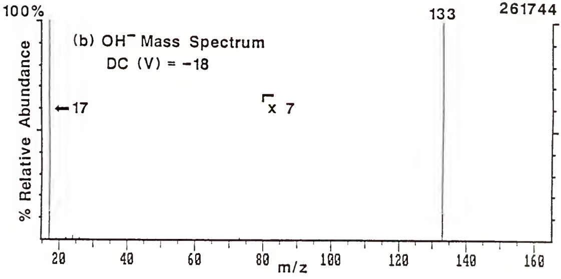

Figure 3.25. The $[OH]^-$ mass-selected NCI mass spectra of n-butylbenzene (mw - 134) with DC voltages of (a) + 14 V ('a_z' = - 0.133), and (b) -18 V ('a_z' = 0.171) and a constant 'q_z' value of 0.738 for m/z 17.

of 0.738) to the ring electrode m/z 17 for water $[OH]^-$ will have an 'a_z' value corresponding to 0.171 (point 'D' on the stability diagram). It is apparent that at this value of 'a_z' a fairly wide range (~ 15 amu wide mass range) of negative ions are stored in the ion trap, but it is also apparent that positive ions are no longer efficiently stored in the ion trap. Hence, the problems associated with positive-negative ion recombination are eliminated. Therefore, for the isolation of negative reactant ions, negative DC voltages were used. Figure 3.26 illustrates the characterization of DC voltage for negative ion isolation. When negative DC voltages (greater than approximately - 18 V, an 'a_z' of 0.171) are applied to the ring electrode, negative ions [Figure 26 (a)] are observed at very high intensities; while positive ions [Figure 26 (b)] are observed at much lower intensities. Once again, with positive DC voltages applied to the ring electrode, some positive ions are still detected in the negative ion spectra [Figure 3.26 (b)]. The other parameters were held constant for this characterization study. The DC voltage at which the m/z 17 intensity was attenuated to one half its maximum value (i.e., - 18 V) was used in the next optimization study.

Negative chemical ionization. The scan function for mass-selected (MS) NCI is the same as the scan function for MS CE (Figure 3.16). The first two parameters (ionization time and isolation of reactant ions) for NCI studies were optimized with the EC experiments. Some of the reactant gases and reactant gas systems examined were water, a 50-50 mixture (by pressure) of nitrous oxide and water, a 50-50 mixture (by pressure) of nitrous oxide and methane [39], nitrous oxide, carbon tetrachloride, and sulfur hexafluoride. The mass spectra of the isolated reactant ions from

Figure 3.26. Characterization of DC voltage for the mass-selected storage of m/z 17 $[OH]^-$ from water (a) negative ions and (b) positive ions.

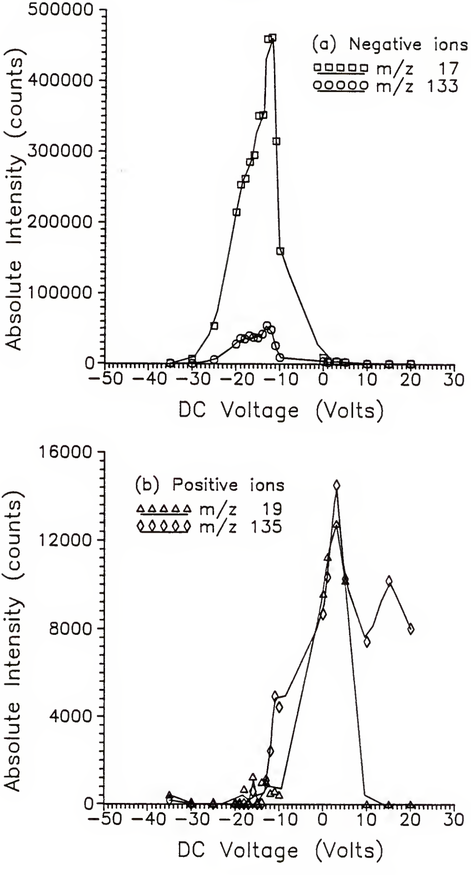
500000
400000
300000
200000
100000
0
Absolute Intensity (counts)
(a) Negative ions
m/z 17
m/z 133
−50 −40 −30 −20 −10 0 10 20 30
DC Voltage (Volts)
16000
12000
8000
4000
0
Absolute Intensity (counts)
(b) Positive ions
m/z 19
m/z 135
−50 −40 −30 −20 −10 0 10 20 30
DC Voltage (Volts)

H_2O, CCl_4, and SF_6 are shown in Figure 3.27. It is clear from these spectra that negative ion isolation with negative DC voltages is very efficient. The CCl_4 mass spectrum of the reactant ions is as expected for this mode of operation. The normal ^{35}Cl to ^{37}Cl isotope ratio is 3 to 1, but here the ratio is ~15 to 1. This is due to the ejection of the ^{37}Cl isotope with the DC voltage.

The next parameter that was optimized was reaction time for the formation of sample ions (period C). This study was performed using the optimum values obtained for ionization time (60 ms) and isolation (DC voltage of -18 V applied for 1 ms) being held constant. The $[OH]^-$ mass-selected NCI spectra of all the sample molecules are shown in Figures 3.28-3.30. The mass spectra (except for those of methylbenzoate and ethylbenzoate) are characterized by little to no fragmentation and the presence of an intense $[M-H]^-$ ion. Hence, this ionization technique is complimentary to proton transfer PCI, which generally produces an intense $[M+H]^+$ ion. Therefore, this ionization technique can be used to provide molecular weight information for a wide range of compounds. The methylbenzoate and ethylbenzoate $[OH]^-$ MS NCI mass spectra both exhibit an intense benzoate anion due to the loss of the ester's ethyl group; the ethylbenzoate mass spectrum also has a fragment ion at m/z 45 ($[COOH]^-$) which is not present in the benzoic acid or methylbenzoate spectra. Therefore, methylbenzoate and ethylbenzoate can be distinguished based upon the presence of this fragment ion. The $[OH]^-$ MS NCI mass spectrum of nitrobenzene [Figure 3.30 (b)] is characterized by an abundant $[M-H]^-$ ion (m/z 122) and a $[NO_2]^{-\cdot}$ ion (m/z 46), as well as a low intensity ion at m/z 92 corresponding to $[M-HNO]^-$. The $[OH]^-$ MS NCI mass spectrum of o-cresol

Figure 3.27. Mass-selected storage mass-spectrum of the reactant ions from (a) water $[OH]^-$, (b) carbon tetrachloride $[Cl]^-$, and (d) sulfur hexafluoride $[SF_6]^-$. The 'q_z' values for the isolated ions were all 0.738, while the 'a_z' values were 0.171, 0.161, and 0.172, and respectively.

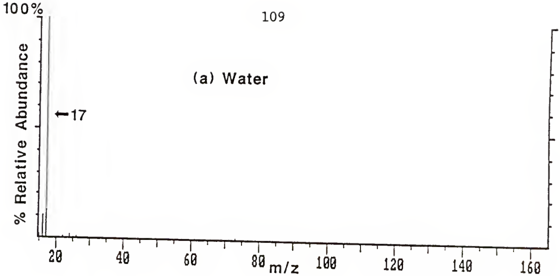
(a) Water

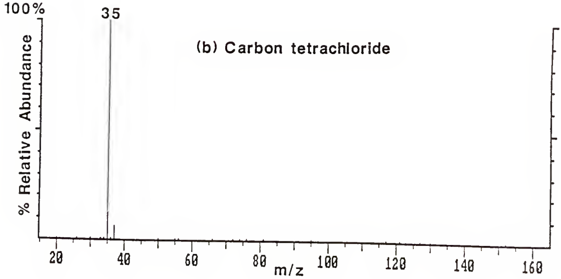
(b) Carbon tetrachloride

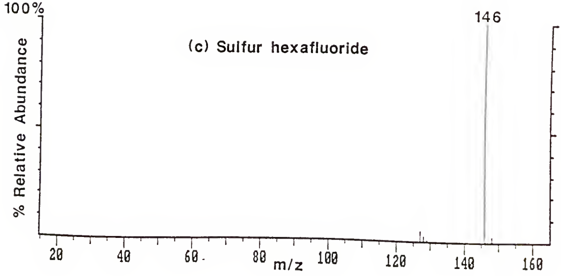
(c) Sulfur hexafluoride

Figure 3.28. The $[OH]^-$ mass-selected NCI mass spectra of (a) glycine, (b) aniline, (c) o-cresol, (d) phenylacetonitrile.

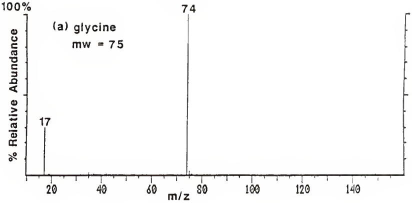
100%
% Relative Abundance
(a) glycine
mw = 75
74
17
20
40
60
80
100
120
140
m/z

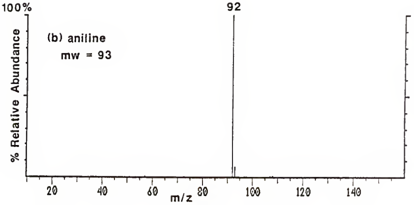
100%
% Relative Abundance
(b) aniline
mw = 93
92
20
40
60
80
100
120
140
m/z

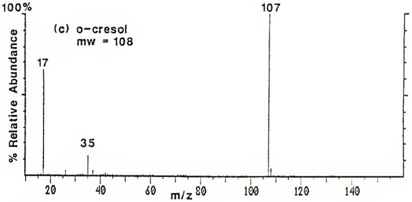
100%
% Relative Abundance
(c) o-cresol
mw = 108
107
17
35
20
40
60
80
100
120
140
m/z

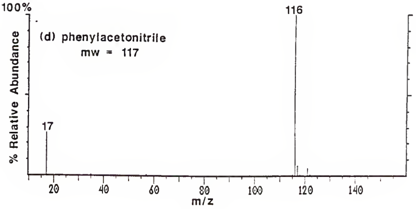
100%
% Relative Abundance
(d) phenylacetonitrile
mw = 117
116
17
20
40
60
80
100
120
140
m/z

Figure 3.29. The $[OH]^-$ mass-selected NCI mass spectra of (a) benzoic acid, (b) methylbenzoate, (c) ethylbenzoate.

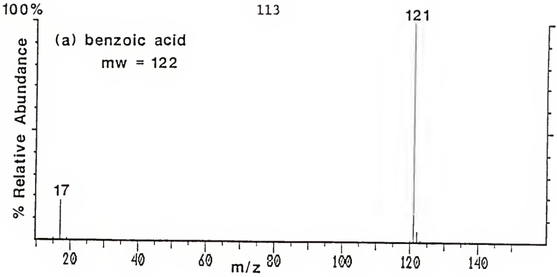
100%
121
(a) benzoic acid
mw = 122
% Relative Abundance
17
20
40
60
m/z
80
100
120
140

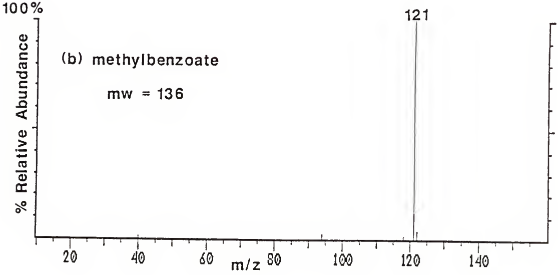
100%
121
(b) methylbenzoate
mw = 136
% Relative Abundance
20
40
60
m/z
80
100
120
140

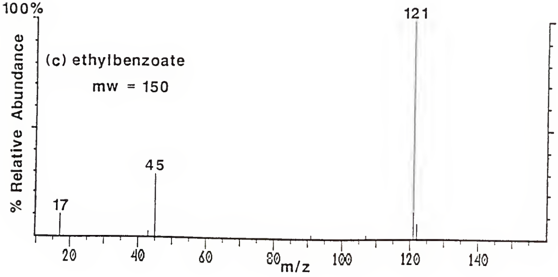
100%
121
(c) ethylbenzoate
mw = 150
% Relative Abundance
45
17
20
40
60
80
m/z
100
120
140

Figure 3.30. The $[OH]^-$ mass-selected NCI mass spectra of (a) benzamide, (b) nitrobenzene, (c) n-butylbenzene.

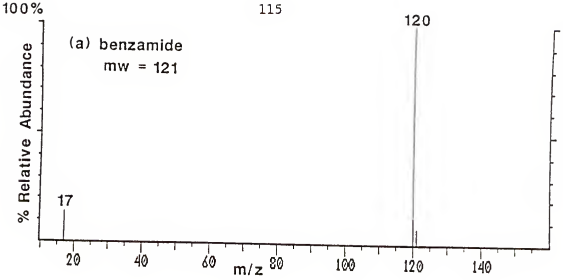
100%
% Relative Abundance
(a) benzamide
mw = 121
120
17
20
40
60
m/z
80
100
120
140

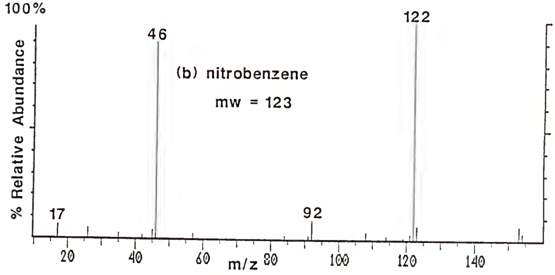
100%
% Relative Abundance
122
46
(b) nitrobenzene
mw = 123
17
92
20
40
60
m/z
80
100
120
140

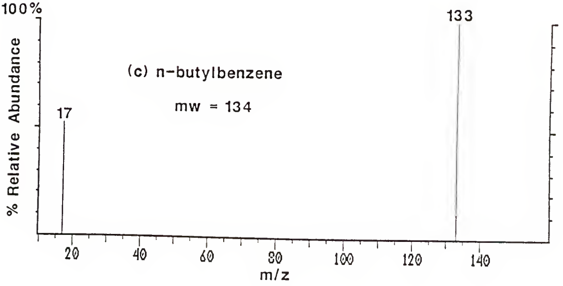
100%
% Relative Abundance
133
(c) n-butylbenzene
mw = 134
17
20
40
60
80
100
120
140
m/z

has some contaminant ions present in the mass spectrum indicated by the presence of m/z 35 (formed from dissociative electron capture of residual CCl_4 from a previous experiment). Similar to positive ion PCI, the optimum NCI reaction time to form sample ions was determined to be the point at which the reactant ion intensity was reduced to less than that of the sample ions. In some cases (Figures 3.27-3.30), indeed all the $[OH]^-$ reactant ion is gone, indicating that the sample ionization time was long enough to use up all the reactant ion. For the $[OH]^-$ NCI studies, the reaction times were on the order of 80 to 100 ms.

The 50-50 mixture of N_2O and H_2O also produced predominately $[OH]^-$ and some $[O]^-$ reactant ions. There does not appear to be any advantage of using this reaction mixture instead of only H_2O for NCI. Therefore the characterization of this reaction mixture will not be discussed further. The other reactant gases and the isolated reactant ions that were examined, ammonia ($[NH_2]^-$), carbon tetrachloride ($[Cl]^-$, and sulfur hexafluoride ($[SF_6]^-$), did not produce negative ions from any of the sample molecules. These reactant ions have been examined with high-pressure NCI studies and have displayed some reactivity with the classes of compounds examined in this work [16,20]. For instance, $[Cl]^-$ has been shown to form adduct ions with nitrated aromatic compounds to form $[M+Cl]^-$ ions [66]. No sample ions were detected with any of these reactant gases. The reason for the lack of reactivity may be readily explained. In high-pressure (~ 1 torr) NCI studies, the reactant and sample ions undergo a number of collisions which can stabilize the negative charge on the respective ions; whereas in the ion trap, the pressures are 1000 times less than in conventional mass spectrometers. Hence, the collisional stabilization that is present in conventional mass spectrometers is absent in the ion trap.

Conclusions

The research presented in this chapter has centered on the use of various electrical fields applied to the ion trap to control the mass range of ions which have stable trajectories, as well as the kinetic energy of these ions. These fields include the fundamental RF voltage applied to the ring electrode, as well as supplemental RF voltage applied across the end cap electrodes at the secular frequency of ions at a specific m/z, and DC voltage applied to the ring electrode in order to provide isolation of ions of a specific mass or a particular polarity. These capabilities provide the opportunity to carefully control the type of ionization that takes place in the ion trap, and the energetics of ionization (and hence degree of fragmentation). These capabilities, as implemented in MS CI and CE ionization, have been demonstrated for a wide variety of reactant ions, and compared to the results of conventional, NMS CI and CE. It was also demonstrated how these approaches are required to make NCI within the ion trap a practical technique.

The NMS ion-molecule reactions in the QITMS were shown to be a result of mixed-mode ionization consisting of a combination of EI, CE, and CI. Other limitations of NMS ionization mode include space charge effects and the inability to achieve NCI in the QITMS. The best results that can be obtained with the popular commercial quadrupole ion trap detector (Finnigan MAT ITD without supplemental RF and without DC) were addressed with the NMS EI, CI and CE results.

The MSE mode in the QITMS (with supplemental RF voltage) did not surmount all of the difficulties associated with mixed-mode ionization, but it provided added control compared to the NMS mode. Ionization of sample molecules by undesired reactant ions can be reduced by mass-selected ejection of a single m/z reactant ion. This ejection will reduce the CE or CI interferences in some cases (e.g., with $[C_2H_5]^+$ CI, the m/z 19 ($[H_3O]^+$) ion which forms by protonation of residual H_2O in the ion trap can be ejected from the ion trap). This ionization technique also suffers from several limitations, including: space charge affects, residual EI ions in CE and CI spectra, and limited negative ionization capabilities. With mass-selection of reactant ions, it was demonstrated that control of the energetics of both the CE and CI ionization processes could be achieved.

The preliminary investigations with negative ionization in the QITMS indicate that NCI and EC are not as sensitive as PCI and EI. This is in contrast to the observation with conventional mass spectrometers of up to a hundredfold increase in sensitivity in the EC negative ionization mode compared to that in positive chemical ionization. The decreased sensitivity associated with negative ionization in the QITMS may be readily explained. Electron capture (EC) for most compounds is favored only for thermal electrons; electrons with higher kinetic energy generally lead to electron ionization to form positive ions. In high-pressure (~ 1 torr) CI sources on conventional mass spectrometers, electrons are thermalized by repeated collisions with a reactant or buffer gas. Even if electrons could undergo enough collisions at the 1000 times lower pressures in the ion trap, they would still not reach thermal energies;

electrons have a m/z value thousands of times lower than the low m/z cut-off of the ion trap. As a result, electrons will have unstable trajectories, and have much too short a time in the trap to be thermalized. Indeed, EC is only observed in the ion trap for compounds with extremely high electron affinities (e.g., SF_6). Dissociative electron capture is observed in the ion trap for a variety of reactant gases including water, ammonia, and carbon tetrachloride. The likelihood of this process is greater than EC, because dissociative EC can occur for electrons with energies up to 15 eV [61].

Negative chemical ionization was a much slower (longer ionization and sample formation reaction times were required) ionization process than positive chemical ionization. The reasons for the longer reaction times required for negative ionization are unclear, since the tabulated rate constants for NCI and PCI are approximately the same. The slower ionization process probably results from the negative reactant ions being present in much lower concentrations than positive reactant ions, even though the same sample and reactant gas pressures were used in each case. In order to obtain reactant ion intensities even close to positive ion intensities requires much longer times; positive ion modes cannot employ such long ionization times without the onset of space charge effects. The presence of positive ions in negative ion spectra in cases where positive reactant ions have not been ejected complicates the interpretation of such spectra. Furthermore, positive ions need to be ejected from the ion trap to prevent positive-negative ion recombination from occurring. This ejection of positive reactant ions from the ion trap was achieved by mass-selectively ejecting m/z 19 ($[H_3O]^+$) with either the supplementary RF voltage or the DC voltage. The MS NCI mode of operation (with DC voltage) was the most effective technique for performing NCI. The results from the QITMS $[OH]^-$ MS NCI studies point out that molecular weight information, in the form of pseudo-molecular ions ($[M-H]^-$), can be obtained from a wide variety of compounds, with very little fragmentation.

CHAPTER 4
ION-MOLECULE REACTIONS FOR POSITIVE CHEMICAL IONIZATION AND CHARGE EXCHANGE IONIZATION IN QUADRUPOLE ION TRAP AND TRIPLE QUADRUPOLE MASS SPECTROMETERS

In this chapter, two forms of ionization will be discussed which produce positive ions by gas-phase ion-molecule reactions, namely chemical ionization (CI) and charge exchange (CE). Electron ionization (EI) will also briefly be discussed in this chapter. The scan functions that were used to obtain the results in this chapter are non-mass-selected EI, non-mass-selected CE or CI, mass-selected ejection CE or CI, and mass-selected CE or CI. Results from the QITMS and from the TQMS (obtained in collaboration with Mark E. Hail) will be compared in this chapter. By the selection of different gaseous reactant ions, the energetics of the gas-phase ion-molecule reactions and the resultant degree of fragmentation that appears in a given spectrum can be controlled.

Chemical ionization via proton transfer to form $[M+H]^+$ will occur if the proton affinity (PA) of a sample molecule, M, is greater than the proton affinity of the conjugate base (R) of the reactant ion, $[R+H]^+$:

$$M + [R+H]^+ \rightarrow [M+H]^+ + R \qquad (4.1).$$

The difference between the PA of the conjugate base of the reactant ion, R, and the PA of the sample molecule (M) will be deposited primarily as internal energy into the newly formed sample ion, $[M+H]^+$ [41]:

$$\Delta H = PA(R) - PA(M) \qquad (4.2).$$

Chemical ionization via hydride abstraction can occur if the hydride ion affinity (HIA) of the reactant ion $[R+H]^+$, is greater than the HIA of the sample ion, $[M-H]^+$ [41]:

$$M + [R+H]^+ \rightarrow [M-H]^+ + [R+2H] \qquad (4.3).$$

The exothermicity of the hydride abstraction reaction will determine the amount of internal energy imparted to the sample ion, $[M-H]^+$ [41]:

$$\Delta H = HIA([M-H]^+) - HIA([R+H]^+) \qquad (4.4).$$

Charge exchange ionization will occur if the ionization energy (IE) of the sample molecule, M, is less than the recombination energy (RE) of the reactant ion, $[R]^{+\cdot}$ [41]:

$$M + [R]^{+\cdot} \rightarrow [M]^{+\cdot} + R \qquad (4.5).$$

The difference between the RE of the reactant ion, $[R]^{+\cdot}$ and IE of the sample molecule, M, will determine the degree of fragmentation of the sample ion, $[M]^{+\cdot}$, with CE [41]:

$$\Delta H = IE(M) - RE([R]^{+\cdot}) \qquad (4.6).$$

The RE of an ion (defined as the amount of energy needed to convert $[R]^{+\cdot}$ to R) is, in principle, the same in magnitude and sign as the IE of the corresponding molecule. The RE of $[R]^{+\cdot}$ will equal the IE of R if there is no transfer of kinetic energy and if the initial and final states of $[R]^{+\cdot}$ are the same [49]. It is important to realize that the RE of a reactant ion which is a fragment (rather than molecular ion) will not simply be the ion's appearance energy (AE) (e.g., NO^+ ion formed from N_2O

has a AE of 14.35 eV, but a RE of 9.26 eV to form NO·). Clearly, knowledge of the IE and RE of the reactant and sample molecules and ions is useful, since it allows one to predict the degree of fragmentation associated with CE ionization. Various methods are available to determine these IE's, including photoionization [34,67], electron ionization [34,68], resonant photoionization [69,70], and Penning ionization [71]. These methods are commonly implemented on specially designed mass spectrometers. The tabulated IE's [Table 4.1] cover the commonly used reactant gases [72], but not the variety of sample compounds that might be of interest. Related research efforts in our group have addressed the need for a routine method for determining the IE's of sample molecules on a computer-controlled TQMS [73].

Traditionally, CI or CE is carried out in a high-pressure ionization source with approximately 1 torr of reactant gas. The gaseous mixture is ionized by EI with high energy (70 - 100 eV) electrons. This results in both the reactant gas and the sample being ionized. Since the reactant gas is in great excess of the sample, it will have a greater probability of ionization. The reactant gas ions are able to interact with neutral reactant gas molecules to form other reactant gas ions, as well as with sample molecules which may result in CI or CE ionization. The mass spectra obtained with such an ion source configuration will include sample ions produced by EI, as well as by CI and/or CE with the variety of reactant ions present. Thus, one problem associated with CI or CE with traditional high-pressure ion sources is that selection of a single reactant ion is not possible. For example, with methane as a reactant gas, a number of reactant ions are produced which can react with the

Table 4.1. Literature Values for Ionization Energies of Reactants and Samples

Species		Ionization Energies (eV)
Gas	Ion	Literature[a]
Helium	$He^{+\cdot}$	24.59 ± 0.01
Nitrogen	N^{+}	14.35 ± 0.02[b]
Argon	$Ar^{+\cdot}$	15.76 ± 0.03
Nitrogen	$N_2^{+\cdot}$	15.58 ± 0.01
Argon	$Ar_2^{+\cdot}$	14.71 ± 0.01
Carbon Dioxide	$CO_2^{+\cdot}$	13.80 ± 0.02
Carbon Dioxide	$CO^{+\cdot}$	14.00 ± 0.01[b]
Nitrous Oxide	$N_2O^{+\cdot}$	12.89 ± 0.00
Methane	$CH_4^{+\cdot}$	12.76 ± 0.24
Water	$H_2O^{+\cdot}$	12.62 ± 0.03
Nitrous Oxide	$O_2^{+\cdot}$	12.08 ± 0.02[b]
Ethylene	$C_2H_4^{+\cdot}$	10.51 ± 0.01
Phenylacetonitrile	$C_8H_7N^{+\cdot}$	9.45 ± 0.05
Nitrous Oxide	NO^{+}	9.26 ± 0.02[b]
n-Butylbenzene	$C_{10}H_{14}^{+\cdot}$	8.69 ± 0.01

[a] Values are averaged values for lowest energy state reported in reference 72, ± the maximum deviation

[b] RE's are reported in cases where the ion does not recombine to form the original species: e.g., RE for $NO^{+} + e^{-} \rightarrow NO^{\cdot}$, not N_2O

sample [46]. Some of the reactant ions observed with methane are m/z 15, 16, 17, 28, 29, and 41 corresponding to $[CH_3]^+$, $[CH_4]^{+\cdot}$, $[CH_5]^+$, $[C_2H_4]^{+\cdot}$, $[C_2H_5]^+$, and $[C_3H_5]^+$, respectively. The resultant mass spectra can contain sample ions produced by a combination of initial EI, proton transfer from $[CH_5]^+$, $[C_2H_5]^+$, and $[C_3H_5]^+$ (with a range of internal energies and degrees of fragmentation), hydride abstraction with $[C_3H_5]^+$, and CE with $[CH_4]^{+\cdot}$ or $[C_2H_4]^{+\cdot}$ (again with a range of internal energies). The proton affinities and hydride ion affinities of samples and reactants are listed in Table 4.2 [41,74].

The above mentioned difficulties associated with CI and CE ionization can be eliminated by taking advantage of the inherent capabilities of tandem mass spectrometry (MS/MS). The ability to mass-select a single reactant ion produced from a given reactant gas and to allow only this ion to interact with a sample molecule in a subsequent step provides a high level of control over sample ionization by CI and CE. In this chapter are reported the advantages of first mass-selecting a reactant ion, which then is used to ionize sample molecules.

The QITMS and the TQMS are uniquely suited to perform mass-selected CI or CE reactions. Some of the important operating parameters for the instruments were listed in Table 1.1. In the TQMS, ionization, mass-selection of the reactant ion, CI or CE, and mass analysis occur in discrete regions of the instrument, and thus MS/MS is tandem-in-space [Figure 1.1(a)]. This is in contrast to tandem mass spectrometry with the QITMS, where these processes occur sequentially in the same region in space, and thus, MS/MS is tandem-in-time [Figure 1.1(b)].

Table 4.2. Proton and Hydride Ion Affinity Values for Species of Interest

Species	Reactant Ion	PA (eV)[a]	HIA (eV)[b]
C_6H_5-CH_2CN	SM[c]	8.50	NF[d]
n-$C_4H_9(C_6H_5)$	SM	8.33	NF
C_3H_4	$C_3H_5^+$	7.89-[e] 8.06	11.01
H_2O	H_3O^+	7.24	NF
C_2H_4	$C_2H_5^+$	7.07	11.79
CH_4	CH_5^+	5.72	11.71

[a] Values reported in reference 41 were converted from kcal/mole to eV

[b] Values reported in reference 74 were converted from kcal/mole to eV

[c] SM - sample molecule

[d] NF - not found in the literature

[e] CH_3-C═CH has a PA of 7.89 eV
H_2C═C═CH_2 has a PA of 8.06 eV

In this chapter, the experimental results from the characterization of non-mass-selected EI, non-mass-selected CE and CI and mass-selected CE and CI with the QITMS and TQMS are presented and compared.

Non-mass-selected Reactions

Electron Ionization

The EI mass spectra of n-butylbenzene and phenylacetonitrile were obtained on the TQMS [Figure 4.1(a) and 4.1(d)] and on the QITMS [Figures 4.2(a) and 4.2(d)]. The $91^+/92^+$ intensity ratio from n-butylbenzene is commonly used to estimate the internal energy imparted during ionization of this molecule [75-77]. These literature values do not correct for the isotopic abundance of ^{13}C (i.e., $[^{13}C_1{}^{12}C_6H_7]^+$) in the 92^+ ion intensity, hence the largest $91^+/92^+$ ratio that can be obtained, given seven carbons and the 1.1% natural abundance of ^{13}C, is 100%/7.7% = 13. The values reported in this work were not corrected for the ^{13}C abundance, so that comparison with literature values could be made. The m/z 91 ion results from a more energetic fragmentation route involving a direct ß-cleavage of the butyl chain and a rearrangement of the benzene ring to form the tropylium ion $[C_7H_7]^+$, while the m/z 92 ion results from a less energetic fragmentation route due to ß-cleavage of the butyl chain with a hydrogen transfer from the butyl chain to form the $[C_7H_8]^{+\cdot}$ ion [Figure 4.3] [78]. The EI mass spectra of n-butylbenzene [Figures 4.1(a) and 4.2(a)] are characterized by a $91^+/92^+$ intensity ratio of 1.7 for both the TQMS and QITMS. For phenylacetonitrile, the $89^+/90^+$ intensity ratio could potentially be used in a similar fashion to estimate the amount of internal energy deposited into this molecule upon ionization. Analogous

Figure 4.1. Non-mass-selected spectra with the TQMS for n-butylbenzene: (a) EI, (b) carbon dioxide CE, and (c) methane CI. Non-mass-selected spectra obtained with the TQMS for phenylacetonitrile: (d) EI, (e) carbon dioxide, and (f) methane CI. Mass scan range was from m/z 15 to 300: except in (e) which had a mass scan range from m.z 80 to 300. Relative abundances of the reactant ions were determined in a separate experiment.

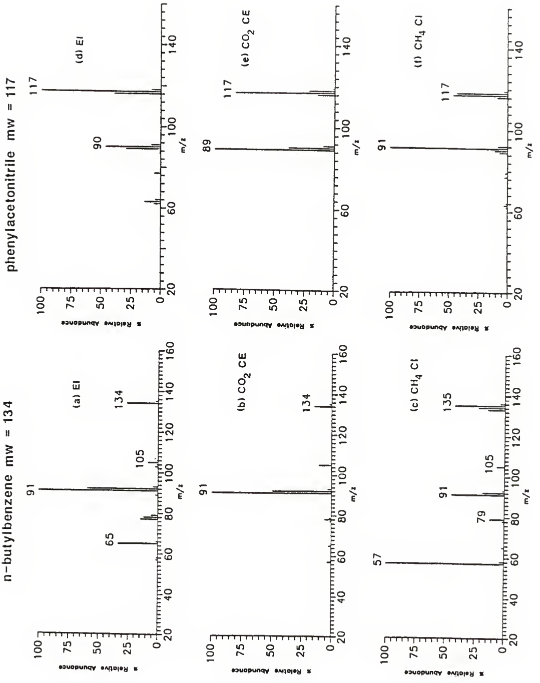
n-butylbenzene mw = 134
phenylacetonitrile mw = 117
(a) EI
(b) CO_2 CE
(c) CH_4 CI
(d) EI
(e) CO_2 CE
(f) CH_4 CI
% Relative Abundance
m/z
100
75
50
25
0
20
40
60
80
100
120
140
160
65
91
105
134
57
79
135
90
117
89

Figure 4.2. Non-mass-selected spectra with the QITMS for n-butylbenzene: (a) EI, (b) carbon dioxide CE, and (c) methane CI. Non-mass-selected spectra obtained with the TQMS for phenylacetonitrile: (d) EI, (e) carbon dioxide, and (f) methane CI. Mass scan range was from m/z 15 to 300.

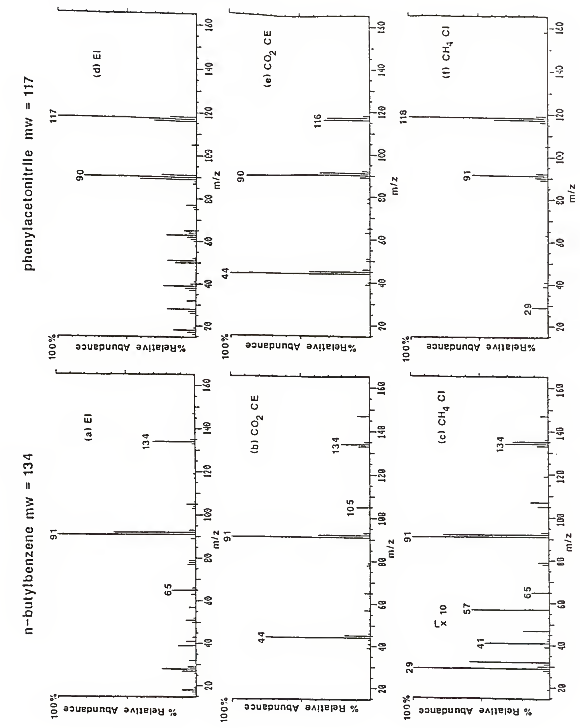
n-butylbenzene mw = 134
phenylacetonitrile mw = 117
(a) EI
(b) CO_2 CE
(c) CH_4 CI
(d) EI
(e) CO_2 CE
(f) CH_4 CI
% Relative Abundance
100%
m/z
20
40
60
80
100
120
140
160
91
65
134
44
105
29
41
57
x 10
117
90
116
118

Figure 4.3. Fragmentation routes for the formation of (a) m/z 92^+ and (b) m/z 91^+ ions [78].

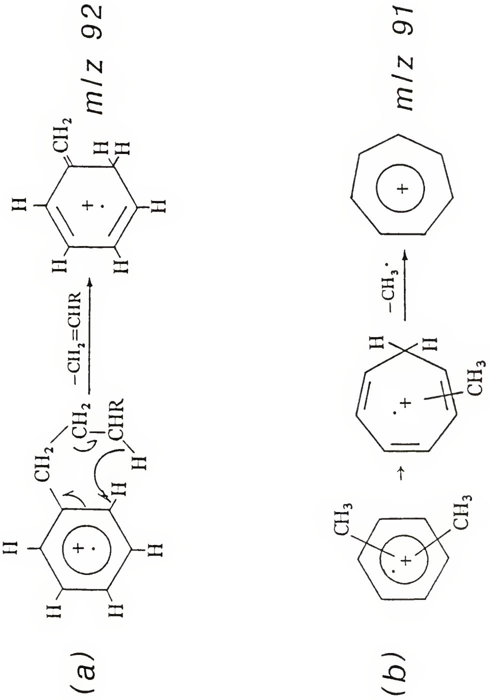
(a)
$-CH_2{=}CHR$
m/z 92
(b)
$-CH_3\cdot$
m/z 91
CH_2
CHR
CH_3
H

to the $91^+/92^+$ intensity ratio for n-butylbenzene, in this work the $89^+/90^+$ intensity ratio was not corrected for the ^{13}C contribution. The energy-resolved CAD breakdown curve (Figure 4.4) of the EI-generated molecular ion of phenylacetonitrile, m/z 117, indicates that the ion at m/z 90 ($[C_7H_6]^{+\cdot}$) results from a low energy fragmentation route, while the ion at m/z 89 ($[C_7H_5]^+$) results from a high energy fragmentation route. The EI mass spectra of phenylacetonitrile [Figure 4.1(d) and 4.2(d)] are characterized by $89^+/90^+$ intensity ratios of 0.63 and 0.51 for the TQMS and QITMS, respectively. The EI mass spectra obtained for both compounds on the QITMS are slightly less energetic than those obtained on the TQMS, as indicated by the fragment ion abundance ratios. This probably results from the lower average electron energy in the QITMS (~30 eV) [58] compared to the TQMS ion source (70 eV).

Charge Exchange Ionization

As stated in the introduction, in CE the difference between the RE of the reactant ion and the IE of the sample molecule determines the internal energy deposited into the sample ion upon ionization by CE. As shown by the values in Table 4.1, ions with a wide range of recombination energies (9.3 to 24.6 eV) are available through the use of different CE reactant gases. However, the selection of a particular reactant gas does not in general result in a single reactant ion; selection of N_2, for example, produces reactant ions with recombination energies ranging from 15.6 to 24.3 eV. Nevertheless, some control of the energetics of the CE ionization reaction (the degree of fragmentation of the resulting $[M]^{+\cdot}$ ion of the sample) can be achieved by selecting various reactant gases,

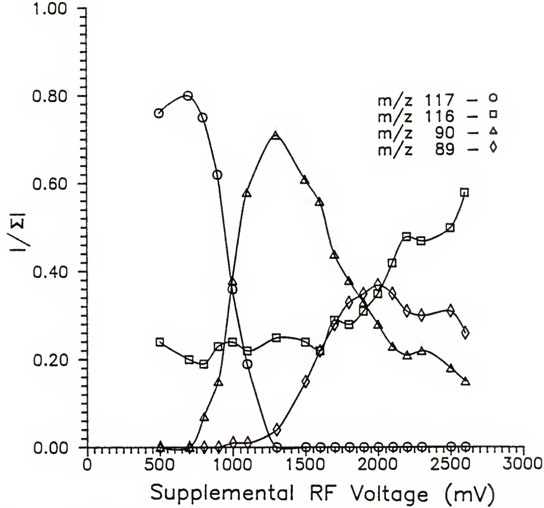

Figure 4.4. Energy resolved breakdown curve for the molecular ion ($[M]^{+\cdot}$) of phenylacetonitrile (mw - 117).

as indicated by the summary of the mass spectra in Tables 4.3(a) and 4.3(b).

The non-mass-selected carbon dioxide CE mass spectra of n-butylbenzene are characterized by $91^+/92^+$ intensity ratios of 2.0 and 2.6 for the TQMS and QITMS, respectively [Figures 4.1(b) and 4.2(b)]. With the RE of $[CO_2]^{+\cdot}$ being 13.8 eV and the IE of n-butylbenzene being 8.7 eV, 5.1 eV of internal energy is deposited into the n-butylbenzene molecule upon CE ionization with $[CO_2]^{+\cdot}$. The non-mass-selected CO_2 CE mass spectra $91^+/92^+$ intensity ratios for n-butylbenzene indicate that these spectra are slightly more energetic than 70 eV EI mass spectra. The non-mass-selected carbon dioxide CE mass spectra of phenylacetonitrile [Figures 4.1(e) and 4.2(e)] are characterized by $89^+/90^+$ intensity ratios of 2.6 and 0.08 for the TQMS and QITMS, respectively. The poor agreement between these spectra on the two instruments can be attributed to differences in the mixture of reactant ions, the relative abundances of these ions, the temperature of the ionization regions, and the ion residence times in the ionization regions of the TQMS and the QITMS. With both instruments, the CE spectra include residual reactant ions which may further complicate spectral interpretation. For example, with the TQMS, ions at m/z 28 ($[N_2]^{+\cdot}$ and/or $[CO]^{+\cdot}$, 40% relative abundance [RA]) and m/z 88 ($[CO_2]_2^{+\cdot}$, 10% RA) are present in addition to the m/z 44 base peak ($[CO_2]^{+\cdot}$, 100% RA]); these ions may contribute to ionization of the sample molecules. The $[N_2]^{+\cdot}$ ion will impart more energy during CE ionization than the $[CO_2]^{+\cdot}$ ion, hence the $89^+/90^+$ ion intensity ratio will be larger than predicted by equation 4.6. This ion appears to be present in the TQMS non-mass-selected CO_2 mass-spectra [Table 4.3(b) and Figure 4.1(e)], which accounts for the very large $89^+/90^+$ ion intensity ratio.

Table 4.3(a). Summary of Non-Mass-Selected CE and CI Reactions with the QITMS

		Reactant Gases							
		Methane	Water	Nitrogen	Ethylene	Argon	Carbon Dioxide	Nitrous Oxide	EI
	m/z	Percent Relative Abundance[a]							
Phenylacetonitrile (mw = 117)	235	22	9	<3	5	<3	<3	<1	<1
	118	100	100	<3	100	<3	6	18	19
	117	39	41	39	37	30	34	100	100
	116	6	10	100	8	100	38	42	31
	92	9	6	<3	<1	8	6	9	<1
	91	55	25	69	73	54	41	34	25
	90	10	19	72	12	62	100	70	81
	89	6	9	78	5	83	8	22	41
n-Butylbenzene (mw = 134)	175	<1	<1	<1	<1	<1	<1	<1	<1
	147	6	3	14	26	<1	9	3	2
	135	26	100	9	66	<1	4	15	4
	134	32	11	25	82	9	21	54	31
	133	9	3	13	34	<1	8	5	2
	119	3	3	<1	11	<1	<1	<1	2
	107	14	<1	<1	<1	<1	<1	<1	<1
	105	8	2	6	10	5	9	5	7
	92	78	23	25	66	42	38	73	60
	91	100	27	100	100	100	100	100	100
	65	14	4	6	<1	13	4	5	18
	57	57	36	7	52	60	4	15	5

[a] Percent relative abundance - relative to most abundant sample ion

Table 4.3(b). Summary of Non-Mass-Selected CE and CI Reactions with the TQMS

		Reactant Gases					
		Methane	Water	Ethylene	Carbon Dioxide	Helium	EI
	m/z	Percent Relative Abundance[a]					
Phenylacetonitrile (mw = 117)	235	<1	<1	<1	<1	<1	<1
	118	43	100	61	22	8	8
	117	46	60	25	83	100	100
	116	9	14	2	15	38	39
	92	8	2	8	<1	<1	<1
	91	100	26	100	10	13	8
	90	11	15	1	39	42	46
	89	7	7	3	100	28	29
n-Butylbenzene (mw = 134)	175	1	<1	7	<1	<1	<1
	147	1	<1	2	<1	<1	<1
	135	42	99	10	2	1	2
	134	22	28	18	15	8	26
	133	15	1	7	1	<1	<1
	119	4	1	4	1	<1	1
	107	14	0	3	<1	<1	<1
	105	6	10	73	11	4	8
	92	19	61	13	50	22	59
	91	45	100	100	100	100	100
	65	2	10	<1	3	9	33
	57	100	33	<1	4	1	<1

[a] Percent relative abundance - relative to most abundant sample ion

Chemical Ionization

The experimental results from non-mass-selected CI reactions are summarized in Tables 4.3(a) and 4.3(b). In order to interpret the CI spectra, it is important to know the proton affinities (PAs) of the compounds of interest, as well as those of the reactant gases (Table 4.2) [11]. The difference between the PA of the conjugate base of the reactant ion and the PA of the sample molecule determines the internal energy that is imparted to the sample ion with CI. As for CE, some control of the energetics (the degree of fragmentation) of this ionization process can be achieved by selecting various reactant gases to produce a variety of reactant ions. For CI, the relative abundances of the fragment ions and the pseudo-molecular ion were used to evaluate the energetics of the CI process.

The TQMS non-mass-selected methane CI mass spectra (with the CH_4 pressure adjusted to make $[C_2H_5]^+$ at least as abundant as $[CH_5]^+$) of n-butylbenzene and phenylacetonitrile are shown in Figures 4.1(c) and 4.1(f), respectively. The QITMS non-mass-selected methane CI mass spectra (with the RF levels adjusted to make $[C_2H_5]^+$ the most abundant reactant ion) of n-butylbenzene and phenylacetonitrile are shown in Figures 4.2(c) and 4.2(f), respectively. The $[C_2H_5]^+$ ion (PA of C_2H_4 is 7.1 eV) was selected as the dominant reactant ion by increasing linearly the RF voltage to eject all ions below m/z 20 during period B [Figure 2.4]. This ejects $[CH_5]^+$ and $[H_3O]^+$, as well as any other ions with m/z less than 20 amu, leaving the $[C_2H_5]^+$ and $[C_3H_5]^+$ reactant ions and EI-produced sample ions with m/z greater than 20. Prior to period C, the RF voltage was lowered to a value corresponding to m/z 10. The $[H_3O]^+$ ions formed by proton transfer during period C were constantly ejected by applying a supplementary RF voltage across the end cap electrodes at the resonant frequency of the m/z 19 ion. Both the TQMS and QITMS non-mass-selected methane CI mass spectrum of n-butylbenzene [Figures 4.1(c) and 4.2(c), respectively] are characterized by ions at m/z 57 ($[C_4H_9]^+$), 91 ($[C_7H_7]^+$), 92 ($[C_7H_8]^{+\cdot}$), 133 ($[M-H]^+$, 134 ($[M]^{+\cdot}$), and 135 ($[M+H]^+$). These spectra show significant differences, including the lower relative abundance of the $[M+H]^+$ ion compared to that of the 91^+ in the QITMS spectrum and the higher abundance of the $[M]^{+\cdot}$ ion compared to $[M+H]^+$ with the QITMS. These differences in the mass spectra obtained with non-mass-selected methane CI experiments on the two instruments may readily be explained. Firstly, the unusually abundant $[M]^{+\cdot}$ ion in the QITMS spectrum points to a larger amount of residual EI-produced or CE-produced ions than in the TQMS. The reactant ion distribution is vastly different in the two instruments. In the TQMS methane non-mass-selected CI experiments, the major reactant ions are $[CH_5]^+$ (100 % RA), $[H_3O]^+$ (9% RA), $[C_2H_5]^+$ (100% RA), and $[C_3H_5]^+$ (20% RA). In the QITMS, the major reactant ions are $[C_2H_5]^+$ (100% RA), $[O_2]^{+\cdot}$ (57% RA), and $[C_3H_5]^+$ (48% RA); ions below m/z 25 (e.g., $[CH_5]^+$ and $[H_3O]^+$) are not stored in the ion trap and therefore cannot lead to ionization. The large abundance of $[CH_5]^+$ (PA = 5.72 eV) in the TQMS ion source will cause the mass spectra to exhibit a higher degree of fragmentation than expected from the QITMS where this reactant ion is absent. The $[O_2]^{+\cdot}$ reactant ion present in the QITMS will lead to CE ionization, producing $[M]^{+\cdot}$ ions in addition to those remaining from EI. The similarities of the QITMS non-mass-selected methane CI spectrum [Figure 4.2(c)] and the QITMS

EI spectrum [Figure 4.2(a)] indicate that the CI spectrum is the result of mixed-mode ionization.

Both the TQMS and QITMS non-mass-selected methane CI mass spectrum of phenylacetonitrile [Figure 4.1(f) and 4.2(f), respectively] are characterized by ions at m/z 91 ($[C_7H_7]^+$), m/z 117 ($[M]^{+\cdot}$), and 118 ($[M+H]^+$). The TQMS methane non-mass-selected mass spectrum is more energetic (exhibits more fragmentation), as would be predicted by the presence of the $[CH_5]^+$ reactant ion. In this case, there is more residual EI with the TQMS than with the QITMS, as reflected in the higher abundance of $[M]^{+\cdot}$ relative to $[M+H]^+$. The difficulty in interpreting the mass spectra from non-mass-selected CE and CI reactions [summarized in Table 4.3] indicate the necessity to mass-select reactant ions if the energetics of the ionization process are to be better controlled.

Mass-selected Ion-molecule Reactions

From the discussion above, it is clear that non-mass-selected CE and CI produce mixed-mode ionization; therefore the degree of fragmentation observed does not always agree with that predicted by theory. The mass spectrometers used here, however, offer the ability to mass-select a particular reactant ion. This should provide CE and CI spectra which show better agreement among various instruments and which are more easily explained by theory.

Charge Exchange Ionization

The mass-selected CE ionization experimental results obtained from phenylacetonitrile and n-butylbenzene are summarized in Tables 4.4(a) and

Table 4.4(a). Summary of Mass-Selected CE Reactions with the QITMS

		Reactant Ions							
		$[Ar]^{+\cdot}$	$[N_2]^{+\cdot}$	$[CO_2]^{+\cdot}$	$[N_2O]^{+\cdot}$	$[H_2O]^{+\cdot}$	$[O_2]^{+\cdot}$	$[C_2H_4]^{+\cdot}$	$[NO]^{+}$
		Internal Energy Imparted By CE (eV)[a]							
Phenylacetonitrile		6.31	6.13	4.35	3.44	3.17	2.63	1.06	-0.19
n-Butylbenzene		7.07	6.89	5.11	4.20	3.93	3.39	1.82	0.57
	m/z	Percent Relative Abundance[b]							
Phenylacetonitrile (mw ~ 117)	235	<1	<1	<1	<1	<1	<1	14	<8
	147	<1	<1	<1	<1	<1	<1	<1	66
	118	3	10	6	18	74	8	57	<8
	117	10	11	13	100	100	100	100	100
	116	60	93	29	13	<1	<1	34	<8
	92	<1	<1	2	<1	<1	<1	<1	<8
	91	37	70	22	37	48	<1	40	<8
	90	19	30	100	86	37	<1	24	<8
	89	100	100	11	<1	<1	<1	25	<8
	63	5	<1	<1	<1	<1	<1	<1	<8
n-Butylbenzene (mw - 134)	175	<1	<1	<1	<3	<1	<3	<1	<1
	147	2	2	2	<3	<1	6	<3	<1
	135	2	3	2	<3	11	<3	21	11
	134	4	4	7	20	24	27	100	100
	133	2	2	3	<3	10	<3	6	<1
	119	<1	<1	<1	<3	5	<3	<1	<1
	107	<1	<1	<1	<3	<1	<3	3	<1
	105	2	2	6	5	11	6	<1	<1
	92	9	7	14	57	65	100	46	<1
	91	100	100	100	100	100	39	22	<1
	65	8	3	2	<3	9	<3	<1	<1
	57	4	6	3	<3	15	<3	15	<1

[a] -ΔH for equation (4.6)

[b] Percent relative abundance - relative to most abundant sample ion

Table 4.4(b). Summary of Mass-Selected CE Reactions with the TQMS

		Reactant Ions								
		$[He]^{+\cdot}$	$[Ar]^{+\cdot}$	$[N_2]^{+\cdot}$	$[Ar_2]^{+\cdot}$	$[N]^{+}$	$[CO_2]^{+\cdot}$	$[CH_4]^{+\cdot}$	$[H_2O]^{+\cdot}$	$[C_2H_4]^{+\cdot}$
		Internal Energy Imparted By CE (eV)[a]								
Phenylacetonitrile		15.14	6.31	6.13	5.26	5.10	4.35	3.31	3.17	1.06
n-Butylbenzene		15.90	7.07	6.89	6.02	5.86	5.11	4.07	3.93	1.82
	m/z	Percent Relative Abundance[b]								
Phenylacetonitrile (mw = 117)	235	<1[c]	<1	<1	<1	<1	<1	<1	<1	<1
	118	2	2	7	<1	13	2	35	51	17
	117	2	10	25	16	100	18	100	100	100
	116	<1	100	100	43	34	35	2	7	2
	92	1	2	3	1	2	1	18	26	1
	91	10	22	38	13	21	12	75	75	5
	90	3	28	47	100	77	100	9	45	2
	89	15	89	71	7	16	1	<1	1	1
	63	56	<1	<1	<1	5	<1	<1	<1	<1
n-Butylbenzene (mw = 134)	175	<1[d]	<1	<1	<1	<1	<1	<1	<1	<1
	147	<1	<1	<1	<1	<1	<1	<1	1	1
	135	<1	<1	<1	<1	<1	1	6	6	21
	134	1	1	3	1	4	5	48	14	100
	133	<1	<1	<1	<1	<1	<1	1	1	1
	119	<1	<1	<1	<1	2	<1	3	2	1
	107	<1	<1	<1	<1	<1	<1	<1	<1	<1
	105	3	2	2	8	8	8	5	13	3
	92	4	9	9	21	98	26	100	88	78
	91	61	100	100	100	100	100	56	100	28
	65	100	<1	<1	<1	<1	<1	<1	3	<1
	57	7	2	2	<1	<1	2	16	15	3

[a] -ΔH for equation (4.6)

[b] Percent relative abundance (%RA) - relative to most abundant sample ion

[c] Other ion present in the phenylacetonitrile $[He]^{+\cdot}$ CE spectra include m/z 27, 39, 40, 51, 63, and 64, with %RA's of 16%, 100%, 39%, 62%, 56%, and 21%; respectively

[d] See Figure 4.8(b) for other ions present in the n-butylbenzene $[He]^{+\cdot}$ CE spectra

4.4(b). The data in these tables illustrate that mass-selected CE ionization mass spectra obtained with the same reactant ion with the QITMS and TQMS are more similar than are the non-mass-selected spectra obtained with the same reactant gas. For example, whereas the non-mass-selected CO_2 CE mass spectra of phenylacetonitrile obtained on the TQMS and QITMS are very different [Tables 4.3(a) and 4.3(b) and Figures 4.1(e) and 4.2(e)], the mass-selected $CO_2^{+\cdot}$ CE mass spectra are very similar [Tables 4.4(a) and 4.4(b)]. The best correlation between the two instruments is with the m/z 40 ($[Ar]^{+\cdot}$) reactant ion from argon, with a $91^+/92^+$ intensity ratio for n-butylbenzene of 11.1 for both instruments. The average difference between the $91^+/92^+$ intensity ratios obtained with the two instruments was 24%. This agreement between instruments is relatively good considering the differences in operating parameters (Table 1.1).

Although the energetics of the ionization could be somewhat controlled with non-mass-selected CE through the use of different reactant gases, the discussion above pointed out that several different reactant ions could be produced from a single reactant gas; thus, mixed-mode ionization and less control of the ionization energetics resulted. One of the most useful features of mass-selected CE on the QITMS and TQMS is that a particular reactant ion with a specific recombination energy can be selected, thus enabling the energetics of CE ionization to be controlled. One example of this can be seen for the $[C_2H_4]^{+\cdot}$ and $[Ar]^{+\cdot}$ reactant ions, which have RE's of 10.5 and 15.8 eV, respectively. These values correspond to approximately 1.8 eV and 7.1 eV, respectively, of internal energy being deposited into n-butylbenzene upon ionization. Thus, the QITMS $[C_2H_4]^{+\cdot}$ CE mass spectrum [Figure 4.5(a)] of n-butylbenzene is

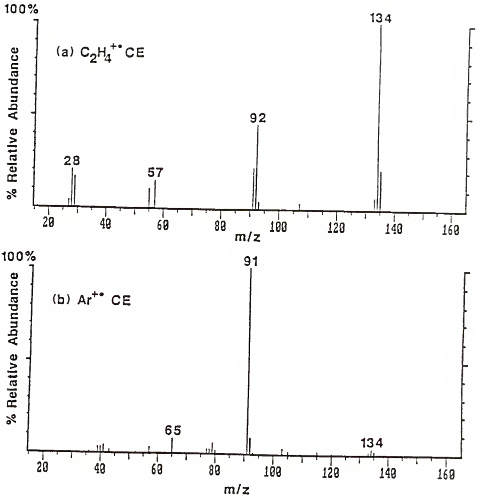

Figure 4.5. QITMS mass-selected CE mass spectra of n-butylbenzene with (a) $[C_2H_4]^{+\cdot}$ (ΔH = -1.8 eV) and (b) $[Ar]^{+\cdot}$ (ΔH = -7.1 eV) as reactant ions. Mass scan range was from m/z 15 to m/z 300.

characterized by a $91^+/92^+$ intensity ratio of 0.5 and a very intense molecular ion. The presence of m/z 29 ($[C_2H_5]^+$) in the $[C_2H_4]^{+\cdot}$ CE mass spectrum may have produced some CI, as indicated by the ions at m/z 57 and 135. The QITMS $[Ar]^{+\cdot}$ CE mass spectrum [Figure 4.5(b)] of n-butylbenzene is characterized by a $91^+/92^+$ intensity ratio of 11.1 and a very low abundance molecular ion at m/z 134 reflecting the larger recombination energy of $[Ar]^{+\cdot}$. Thus, this example of mass-selected CE illustrates the analytical utility of this ionization technique. If molecular weight information is desired, the $[C_2H_4]^{+\cdot}$ ion can be selected for CE; conversely, if structural information is desired, the $[Ar]^{+\cdot}$ ion can be selected.

As demonstrated above, a single reactant gas can produce different reactant ions, each with its specific recombination energy. Thus, different reactant ions from a single gas can be mass-selected to control the degree of fragmentation desired from the molecular ion. For example, when 0.70 torr of argon is present in the ion source of the TQMS, both $[Ar]^{+\cdot}$ (RE = 15.8 eV) and $[Ar_2]^{+\cdot}$ (RE = 14.7 eV) are generated and can be mass-selected as reactant ions. The TQMS mass-selected $[Ar]^{+\cdot}$ and $[Ar_2]^{+\cdot}$ CE mass spectra [Figure 4.6] of n-butylbenzene are characterized by $91^+/92^+$ intensity ratios of 11.1 and 4.8, respectively. These results were predicted since $[Ar_2]$+. has a lower recombination energy than $[Ar]^{+\cdot}$. A more dramatic example of the differences in the fragmentation that can be obtained with different reactant ions of the same reactant gas is demonstrated when nitrous oxide is used as a reactant gas. Nitrous oxide produces three reactant ions with different RE's: $[N_2O]^{+\cdot}$ (RE = 12.9 eV), $[O_2]^{+\cdot}$ (RE = 12.1 eV), and $[NO]^+$ (RE = 9.3 eV). The QITMS non-mass-

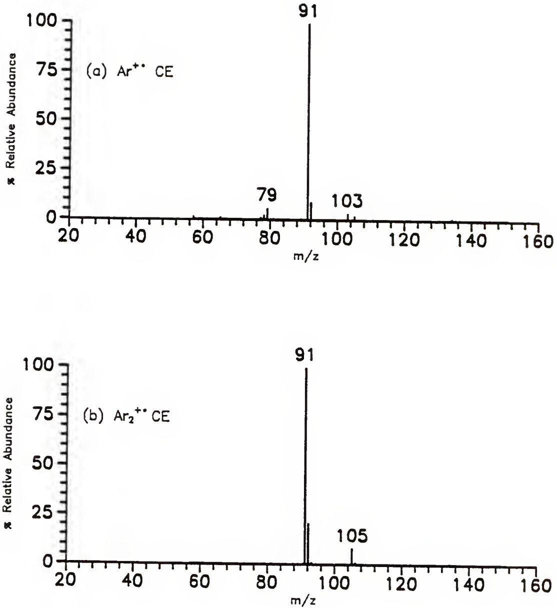

Figure 4.6. TQMS mass-selected CE mass spectra with argon as the reactant gas: (a) mass-selected $[Ar]^{+\cdot}$ CE (ΔH = -7.1 eV), and (b) mass-selected $[Ar_2]^{+\cdot}$ CE (ΔH = -6.0 eV). The mass scan ranges were from m/z 45 to m/z 300 and m/z 85 to m/z 300 for mass-selected $[Ar]^{+\cdot}$ CE and mass-selected $[Ar_2]^{+}$ CE, respectively.

selected and mass-selected N_2O spectra of n-butylbenzene are shown in Figure 4.7. The QITMS non-mass-selected N_2O CE mass spectrum [Figure 4.7(a)] is characterized by a $91^+/92^+$ intensity ratio of 1.4 and an intense molecular ion at m/z 134. The three N_2O reactant ions can all contribute to CE of the sample molecules. In addition, the presence of $[H_3O]^+$ (m/z 19) may have produced some proton-transfer CI, as indicated by the presence of ions at m/z 57 and m/z 135. The QITMS mass-selected $[NO]^+$ CE mass spectrum [Figure 4.7(b)] is characterized by the molecular ion at m/z 134 with no fragmentation observed. The lack of fragmentation is predicted since the amount of internal energy imparted to the molecule during ionization is only 0.6 eV. Mass-selection of the $[O_2]^{+\cdot}$ and $[N_2O]^{+\cdot}$ reactant ions produces CE mass spectra which are dominated by the 91^+ and 92^+ fragment ions, with $91^+/92^+$ ion intensity ratios of 0.4 and 1.8, respectively [Figures 4.7(c) and 4.7(d)]. It is interesting to note the dramatic change in the $91^+/92^+$ ion intensity ratios as the internal energy of the $M^{+\cdot}$ ion is varied from 3.4 to 4.2 eV with the use of $[O_2]^{+\cdot}$ and $[N_2O]^{+\cdot}$ as reactant ions, respectively. The mass-selected $[N_2O]^{+\cdot}$ CE spectrum also exhibits an intense $[O_2]^{+\cdot}$ ion, which increases with reaction times greater than approximately 20 ms, either due to CE of residual O_2 by $[N_2O]^{+\cdot}$ or due to reactions of $[N_2O]^{+\cdot}$ with neutral N_2O [50]. This illustrates one limitation of mass-selected reactions with the QITMS: with long reaction times, other reactant ions may form and may lead to mixed mode ionization. However, the magnitude of this problem is much less than that which occurs when no mass-selection of the reactant ion occurs. An important advantage of the TQMS is that spatial separation of the initial ionization and CE/CI regions allows the interfering reactant ions formed

Figure 4.7. QITMS non-mass-selected and mass-selected CE mass spectra with nitrous oxide as the reactant gas: (a) non-mass-selected CE, (b) mass-selected $[NO]^{+}$ CE (ΔH = -0.3 eV), (c) mass-selected $[O_2]^{+\cdot}$ CE (ΔH = -3.0 eV), and (d) mass-selected $[N_2O]^{+\cdot}$ CE (ΔH = -4.0 eV). Mass scan range was from m/z 15 to m/z 300.

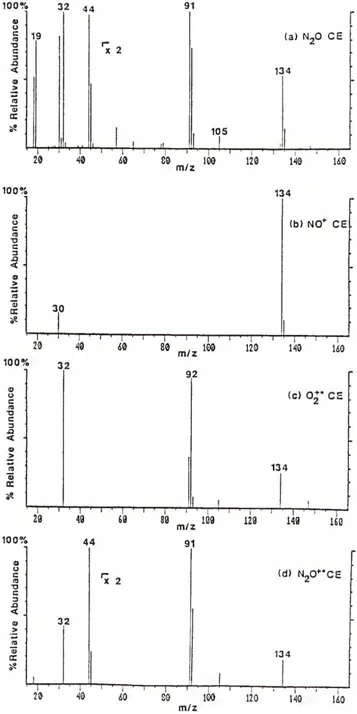
100%
% Relative Abundance
19
32
44
91
x 2
(a) N_2O CE
134
105
20
40
60
80
100
120
140
160
m/z
100%
134
(b) NO^+ CE
% Relative Abundance
30
20
40
60
80
100
120
140
160
m/z
100%
32
92
(c) $O_2^{+\bullet}$ CE
% Relative Abundance
134
20
40
60
80
100
120
140
160
m/z
100%
44
91
x 2
(d) $N_2O^{+\bullet}$ CE
% Relative Abundance
32
134
20
40
60
80
100
120
140
160
m/z

in the ionization region to be eliminated during the first stage of mass analysis. Although some interfering reactant ions can be generated in Q2 from CE/CI of residual gases in Q2, the abundances of these ions are usually very low relative to the mass-selected reactant ion and their contribution to the ionization of the sample is probably insignificant. Interferent ions with an m/z lower than that of the selected reactant ion can be eliminated by increasing the Q2 RF voltage such that they are unstable and not transmitted. The experimental results from mass-selected CE are summarized in Tables 4.4(a) and 4.4(b).

A comparison of non-mass-selected and mass-selected ion molecule reactions in the TQMS is shown in Figure 4.8. It should be noted that $[He]^{+\cdot}$ CE could not be performed with the QITMS, since the low mass cut-off of the ion trap prevents helium ions from being stored. The non-mass-selected helium CE mass spectrum of n-butylbenzene is shown in Figure 4.8 (a), while the mass-selected $[He]^{+\cdot}$ CE spectrum is shown in Figure 4.8 (b). The non-mass-selected spectrum is characterized by a $91^+/92^+$ intensity ratio of 4.5, a value that is unexpectedly low given the extremely high recombination energy (24.6 eV) of $[He]^{+\cdot}$. In contrast the TQMS $[He]^{+\cdot}$ CE mass-selected spectrum of n-butylbenzene is characterized ions [e.g., $H_2O]^{+\cdot}$ (RE = 12.6 eV), $[N_2]^{+\cdot}$ (RE = 15.6 eV), and $[O_2]^{+\cdot}$ (RE = 12.1 eV)] when the non-mass-selected ionization mode is used. If CE occurs with any of the extraneous reactant ions, the $91^+/92^+$ ion intensity ratio would be less than that predicted for $[He]^{+\cdot}$ CE. With mass-selection of the $[He]^{+\cdot}$ ion, this mixed-mode ionization is avoided.

The mass-selected CE ionization experimental results for n-butylbenzene are summarized and compared with CE ionization data for n-butylbenzene

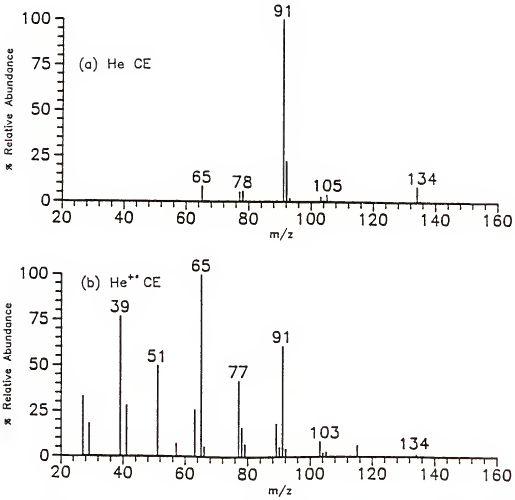

Figure 4.8. TQMS non-mass-selected and mass-selected CE mass spectra with helium as the reactant gas: (a) non-mass-selected CE, and (b) mass-selected $[\text{He}]^{+\cdot}$ CE ($\Delta H = -15.9$ eV). The mass scan ranges were from m/z 50 to m/z 300 and m/z 20 to m/z 300 for non-mass-selected CE and mass-selected CE, respectively.

obtained by Harrison and Lin [77] in Figure 4.9(a). The plots of experimental data and literature data follow the same trends, which would be expected from theory: as the recombination energy of the reactant ion increases, the internal energy of the n-butylbenzene molecular ion increases; thus, the $91^+/92^+$ intensity ratio increases. The large difference between the literature values and the values obtained in this work may be attributed to the mass-selection of the reactant ions that interact with the sample molecules. For example, Harrison and Lin reported a $91^+/92^+$ intensity ratio of 6.9 with non-mass-selected N_2 CE, while the $91^+/92^+$ intensity ratio observed in this work for the QITMS mass-selected $[N_2]^{+\cdot}$ CE was 14.3. Note that the values of the $91^+/92^+$ intensity ratio in this work sometimes exceed the calculated maximum value of 13; this may be attributed to small errors in zeroing and poor ion statistics for the 92^+ ion. As has been demonstrated here, without mass-selection of a single reactant ion for a particular reactant gas, mixed-mode ionization can result in the $91^+/92^+$ intensity ratio not accurately reflecting the energetics as predicted based on the assumption of only one reactant ion. A similar graph appears in Figure 4.9(b) for the experimental results with phenylacetonitrile. Similar to the behavior observed for the $91^+/92^+$ intensity ratios of n-butylbenzene, the $89^+/90^+$ intensity ratio increases with increasing amounts of internal energy. Note that the $[C_2H_4]^{+\cdot}$ data do not fit on either curve for phenylacetonitrile. This may be attributed to the fact that m/z 28 may be one of or a combination of the following species: $[C_2H_4]^{+\cdot}$ (RE = 10.5 eV) $[CO]^{+\cdot}$ (RE = 14.0 eV), and $[N_2]^{+\cdot}$ (RE = 15.6 eV). The presence of the $[N_2]^{+\cdot}$ and $[CO]^{+\cdot}$ ions in the mass-

Figure 4.9. Experimental and literature values as a function of internal energy deposited during CE ionization of n-butylbenzene and phenylacetonitrile. (a) $91^+/92^+$ intensity ratio as a function of internal energy deposited for n-butylbenzene and (b) $89^+/90^+$ intensity ratio as a function of internal energy deposited for phenylacetonitrile.

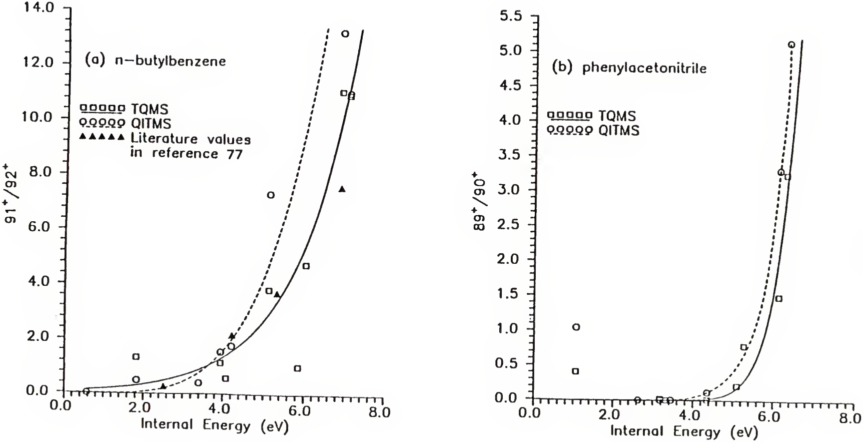
(a) n–butylbenzene
TQMS
QITMS
Literature values in reference 77
91⁺/92⁺
14.0
12.0
10.0
8.0
6.0
4.0
2.0
0.0
0.0
2.0
4.0
6.0
8.0
Internal Energy (eV)
(b) phenylacetonitrile
TQMS
QITMS
89⁺/90⁺
5.5
5.0
4.5
4.0
3.5
3.0
2.5
2.0
1.5
1.0
0.5
0.0
0.0
2.0
4.0
6.0
8.0
Internal Energy (eV)

selected $[C_2H_4]^{+\cdot}$ CE mass spectra would cause the $89^+/90^+$ intensity ratio to be larger than predicted by equation 4.6.

Chemical Ionization

The mass-selected CI mass spectra of n-butylbenzene and phenylacetonitrile are summarized in Tables 4.5(a) and 4.5(b). Once again, the capabilities of the QITMS and TQMS allow reactant ions with various PA's to be mass-selected; thus, the energetics of the CI process can be controlled. The reactant ions $[CH_5]^+$ and $[C_2H_5]^+$ were selected from methane reactant gas with the mass-selected scan mode of the QITMS. The amount of internal energy deposited into the n-butylbenzene molecule upon ionization by $[CH_5]^+$ and $[C_2H_5]^+$ CI is calculated to be 2.6 eV and 1.3 eV, respectively. The mass-selected $[CH_5]^+$ and $[C_2H_5]^+$ CI mass spectra of n-butylbenzene [Table 4.5(a) and Figure 4.10] are characterized by ions at m/z 57 ($[C_4H_9]^+$), 91 ($[C_7H_7]^+$), 133 ($[M\text{-}H]^+$), and 135 ($[M+H]^{+\cdot}$). The higher degree of fragmentation observed in the $[CH_5]^+$ CI mass spectra is as anticipated by the large energy deposition calculated with equation 4.2. Even with mass-selection of a single reactant ion, due to the nature of the QITMS (tandem-in-time), interferent reactant ions were regenerated after the mass-selection step; their intensities were observed to increase with increasing ion-molecule reaction time. Thus, the presence of $[C_2H_5]^+$ and $[H_3O]^+$ in the mass-selected $[CH_5]^+$ and $[C_2H_5]^+$ CI mass spectra, respectively, would cause a decrease in the predicted degree of fragmentation of the pseudo-molecular ion of n-butylbenzene. Comparison of the QITMS mass-selected $[C_2H_5]^+$ CI mass spectrum [Figure 4.10(b)] to the QITMS non-mass-selected methane CI and EI spectra [Table 4.5(a) and

Table 4.5(a). Summary of Mass-Selected CI Reactions with the QITMS

		Reactant Ions				
		$[CH_5]^{+a}$	$[C_2H_5]^{+a}$	$[C_2H_5]^{+b}$	$[H_3O]^+$	$[C_3H_5]^{+b}$
		Internal Energy Imparted by CI[c]				
Phenylacetonitrile		2.78	1.43	1.43	1.26	0.52[d]
n-Butylbenzene		2.61	1.26	1.26	1.09	0.35[d]
	m/z	Percent Relative Abundance[e]				
Phenylacetonitrile (mw - 117)	235	10	20	<1	39	<1
	158	<1	<1	<1	<1	62
	130	<1	<1	1	<1	100
	118	37	100	100	100	83
	117	11	15	6	<1	7
	116	2	<1	2	<1	4
	92	10	<1	12	<1	6
	91	100	45	64	11	33
	90	3	<1	3	<1	<1
	89	<1	<1	1	<1	<1
n-Butylbenzene (mw - 134)	175	<1	<1	<1	<1	11
	147	7	3	8	<1	92
	135	70	100	100	100	11
	134	6	6	19	<1	12
	133	18	8	22	<1	100
	119	<1	<1	<1	<1	29
	107	3	20	27	<1	<1
	105	4	2	<1	<1	15
	92	3	2	12	<1	6
	91	27	8	16	<1	41
	65	<1	<1	<1	<1	<1
	57	100	27	60	27	28

[a] Reactant ion derived from methane
[b] Reactant ion derived from ethylene
[c] -ΔH for equation (4.2) [proton transfer]
[d] -ΔH for equation (4.4) [hydride abstraction] cannot be calcualted, since HIA's are not tabulated for phenylacetonitrile and n-butylbenzene
[e] Percent relative abundance - relative to most abundant sample ion

Table 4.5(b). Summary of Mass-Selected CI Reactions with the TQMS

		Reactant Ions				
		$[CH_5]^{+a}$	$[C_2H_5]^{+a}$	$[C_2H_5]^{+b}$	$[H_3O]^+$	$[C_3H_5]^{+b}$
		Internal Energy Imparted by CI[c]				
Phenylacetonitrile		2.78	1.43	1.43	1.26	0.52[d]
n-Butylbenzene		2.61	1.26	1.26	1.09	0.35[d]
	m/z	Percent Relative Abundance[e]				
Phenylacetonitrile	235	<1	<1	<1	<1	<1
(mw = 117)	130	<1	<1	<1	<1	62
	118	85	100	50	100	100
	117	1	<1	100	<1	4
	116	1	1	2	<1	9
	92	19	8	5	3	6
	91	100	98	74	45	80
	90	<1	<1	2	<1	<1
	89	<1	<1	<1	<1	<1
n-Butylbenzene	175	<1	<1	<1	<1	5
(mw = 134)	147	<1	<1	1	1	90
	135	6	22	42	37	15
	134	1	4	100	5	6
	133	6	8	9	3	53
	119	1	<1	1	1	16
	107	<1	7	10	<1	<1
	105	5	2	2	3	19
	92	3	5	43	6	6
	91	35	60	57	22	100
	65	<1	<1	<1	<1	<1
	57	100	100	94	100	76

[a] Reactant ion derived from methane
[b] Reactant ion derived from ethylene
[c] -ΔH for equation (4.2) [proton transfer]
[d] -ΔH for equation (4.4) [hydride abstraction] cannot be calcualted, since HIA's are not tabulated for phenylacetonitrile and n-butylbenzene
[e] Percent relative abundance - relative to most abundant sample ion

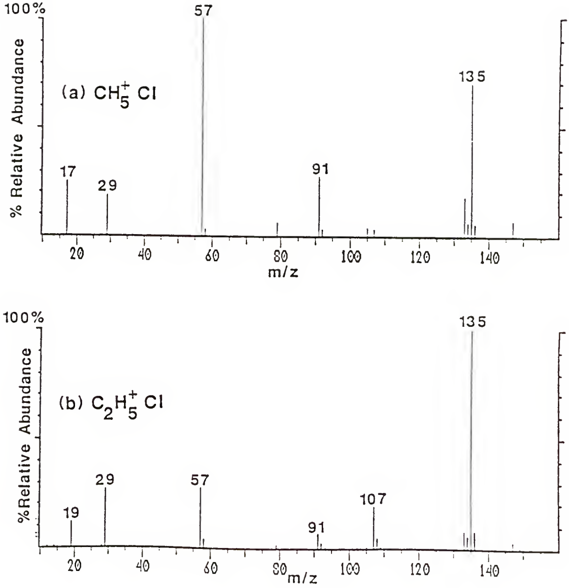

Figure 4.10. QITMS mass-selected CI mass spectra with methane as the reactant gas: (a) mass-selected $[CH_5]^+$ proton-transfer CI (ΔH = - 2.6 eV), and (b) mass-selected $[C_2H_5]^+$ proton-transfer CI (ΔH = - 1.3 eV). Mass scan range was from m/z 15 to m/z 300.

Figures 4.2(a) and 5(b), respectively] indicates that the non-mass-selected CI spectrum is the result of mixed-mode ionization.

The QITMS results with ethylene as a reactant gas provide another comparison of non-mass-selected and mass-selected ion-molecule reactions [Tables 4.3(a), 4.4(a), and 4.5(a) and Figure 4.11]. A unique feature of ethylene reactant gas is the availability of reactant ions for CE ($[C_2H_4]^{+\cdot}$), as well as both proton-transfer and hydride-abstraction CI ($[C_2H_5]^+$ and $[C_3H_5]^+$, respectively). The QITMS non-mass-selected ethylene mass spectrum [Figure 4.11(a)] is a composite of at least four ionization processes: EI, CE with $[C_2H_4]^{+\cdot}$, proton-transfer CI with $[C_2H_5]^+$, and hydride-abstraction CI with $[C_3H_5]^+$. The need to mass-select the reactant ion for CE or CI is apparent from this example. The QITMS mass-selected $[C_2H_4]^{+\cdot}$ (RE = 10.5 eV) CE mass spectrum [Figure 4.11(b)] of n-butylbenzene is characterized by a very intense molecular ion $[M]^{+\cdot}$ (m/z 134) and a very low $91^+/92^+$ intensity ratio of 0.5. Due to the inability to completely eliminate the $[C_2H_5]^+$ ion with the RF/DC conditions used in this experiment, some proton-transfer CI also occurred, as evidenced by the presence of the m/z 57 fragment ion. The QITMS mass-selected $[C_2H_5]^+$ (PA = 7.1 eV) CI mass spectrum of n-butylbenzene has the $[M+H]^+$ ion (m/z 135) as its base peak; thus, proton-transfer CI ion-molecule reactions dominates the ionization processes [Figure 4.11(c)]. The QITMS mass-selected $[C_3H_5]^+$ CI mass spectrum is dominated by the ions at m/z 133 and 147 resulting from two different CI processes [Figure 4.11(d)]. The m/z 133 is the $[M-H]^+$ ion which results from the hydride-abstraction CI reaction which dominates the $[C_3H_5]^+$ CI processes. The fact that hydride ion abstraction is more likely with $[C_3H_5]^+$ than with $[C_2H_5]^+$ is predicted

Figure 4.11. QITMS non-mass-selected and mass-selected CE mass spectra with ethylene as the reactant gas: (a) non-mass-selected CI, (b) mass-selected $[C_2H_4]^{+\cdot}$ CE (ΔH = -1.8 eV), (c) mass-selected $[C_2H_5]^+$ proton-transfer CI (ΔH = - 1.3 eV), and (d) mass-selected $[C_3H_5]^{+\cdot}$ hydride-abstraction CI. Mass scan range was from m/z 15 to m/z 300.

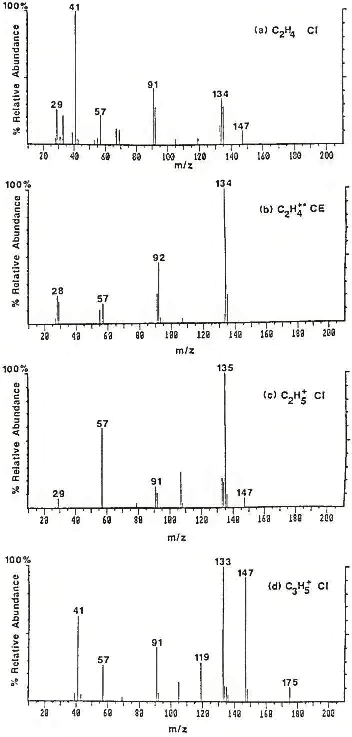
100%
% Relative Abundance
(a) C2H4 CI
41
29
57
91
134
147
20
40
60
80
100
120
140
160
180
200
m/z
100%
% Relative Abundance
(b) C2H4+• CE
134
92
28
57
20
40
60
80
100
120
140
160
180
200
m/z
100%
% Relative Abundance
(c) C2H5+ CI
135
57
91
29
147
20
40
60
80
100
120
140
160
180
200
m/z
100%
% Relative Abundance
(d) C3H5+ CI
133
147
41
91
57
119
175
20
40
60
80
100
120
140
160
180
200
m/z

based upon the literature values for the HIA's of these ions (Table 4.2). The HIA of the $[M-H]^+$ ion of n-butylbenzene could not be found in the literature. Therefore, the amount of internal energy imparted to this ion cannot be calculated. Very little proton-transfer CI occurs with $[C_3H_5]^+$, as evidenced by the relatively low abundance of the m/z 135 ion. The second major CI process is that due to adduct ion formation which produces the $[M+C_3H_5]^+$ ion at m/z 175. This adduct ion is commonly encountered when $C_3H_5^+$ is present as a reactant ion (e.g., non-mass-selected CH_4 CI) [3]. This adduct ion easily fragments (by the loss of C_2H_4) to form the m/z 147 fragment ion. Similar adduct ion formation processes occur with mass-selected $[CH_5]^+$ and $[C_2H_5]^+$ CI in the QITMS, as there are m/z 147 ions in these mass spectra as well [Table 4.5(a)]. With mass-selected CI reactions on the TQMS, this $[M+41]^+$ adduct ion is formed only with $[C_3H_5]^+$ as the reactant ion. The ability to produce, by the selection of various reactant ions from ethylene, $[M]^{+\cdot}$, $[M+H]^+$, and $[M-H]^+$, ions of a compound, and to control the degree of fragmentation, may prove to be a valuable tool for analytical mass spectrometry.

Conclusions

With mass-selection of reactant ions, it was demonstrated that control of the energetics of both the CE and CI ionization processes could be achieved. The non-mass-selected ion-molecule reactions in both instruments were shown to be a result of mixed-mode ionization consisting of a combination of EI, CE, and CI. Thus, the spectra obtained from non-mass-selected ion-molecule reactions were difficult to interpret based upon the energetics of the ionization processes. In addition, the non-mass-selected spectra obtained with the TQMS and QITMS were very different. However, mass-selected ion-molecule reactions in the QITMS and the TQMS yielded very similar spectra which were easily interpreted based upon the energetics of the ionization of the sample by the selected reactant ion. Hence, both the utility and feasibility of performing ion-molecule reactions in the center quadrupole of a TQMS, as well as in the QITMS, have been demonstrated. With the tandem-in-space configuration of the TQMS, the spatial separation of the reactant ionization region (the ion source) from the sample ionization region (Q2) permitted the elimination of interfering reactant ions by the first stage of mass analysis (Q1). Although the interfering reactant ions can be ejected initially from the QITMS, they may reappear during the sample ionization reaction period. This problem appears to become significant when reaction times greater than ~20 ms are used.

CHAPTER 5
CONCLUSIONS AND FUTURE WORK

The research presented in this thesis has centered on fundamental studies of ionization processes in the quadrupole ion trap mass spectrometer (QITMS). Ionization methods studied have included positive ion production by electron ionization (EI), chemical ionization (CI) with proton-transfer and hydride abstraction, and charge exchange (CE), as well as negative ion production by proton abstraction (NCI) and electron capture (EC). A major theme of this work has been the use of various electrical fields applied to the ion trap to control the mass range of ions which have stable trajectories, as well as the kinetic energy of these ions. These fields include the fundamental RF voltage applied to the ring electrode, as well as supplemental RF voltage applied across the end cap electrodes at the secular frequency of ions of a specific m/z, and DC voltage applied to the ring electrode in order to provide isolation of ions of a specific mass or a particular polarity. These capabilities provide the opportunity to carefully control the type of ionization that takes place in the ion trap, and the energetics of ionization (and hence degree of fragmentation). These capabilities, as implemented in mass-selected CI and CE, have been demonstrated for a wide variety of reactant ions, and compared to the results of conventional, non-mass-selected CI and CE. A comparison has also been made of these ionization methods with the QITMS and the triple quadrupole mass spectrometer (TQMS). It was also demonstrated how these approaches make NCI within the ion trap a practical technique.

The non-mass-selected ion-molecule reactions in both QITMS and TQMS instruments were shown to be a result of mixed-mode ionization consisting of a combination of EI, CE, and CI. Thus, the spectra obtained from non-mass-selected ion-molecule reactions were difficult to interpret based upon the energetics of the ionization processes. In addition, the non-mass-selected spectra obtained with the TQMS and QITMS were very different. Other limitations of non-mass-selected ionization mode include space charge affects and the inability to achieve NCI in the QITMS. The best results that can be obtained with the popular commercial quadrupole ion trap detector (Finnigan MAT ITD without supplemental RF and without DC) were addressed with the non-mass-selected EI, CI and CE results.

The mass-selected ejection mode in the QITMS (with supplemental RF voltage) did not surmount all of the difficulties associated with mixed-mode ionization, but it provided added selectivity compared to the non-mass-selected mode. Ionization of sample molecules by undesired reactant ions can be reduced by mass-selected ejection of a single m/z reactant ion. This ejection will reduce the CE or CI interferences in some cases (e.g. with $[C_2H_5]^+$ CI, the m/z 19 ($[H_3O]^+$) ion which forms by protonation of residual H_2O in the ion trap can be ejected from the ion trap). This ionization technique also suffers from several limitations, including: space charge affects, residual EI ions in CE and CI spectra, and limited negative ionization capabilities.

With mass-selection of reactant ions, it was demonstrated that control of the energetics of both the CE and CI ionization processes could be achieved. The mass-selected ion-molecule reactions in the QITMS and the TQMS yielded very similar spectra which were easily interpreted based upon the energetics of the ionization of the sample by the selected reactant ion. Hence, both the utility and feasibility of performing ion-molecule reactions in the center quadrupole of a TQMS, as well as in the QITMS, have been demonstrated. With the tandem-in-space configuration of the TQMS, the spatial separation of the reactant ionization region (the ion source) from the sample ionization region (Q2) permitted the reduction of interfering reactant ions by the first stage of mass analysis (Q1). Although the interfering reactant ions can be ejected initially from the QITMS, they may reappear during the sample ionization reaction period. This problem appears to become significant when reaction times greater than ~20 ms are used.

The preliminary investigations with negative ionization in the QITMS indicate that NCI and EC are not as sensitive as PCI and EI. This is in contrast to the observation with conventional mass spectrometers of up to a hundred-fold increase in sensitivity in the EC negative ionization mode compared to that in positive chemical ionization. The decreased sensitivity associated with EC in the QITMS may be readily explained. Electron capture for most compounds is favored only for thermal electrons; electrons with higher kinetic energy generally lead to electron ionization (to form positive ions). Electrons have a m/z value thousands of times lower than the low m/z cut-off of the ion trap. As a result, electrons will have unstable trajectories, and have much too short a time in the trap to be thermalized. Indeed, EC is only observed in the ion trap for compounds with extremely high electron affinities (eg. SF_6). However, dissociative electron capture is observed in the ion trap for a variety of reactant gases including water, ammonia, and carbon tetrachloride. The likelihood of dissociative EC is greater than EC, since it can occur with electrons with energies up to 15 eV.

Negative chemical ionization was a much slower (longer ionization and sample formation reaction times were required) ionization process than positive chemical ionization. The reasons for the longer reaction times required for negative ionization is unclear, since the tabulated rate constants for NCI and PCI are approximately the same. The slower ionization process probably results from the negative reactant ions being present in much lower concentrations than positive reactant ions, even though the same sample and reactant gas pressures were used in each case. The presence of positive ions within the ion trap indicated the need to eject positive ions, in order to prevent positive-negative ion recombination from occurring. This ejection of positive interferent ions from the ion trap, in NCI experiments, was achieved by mass-selectively ejecting m/z 19 ($[H_3O]^+$) with the supplementary RF voltage and with the DC voltage. The mass-selected NCI mode of operation (with DC voltage) was the most effective technique for performing NCI studies. The results from the QITMS $[OH]^-$ mass-selected NCI studies point out that molecular weight information, in the form of pseudo-molecular ions ($[M-H]^-$), can be obtained from a wide variety of compounds, with very little fragmentation.

Future directions suggested for this project include the study of ion-molecule reactions in the center quadrupole of a TQMS and in the QITMS with samples introduced via gas chromatography. These experiments would be designed to evaluate the analytical utility, selectivity, and sensitivity of this method of performing ion-molecule reactions. Future work should also include various applications of the ionization techniques (mass-selected CE, CI, and EC) for "real world" samples. The studies in this work focused on pure model compounds. In order to illustrate the analytical usefulness of these ionization techniques, applications with mixtures containing a variety of matrices need to be performed. The analytical figures of merit such as linear dynamic range and limit of detection need to be evaluated for the ionization techniques.

Future experiments with electron capture in the ion trap could include the examination of various electron energies in the ion trap, as well as pressure studies with a variety of reactant gases. The ideal reactant gas would have a large collisional cross section and be non-reactive. Xenon and argon are two candidates for reactant gases; however in both cases, the electron energy would have to be adjusted to prevent ionizing the reactant gas molecules. The NCI mass spectra exhibited abundant pseudo-molecular ions and very little or no fragmentation, hence little structural information. This lack of structural information provided in these studies indicates the need for further work utilizing the MS^n capabilities of the ion trap. This analysis would include the following segments: formation by EI and mass selection of the reactant ion, formation by NCI and mass selection of the parent ion ($[M-H]^-$), collisionally-activated dissociation of this parent ion, and mass analysis of the fragment ions. The examination of pentafluorobenzene (a compound often incorporated in common derivatives prepared for high sensitivity GC/MS with EC ionization) in the negative ionization mode, is a suggested preliminary investigation to perform. It is predicted, based upon the examination of sulfur hexafluoride, that this compound should form a very stable negative ion in the QITMS, although the high sensitivity associated with this molecule in conventional mass spectrometers is not expected. After this preliminary investigation, derivitized samples (introduced by means of gas chromatography) should be evaluated with the QITMS operated for the detection of negative ions. Once again, this study would include the determination of linear dynamic range and limits of detection for these samples.

A long-range future project would center around the ability to create a universal library for CE with mass-selected ion-molecule reactions. The basic principles for this project have been demonstrated in this work, since the mass-selected CE mass spectra obtained in this study appear to be independent of the instrumentation. Hence, the creation of a universal data base (one designed for ion-molecule reactions and applicable to any instrument) that would be similar to the standard EI database (libraries) which are currently used is possible. The work required for the creation of this database could be divided amongst several laboratories throughout the world.

LITERATURE CITED

1) W. Paul, H. Reinhard, and V.Z. von Zahn, Z. Physik, 156 (1959) 1.

2) W. Paul, O. Osberghaus, and E. Fischer, Forschungsber. Wirtsch. Ver Kehrsministeriums Nordheim Westfalen, No. 415 (1958).

3) E. Fischer, Z. Physik, 156 (1959) 26.

4) G. Lawson, and J.F.J. Todd, Chem. Brit., 8 (1972) 373.

5) P.H. Dawson, J.W. Hedman, and N.R. Whettten, Rev. Sci. Instrum., 40 (1969) 1444.

6) J.F.J. Todd, D.A. Freer, and R.M. Waldren, Int. J. Mass Spectrom. Ion Phys., 36 (1980) 371.

7) M.N. Kishore, and P.K. Ghosh, Int. J. Mass. Spectrom. Ion. Phys., 29 (1976) 345.

8) R.F. Bonner, G. Lawson, and J.F.J. Todd, Int. J. Mass Spectrom. Ion Phys., 10 (1973) 197.

9) R.F. Bonner, G. Lawson, J.F.J. Todd, and R.E. March, in A.R. West (Ed.) Advances in Mass Spectrometry, Applied Science, London, 1974, pp. 377-384.

10) R.M. Waldren, and J.F.J. Todd, Int. J. Mass Spectrom. Ion. Phys., 29 (1979) 315.

11) R.E, Mather, and J.F.J. Todd, Int. J. Mass Spectrom. Ion Phys., 33 (1980) 159.

12) P.H. Dawson, and C. Lambert, Int. J. Mass Spectrom. Ion Phys., 14 (1974) 339.

13) J.F.J. Todd, in D. Price, and J.F.J. Todd (Eds.) Dynamic Mass Spectrometry, Heyden, London, 1981, pp. 44-70.

14) G.C. Stafford Jr., P.E. Kelley, J.E.P. Syka, W.E. Reynolds, and J.F.J. Todd, Int. J. Mass Spectrom. Ion Proc., 60 (1984) 85.

15) D.B. Tucker, C.H. Hameister, S.C. Bradshaw, D.J. Hoekman, and M. Weber-Grabau, Proc. 36th Ann. Conf. Mass Spectrom. Allied Top., San Franscisco, 1988, 628.

16) M. Weber-Grabau, M., P.E. Kelley, J.E.P. Syka, S.C. Bradshaw, and J.S. Brodbelt, Proc. 35th Ann. Conf. Mass Spectrom. Allied Top., Denver, 1987, 1114.

17) M. Weber-Grabau, P.E. Kelley, S.C. Bradshaw, and D.J. Hoekman, Proc. 36th Ann. Conf. Mass Spectrom. Allied Top., San Francisco, 1988, 1106.

18) G.C. Stafford, D.M. Taylor, S.C. Bradshaw, J.E.P. Syka, and M. Uhrich, Proc. 35th Ann. Conf. Mass Spectrom. Allied Top., Denver, 1987, 775.

19) J.N. Louris, R.G. Cooks, J.E.P. Syka, P.E. Kelley, G.C. Stafford Jr., and J.F.J. Todd, Anal. Chem., 59 (1987) 1677.

20) P.H. Dawson, Quadrupole Mass Spectrometry and Its Applications, Elsevier Scientific Publishing Company, Amsterdam, 1976, pp. 1-119.

21) J.S. Brodbelt, J.N. Louris, and R.G. Cooks, Anal. Chem., 59 (1987) 1278.

22) S.A. McLuckey, G.L. Glish, and P.E Kelley, Anal. Chem., 59 (1987) 1670.

23) R.L. Hunter, and R.T. McIver Jr., Anal. Chem., 51 (1979) 699.

24) W.T. Huntress Jr., and R.F. Pinizzotto Jr., J. Chem. Phys., 59 (1973) 4742.

25) S. Ghaderi, P.S. Kulkarni, E.B. Ledford Jr., C.L. Wilkins, M.L. Gross, Anal. Chem., 53 (1981) 428.

26) C.L. Wilkins, and M.L. Gross, Anal. Chem., 53 (1981) 1661A.

27) K.R. Jennings, and R.S. Mason, in F.W. McLafferty (Ed.) Tandem Mass Spectrometry, John Wiley & Sons, New York, 1983, 197-222.

28) R.A. Yost, and D.D. Fetterolf, Mass Spec. Rev. 1983, 2, 1-45.

29) R.A. Yost, and C.G. Enke, in F.W. McLafferty (Ed.) Tandem Mass Spectrometry, John Wiley & Sons, New York, 1983, 175-195.

30) H. Degn, R.P. Cox, and D. Lloyd, Methods Biochem. Anal., 31 (1984) 166.

31) P.H. Dawson, Int. J. Mass Spectrom. Ion Proc., 67 (1985) 267.

32) J.E.P. Syka, and W.J. Fies Jr., Proc. 35th Ann. Conf. Mass Spectrom. Allied Top., Denver, 1987, 767.

33) K.R. Jennings, Anal. Proc., 18 (1980) 320.

34) H.E. Duckworth, R.C. Barber, and V.S. Venkatasubramanian, in M. Berry, P.C.W. Davies, C.J. Isham, and I.G. Main (Eds.) Mass Spectroscopy, Cambridge University Press, New York, 1986, pp. 40-69.

35) J.R. Chapman, Practical Organic Mass Spectrometry, John Wiley & Sons, New York, 1985, pp. 46-100.

36) E.D. Lee, S.H. Hsu, and J.D. Henion, Anal. Chem., 60 (1988) 1990.

37) D.F. Hunt, and J.P. Gale, Anal. Chem., 56 (1984) 1111.

38) J.H. Bowie, Mass Spectrom. Rev., 3 (1984) 161.

39) H. Bradenberger, in A. Frigerio (Ed.) Recent Developments In Mass Spectrometry in Biochemistry And Medicine, Plenum, New York, 1979, 85-110.

40) J.G. Dillard, Chem. Rev., 73 (1973) 589.

41) A.G. Harrison, Chemical Ionization Mass Spectrometry, CRC Press Inc, Boca Raton, 1983, pp. 1-160.

42) H. Budzikiewicz, Mass Spec. Rev., 5 (1986) 345.

43) D.F. Hunt, and S.K. Sethi, in M.L. Gross (Ed.) High Performance Mass Spectrometry: Chemical Applications, American Chemical Society, Washington, 1978, 150-178.

44) S.C. Subba Rao, and C.C. Fenselau, Anal. Chem., 50 (1978) 511.

45) J.T. Watson, Introduction to Mass Spectrometry, Raven, New York, 1985, pp. 184-202.

46) F.P. Abramson, and J.H. Futrell, J. Chem. Phys., 45 (1966) 1925.

47) P.H. Dawson, and W.F. Sun, Int. J. Mass Spectrom. Ion Phys., 44 (1982) 51.

48) C.S. Hsu, and R.G. Cooks, Org. Mass Spectrom., 11 (1976) 975.

49) A.G. Harrison, in M.A. Alomoster Ferreira (Ed.) Ionic Processes in the Gas Phase, Kluwer Academic, Norwell, 1984, pp. 23-39.

50) E. Lindholm, in J.L. Franklin (Ed.) Ion-Molecule Reactions, Plenum Press, New York, 1972, pp. 457-483.

51) P. Jonathan, A.G. Brenton, and J.H. Beynon, Org. Mass Spectrom., 23 (1988) 114.

52) C.J. Proctor, C.J. Porter, A.G. Brenton, and J.H. Beynon, Int. J. Mass Spectrom. Ion Phys., 39 (1981) 9.

53) K.L. Busch, T.L. Kruger, and R.G. Cooks, Anal. Chim. Acta, 119 (1980) 153.

54) G.G. Dolnikowski, M.J. Kristo, C.G. Enke, and J.T. Watson, Int. J. Mass Spectrom. Ion Processes, 82 (1988) 1.

55) M. Weber-Grabau, P.E. Kelley, S.C. Bradshaw, and D.J. Hoekman, Proc. 36th Ann. Conf. Mass Spectrom. Allied Top., San Francisco, 1988, 1106.

56) D.B. Tucker, C.H. Hameister, S.C. Bradshaw, D.J. Hoekman, and M. Weber-Grabau, Proc. 36th Ann. Conf. Mass Spectrom. Allied Top., San Francisco, 1988, 628.

57) G.L. Glish, G.J. Van Berkel, K.G. Asano, and S.A. McLuckey, Proc. 36th Ann. Conf. Mass Spectrom. Allied Top., San Francisco, 1988, 1112.

58) R.E. Pedder, and R.A. Yost, Proc. 36th Ann. Conf. Mass Spectrom. Allied Top., San Francisco, 1988, 632.

59) J.F.J. Todd, R.M. Waldren, R.E. Mather, Int. J. Mass Spectrom. Ion Phys., 34 (1980) 325.

60) S.A. McLuckey, K.G. Asano. G.L. Glish, Proc. 36th Ann. Conf. Mass Spectrom. Allied Top., San Franscisco, 1988, 1108.

61) R.C. Dougherty, Anal. Chem., 53 (1981) 625A-636A.

62) J.G. Dillard, in G.R. Waller, and O.C. Dermer (Eds.) Biochemical Applications Of Mass Spectrometry, John Wiley & Sons, New York, 1980, pp. 927-950.

63) G.C. Stafford, J.R. Reeher, R.D. Smith, and M.S. Story, in D. Price, and J.F.J. Todd (Eds.) Dynamic Mass Spectrometry, Heyden and Son, London, Volume 5, 1978, pp. 55-57.

64) R.C. Dougherty, J. Daulton, and F.J. Biros, Org. Mass Spectrom., 6 (1972) 1171.

65) G. Boand, R. Houriet, and T. Gaumann, in A. Quayle (Ed.) Advances In Mass Spectrometry, Heyden & Son, London, Vol. 8A, 1980, pp. 238-245.

66) A.L.C. Smit, and F.H. Field, J. Am. Chem. Soc., 99 (1977) 6471. Formation of OH^- from N_2O and CH_4.

67) W.A. Chupka, in J.L. Franklin (Ed.), Ion-Molecule Reactions, Plenum Press, New York, 1972, pp. 33-76.

68) K. Maeda, G.P. Semeluk, and F.P. Lossing, Int. J. Mass Spectrom. Ion Phys., 1 (1968) 395.

69) W.B. Peatman, T.B. Borne, and E.W. Schlag, Chem. Phys. Lett., 3 (1969) 492.

70) D. Villarejo, R.R. Herm, and M.G. Ingrham, J. Chem. Phys., 46 (1967) 4995.

71) C.E. Brion, C.A. McDowell, and W.B. Stewart, Chem. Phys. Lett., 13 (1972) 79.

72) H.M. Rosenstock, K. Draxl, B.W. Steiner, and J.T. Herron, J. Phys. Chem. Ref. Data Supp., 6 (1977) 1.

73) M.E. Hail, Ph.D. Dissertation, University of Florida, Gainesville, FL, 1989.

74) S.G. Lias, J.F. Liebman, and R.D. Levin, J. Phys. Chem. Ref. Data, 13 (1984) 695.

75) I.W. Griffiths, F.M. Harris, E.S. Mukhtar, and J.H. Beynon, Int. J. Mass Spectrom. Ion Phys., 41 (1981) 83.

76) I.W. Griffiths, E.S. Mukhtar, R.E. March, F.M. Harris, and J.H. Beynon, Int. J. Mass Spectrom. Ion Phys., 39 (1981) 125.

77) A.G. Harrison, and M.S. Lin, Int. J. Mass Spectrom. Ion Phys., 51 (1983) 353.

78) R.M. Silverstein, G.C. Bassler, and T.C. Morrill, Spectrometric Identification Of Organic Compounds, John Wiley & Sons, New York, 1981, pp. 18-20.

BIOGRAPHICAL SKETCH

David Wayne Berberich was born in Kansas City, Missouri, on December 3, 1961. He attended Ingels Elementary School for grades 1-6 and for grades 7-9 he attended Smith-Hale Junior High School. He graduated from Ruskin High School in Kansas City, Missouri, in 1980. After high school he attended Avila College in Kansas City, Missouri, earning a Bachelor of Arts degree in 1984 with majors in chemistry and mathematics. At Avila, he received the following awards: Presidential Scholarship, Chemistry Alumni Scholarship, The American Institute of Chemist Award, and membership into the Delta Epsilon Sigma (National Scholastic Honor Society). After graduation from Avila, he married Kathleen Mary Kennedy on May 25, 1984. In the fall of 1984, he entered the University of Florida to begin work for the degree of Doctor of Philosophy. He remained at the University of Florida, under the direction of Dr. Richard A. Yost, to complete work on the Ph.D. in analytical chemistry.

I certify that I have read this study and that in my opinion it conforms to acceptable standards of scholarly presentation and is fully adequate, in scope and quality, as a dissertation for the degree of Doctor of Philosophy.

Richard A. Yost, Chairman
Associate Professor of Chemistry

I certify that I have read this study and that in my opinion it conforms to acceptable standards of scholarly presentation and is fully adequate, in scope and quality, as a dissertation for the degree of Doctor of Philosophy.

John G. Dorsey
Associate Professor of Chemistry

I certify that I have read this study and that in my opinion it conforms to acceptable standards of scholarly presentation and is fully adequate, in scope and quality, as a dissertation for the degree of Doctor of Philosophy.

Gerhard M. Schmid
Associate Professor of Chemistry

I certify that I have read this study and that in my opinion it conforms to acceptable standards of scholarly presentation and is fully adequate, in scope and quality, as a dissertation for the degree of Doctor of Philosophy.

Kenneth B Wagener

Kenneth B. Wagener
Associate Professor of Chemistry

I certify that I have read this study and that in my opinion it conforms to acceptable standards of scholarly presentation and is fully adequate, in scope and quality, as a dissertation for the degree of Doctor of Philosophy.

Charles W. Thomas
Professor of Sociology

This dissertation was submitted to the Graduate Faculty of the Department of Chemistry in the College of Liberal Arts and Sciences and to the Graduate School and was accepted as partial fulfillment of the requirements for the degree of Doctor of Philosophy.

May 1989

Dean, Graduate School